The role of host-stress in the infection by the bacterial pathogen *Shigella flexneri*

Die Rolle von Wirtszellstress in der Infektion mit dem bakteriellen Krankheitserreger *Shigella flexneri*

Doctoral thesis for a doctoral degree
at the Graduate School of Life Sciences,
Julius-Maximilians-Universität Würzburg,

Section Infection and Immunity

submitted by

Caroline S. Tawk

from Moscow

Würzburg **2017**

Submitted on:

Members of the *Promotionskomitee*:

Chairperson: Prof. Dr. Thomas Dandekar

Primary Supervisor: Prof. Dr. Jörg Vogel

Supervisor (Second): Dr. Ana Eulalio

Supervisor (Third): Prof. Dr. Utz Fischer

Date of Public Defence:

Date of Receipt of Certificates:

SUMMARY

The human-bacterial pathogen interaction is a complex process that results from a prolonged evolutionary arms race in the struggle for survival. The pathogen employs virulence strategies to achieve host colonization, and the latter counteracts using defense programs. The encounter of both organisms results in drastic physiological changes leading to stress, which is an ancient response accompanying infection. Recent evidence suggests that the stress response in the host converges with the innate immune pathways and influences the outcome of infection. However, the contribution of stress and the exact mechanism(s) of its involvement in host defense remain to be elucidated. Using the model bacterial pathogen *Shigella flexneri*, and comparing it with the closely related pathogen *Salmonella* Typhimurium, this study investigated the role of host stress in the outcome of infection.

Shigella infection is characterized by a pronounced pro-inflammatory response that causes intense stress in host tissues, particularly the intestinal epithelium, which constitutes the first barrier against *Shigella* colonization. In this study, inflammatory stress was simulated in epithelial cells by inducing oxidative stress, hypoxia, and cytokine stimulation. *Shigella* infection of epithelial cells exposed to such stresses was strongly inhibited at the adhesion/binding stage. This resulted from the depletion of sphingolipid-rafts in the plasma membrane by the stress-activated sphingomyelinases. Interestingly, *Salmonella* adhesion was not affected, by virtue of its flagellar motility, which allowed the gathering of bacteria at remaining membrane rafts. Moreover, the intracellular replication of *Shigella* lead to a similar sphingolipid-raft depletion in the membrane across adjacent cells inhibiting extracellular bacterial invasion.

Additionally, this study shows that *Shigella* infection interferes with the host stress granule-formation in response to stress. Interestingly, infected cells exhibited a nuclear depletion of the global RNA-binding stress-granule associated proteins TIAR and TIA-1 and their accumulation in the cytoplasm.

Overall, this work investigated different aspects of the host stress-response in the defense against bacterial infection. The findings shed light on the importance of the host stress-pathways during infection, and improve the understanding of different strategies in host-pathogen interaction.

ZUSAMMENFASSUNG

Die Interaktion von Mensch und bakteriellem Krankheitserreger ist ein komplexer Prozess, der aus dem anhaltenden evolutionären Wettrüsten im Kampf ums Überleben resultiert. Der Erreger setzt Virulenzstrategien zur Kolonisierung des Wirtes ein und dieser nutzt Verteidigungsprogramme um dem entgegenzuwirken. Die Begegnung der beiden Organismen resultiert in drastischen physiologischen Veränderungen, welche zu Stress führen, der eine klassische infektionsbegleitende Reaktion ist.

Neuere Untersuchungen deuten darauf hin, dass die Stressantwort des Wirtes mit den Signalwegen der angeborenen Immunantwort konvergiert und im Ergebnis die Infektion beeinflusst. Jedoch bleiben die Bedeutung des Stresses und der exakte Mechanismus wie Stress an der Verteidigung des Wirtes beteiligt ist, noch zu klären. In dieser Studie dienten der bakterielle Krankheitserreger *Shigella flexneri* und vergleichend dazu der nah verwandte Erreger *Salmonella* Typhimurium als Modellorganismen, um die Rolle von Wirtszellstress für den Ausgang der Infektion zu untersuchen.

Die Infektion mit Shigellen ist durch eine ausgeprägte pro-inflammatorische Reaktion gekennzeichnet. Diese versursacht in den Wirtsgeweben, insbesondere im Darmepithel, einen starken Stress, der die erste Barriere gegen die Besiedelung mit Shigellen darstellt. In der vorliegenden Arbeit wurde entzündlicher Stress in Epithelzellen durch die Induktion von oxidativem Stress, Hypoxie und Zytokinstimulation simuliert. Die Shigelleninfektion von Epithelzellen, die solchen Belastungen ausgesetzt waren, war stark im Adhäsions-/ Bindungsstadium gehemmt. Dies resultierte aus der Verarmung von Sphingolipidflößen in der Plasmamembran durch stressaktivierte Sphingomyelinasen. Interessanterweise wurde die Adhäsion von Salmonellen, aufgrund ihrer Flaggellenvermittelten Beweglichkeit, nicht beeinträchtigt und ermöglichte so die Ansammlung von Bakterien an den verbleibenden Membranflößen. Darüber hinaus führte die intrazelluläre Replikation von Shigellen zu einer ähnlichen Verminderung von Sphingolipidflößen in der Membran benachbarter Zellen, wodurch die extrazelluläre bakterielle Invasion gehemmt wurde.

Zusätzlich zeigt diese Studie, dass eine Infektion mit Shigellen mit der Bildung von Stressgranula in der Wirtszelle interferiert. Interessanterweise zeigten infizierte Zellen

eine nukleäre Depletion der globalen RNA-bindenden und Stressgranula assoziierten Proteine TIAR und TIA-1 sowie deren Akkumulation im Zytoplasma.

Insgesamt untersuchte diese Arbeit verschiedene Aspekte der Stressreaktion der Wirtszelle bei der Verteidigung gegen bakterielle Infektionen. Die Ergebnisse beleuchten die Bedeutung der Stresssignalwege im Wirt während der Infektion und verbessern das Verständnis der verschiedenen Strategien in der Interaktion von Wirt und Krankheitserreger.

ACKNOWLEDGEMENTS

I am grateful to my primary supervisor, Jörg Vogel, for giving me the opportunity to be part of his lab. I have learned and developed a lot scientifically, professionally, and personally. Being in the Vogel lab is an extraordinary experience in itself. Thank you for your support especially in the final period of my PhD.

I would like to thank my supervisor, Ana Eulalio, thank you for giving me this 'small' project initially. I think it turned out to be a very nice thesis and I enjoyed a great deal of my time in the Eulalio lab! Thank you for supporting me throughout the years we worked together, I really appreciate that.

I would like to thank my third committee member, Utz Fischer. Thank you for taking the time and always making the trips from Hubland.

I would like to thank all the past and present members in both the Vogel and Eulalio labs. I would like to thank Claire Maudet for her advice and help. I thank Stan Gorski for always being positive and supportive. All the lab technicians in both labs, whose work is so essential and helpful, thank you. Special thanks to my PhD sister Malvika Sharan, we have worked together and shared our frustrations, thank you for this priceless friendship.

I would like to thank Lars Dölken for the discussions on my project. He helped me coin the role of the sphingomyelinases in the inhibition of infection. I think this is how science should be about sharing knowledge and views, it is essential for progress.

I cannot thank Hilde Merkert enough! for everything you have done to help me professionally, the beautiful microscopy would not have been possible without you, and of course for being such a great friend.

A very special thank you to my great friends at the institute: Amelie, Carolin, Charlotte, Clivia, Jens, Gianluca, Emmanuel, Carmen, Ushasree, Sasha, Laura, Chuan, Gaurav, Nadja and everyone else. You guys are the best! Special thanks to Charlotte (les mots ne suffiront jamais pour t'exprimer mon appreciation et amour pour toi) and Carmen for reading my thesis draft. Kiki (well not only for that, you know how much I thank you) of course for the summa cum abstract in German!

Thank you infinitely Yanjie, mostly for being such a wonderful and loving person, but also for teaching me so much in the lab and sharing with me the passion for science.

I would not have been able to pull through without all the wonderful people at the institute who have always been there with their cheerfulness and great company. I am so happy I have shared so many memorable moments with all of you at IMIB and RVZ, I will run out of space if I name everyone who marked me.

I am grateful to the GSLS for supporting me and giving me the opportunity to become a fellow.

Finally, I would like to thank my precious friend Denise, I am incredibly fortunate to have you. Thank you to my eternal friend Clara. You both girls are family. I am always grateful to Colin and Ingrid Smith who have launched me so well on this journey. I am infinitely grateful to my lovely family for their support especially Hiaf.
Last but not least, my stars, my mom and my sister Sandra, I dedicate this work to you.

LIST OF ABBREVIATIONS

% (v/v)	% (volume/volume)
% (w/v)	% (weight/volume)
°C	degree Celsius
3D	3 dimension
A	adenosine
aa	amino acid
Amp	ampicillin
ASM	acid sphingomyelinase
ATP	adenosine triphosphate
bp	base pair
C	cytosine
cDNA	complementary DNA
CDS	coding sequence
CDS	cytosolic DNA sensor
CGD	chronic granulomatous disease
Ci	Curie
CLR	C-type lectin receptor
Cm	chloramphenicol
Cox-2	cyclooxygenase 2
Da	Dalton
DAMP	damage-associated molecular pattern
DMSO	dimethylsulfoxide
DNA	deoxyribonucleic acid
dNTP	deoxyribonucleotide
DTT	dithiothreitol
E. coli	*Escherichia coli*
EDTA	ethylene diamine tetraacetic acid
EGTA	ethylene glycol tetraacetic acid
EIF	eukaryotic initiation factor
EMSA	electrophoretic mobility shift assay
ER	endoplasmic reticulum
ERK	extracellular signal–regulated kinase
Fig	figure
G	guanosine
g	gravitational acceleration
G3BP-1	Ras GTPase-activating protein-binding protein 1
GCN2	general control nonderepressible 2
gDNA	genomic DNA
GFP	green fluorescent protein
GTP	guanosine triphosphate
H_2O_2	hydrogen peroxide
HCT-8	human epithelial colorectal adenocarcinoma cell line
HCV	hepatitis C virus
HeLa	human epithelial cervical adenocarcinoma cell line

HIF1-α	hypoxia-inducible factor 1-alpha
hpi	hours post infection
IAV	influenza A virus
iCLIP	individual-nucleotide resolution UV crosslinking and immunoprecipitation of protein-RNA complexes
IL	interleukin
JNK	c-Jun N-terminal kinase
Kan	kanamycin
LB	Lennox-broth
lncRNA	long non-coding RNA
LPS	lipopolysaccharide
M	molar
MAPK	Mitogen-activated protein kinase
M-cells	microfold cell
min	minute
miRNA	microRNA
MOI	multiplicity of infection
mRNA	messenger RNA
$NaAsO_2$	sodium arsenite
NaCl	sodium chloride
NADPH	nicotinamide adenine dinucleotide phosphate-oxidase
NFκB	Nuclear factor-κB
NLR	NOD-like receptor
NS1	non-structural protein 1
NSM	neutral sphingomyelinase
nt	nucleotide
OD600	optical density at 600 nm
ON	overnight
ORF	open reading frame
P:C:I	phenol:chloroform:isoamyl alcohol
p38	p38 mitogen-activated protein kinase
PAA	polyacrylamide
PAMP	pathogen-associated molecular pattern
p-bodies	processing bodies
PCR	polymerase chain reaction
PK	proteinase K
PKR	protein kinase R
PMN	polymorphonuclear leukocytes
PNK	polynucleotide kinase
PRD	prion-related domain
PRR	pattern recognition receptor
qRT-PCR	quantitative real-time PCR
RACK1	Receptor for activated C kinase 1
RBP	RNA-binding protein
RLR	RIG-I-like receptor
RNA	ribonucleic acid
RNAP	RNA polymerase

RNase	ribonuclease
RNP	ribonucleoprotein particle
ROS	reactive oxygen species
rpm	revolutions per minute
RRM	RNA recognition motif
rRNA	ribosomal RNA
SCV	*Salmonella*-containing vacuole
SDS	sodium dodecyl sulfate
SDS-PAGE	sodium dodecyl sulfate polyacrylamide gel electrophoresis
sec	second
SG	stress granule
siRNA	small interfering RNA
SMCV	encephalomyocarditis virus
SPI	*Salmonella* pathogenicity island
Supp Fig	supplementary figure
t	time
T3SS	type III secretion system
TEMED	N,N,N,N,-Tetramethylethylendiamin
TIA-1	T-cell intracellular antigen 1
TIAR	T-cell-restricted intracellular antigen 1-related protein
TLR	Toll-like receptor
TNF-α	tumor necrosis factor alpha
TTP	tristetraprolin
U	unit
U	uridine
UTR	untranslated region
UV	ultraviolet light
vol	volume
WB	Western blot
WT	wild-type

LIST OF FIGURES

Figure 1.1 Host innate defense mechanisms

Figure 1.2 *Shigella* and *Salmonella* invasion of the gut epithelium

Figure 1.3 Membrane lipid rafts and the sphingomyelinase pathways

Figure 1.4 Involvement of reactive oxygen species in stress and immune signaling

Figure 1.5 Stress granules at the crossroads of stress and innate immunity

Figure 2.1.1 *Shigella* infection of arsenite stressed epithelial cells is inhibited

Figure 2.1.2 *Shigella* infection of epithelial cells experiencing oxidative stress is inhibited

Figure 2.1.3 *Shigella* adhesion to stressed host cells is inhibited

Figure 2.1.4 Sphingolipid-rafts depletion by the stress-activated ASM and NSM inhibits *Shigella* infection

Figure 2.1.5 Stress-activated ASM localizes to the cell membrane and forms ceramide-rich platforms

Figure 2.1.6 The inhibition of *Shigella* infection in stressed cells is dependent on MAPK p38 activation

Figure 2.1.7 *Salmonella* motility compensates for the depletion of lipid-rafts in stressed cells

Figure 2.1.8 *Shigella* replication in cells inhibits re-infection by extracellular bacteria

Figure 2.1.9 *Salmonella* motility compensates for the inhibition caused by infected cells

Figure 2.1.10 *Shigella* replication in cells induces host-cell membrane remodeling

Figure 2.1.11 ASM knockdown reverts the inhibition of extracellular Shigella by infected cells

Figure 2.2.1 *Shigella* infected cells inhibit SG-aggregation in response to stress

Figure 2.2.2 *Shigella* intracellular replication inhibits generic SG-aggregation

Figure 2.2.3 Replication in the cytoplasm inhibits SG-formation independently of the bacterial pathogen

Figure 2.2.4 *Shigella* infection induces nuclear depletion and cytosolic accumulation of TIAR and TIA-1

Figure 2.2.5 TIAR and TIA-1 RNA targets are upregulated during *Shigella* infection

Figure 2.2.6 TIAR and TIA-1 interactome capture during *Shigella* infection using iCLIP

Figure 3.1.1 Model for the inhibition of bacterial infection by inflammatory stress cues

Figure 3.1.2 Model for the inhibition of re-infection by intracellular bacterial replication

Figure 3.2.1 Model for the inhibition of SG-aggregation and induction of TIAR/TIA-1 cytoplasmic accumulation by intracellular *Shigella*

Figure 4.1 *Shigella* infection of arsenite stressed epithelial cells is inhibited

Figure 4.2 *Shigella* infection of epithelial cells experiencing oxidative stress is inhibited

Figure 4.3 Sphingolipid-rafts depletion by the stress-activated ASM and NSM inhibits *Shigella* infection

Figure 4.4 *Salmonella* motility compensates for the depletion of lipid-rafts in stressed cells

Figure 4.5 *Shigella* replication in cells inhibits re-infection by extracellular bacteria

Figure 4.6 *Shigella* replication in cells induces host-cell membrane remodeling

LIST OF TABLES

Table 4.1 Single effector knockout mutants of *Shigella flexneri* M90T serotype 5a

Table 4.2.1 TIAR and TIA-1 RNA-targets upregulated during *Shigella* infection

Table 4.2.2 TIAR and TIA-1 RNA-targets downregulated during *Shigella* infection

Table 5.1 Instruments

Table 5.2 Consumables and commercial kits

Table 5.3 Chemicals

Table 5.4 Enzymes

Table 5.5 Antibiotics

Table 5.6 Drugs, inhibitors, and chemicals for cell culture

Table 5.7 Antibodies

Table 5.8 Secondary antibodies

Table 5.9 Cell dyes

Table 5.10 Bacterial strains

Table 5.11 List of plasmids

Table 5.12 Synthetic Oligonucleotides

Table 5.13 Primers for Sybr Realtime qRT-PCR

Table 5.14 siRNAs

INDEX

SUMMARY.....I

ZUSAMMENFASSUNG.....II

ACKNOWLEDGEMENTS.....IV

LIST OF ABREVIATIONS.....V

LIST OF FIGURES.....VIII

LIST OF TABLES.....X

1 INTRODUCTION.....1

1.1 Host-pathogen interaction during bacterial infection.....1

1.1.1 The host innate defense mechanisms.....1

1.1.2 Virulence strategies in model bacterial pathogens:

Shigella flexneri and *Salmonella enterica* serovar Typhimurium.....5

i) *Shigella flexneri*.....5

ii) *Salmonella* Typhimurium.....6

1.2 The role of membranes and lipid-rafts in the defense against pathogens.....9

1.3 The role of stress in host defense during infection.....12

1.3.1 Inflammation at the intersection of stress and immunity.....12

1.3.2 Oxidative stress as a danger signal.....14

1.4 Pathogen interference with host stress granules.....17

1.4.1 The role of stress-granules in infection.....17

1.4.2 The role of RNA-binding proteins in the post-transcriptional regulation

of the innate immune response.....21

1.5 Aims of the study.....22

2 RESULTS.....23

2.1 Cellular stress inhibits *Shigella* infection.....23

2.1.1 Cellular stress inhibits *Shigella* infection in epithelial cells……..23

2.1.2 *Shigella* infection of epithelial cells experiencing oxidative stress is inhibited……25

2.1.3 *Shigella* adhesion to stressed host cells is inhibited……28

2.1.4 Depletion of sphingolipid-rafts by sphingomyelinases in stressed cells inhibits *Shigella* adhesion……30

2.1.5 P38 MAPK is required for the inhibition of infection in stressed cells……37

2.1.6 *Salmonella* motility compensates for the depletion of sphingolipid-rafts in stressed cells……40

2.1.7 *Shigella* replication in cells inhibits re-infection by extracellular bacteria.....45

2.1.8 *Shigella* intracellular replication remodels the cell membrane through the activation of ASM and NSM……49

2.1.9 Concluding remarks……52

2.2 Intracellular bacterial replication inhibits SG-formation and affects TIAR/TIA-1 localization……54

2.2.1 *Shigella* replication inhibits generic SG-aggregation……54

2.2.2 Intracellular cytosolic replication inhibits SG-aggregation……58

2.2.3 *Shigella* replication in the host cytoplasm promotes nuclear/cytosolic re-localization of the RBPs TIAR and TIA-1……61

2.2.4 TIAR and TIA-1 RNA targets are upregulated during *Shigella* infection……65

2.2.5 Concluding remarks……67

3 DISCUSSION……68

3.1 Stress-pathways as defense strategies against bacterial infection……68

3.1.1 Host stress-response contributes to the reinforcement of the epithelial barrier to *Shigella* intrusion……68

3.1.2 Cellular stress leads to sphingolipid-raft depletion and impedes bacterial adhesion……70

3.1.3 A defense strategy involving membrane remodeling by stress-activated sphingomyelinases……72

3.1.4 To be motile or not to be……74

3.1.5 A defense strategy involving the propagation of the danger signal into adjacent cells……74

3.1.6 Conclusion and perspectives……75

3.2 Involvement of SGs and TIAR/TIA-1 in the infection by cytosolic bacteria……78

3.2.1 *Shigella* infection inhibits the aggregation of SGs in response to exogenous stress……78

3.2.2 Intracellular cytoplasmic replication of bacterial pathogens interferes with SG-assembly……79

3.2.3 *Shigella* infection favors the cytosolic function of TIAR and TIA-1……80

3.2.4 Conclusion and perspectives……82

4 APPENDIX……84

5 MATERIALS AND METHODS……107

5.1 General equipment……107

5.2 Consumables and commercial kits……108

5.3 Chemicals……109

5.4 Enzymes……110

5.5 Antibiotics……110

5.6 Drugs, inhibitors, and chemicals for cell culture……110

5.7 Antibodies……111
5.8 Bacterial strains……112
5.9 Plasmids……115
5.10 Synthetic oligonucleotides……115
5.11 Media……121
5.12 Buffers and solutions……121
5.13 Methods……126
5.13.1 Cell lines and cell culture……126
5.13.2 Treatment of cells……126
5.13.3 siRNA reverse transfections……126
5.13.4 Plasma membrane sphingomyelin activity assays……127
5.13.5 Nuclear and cytoplasmic cell fractionation……127
5.13.6 Infection assays……127
i) *Shigella*……127
ii) *Salmonella*……128
iii) *Listeria*……128
iv) Adhesion assays……128
v) Re-infection assays……128
5.13.7 Quantification of colony forming units (CFU)……128
5.13.8 Isolation of total RNA……128
5.13.9 Determination of concentration of nucleic acids……129
5.13.10 cDNA synthesis and Quantitative reverse transcription PCR qRT-PCR...129
i) DNase treatment……130
ii) reverse transcription……130
iii) Quantitative reverse transcription PCR (qRT-PCR)……130
5.13.11 Microscopy methods……130
i) Immunofluorescence staining and confocal imaging……130
ii) 3D conversion……130
5.13.12 Western blot analysis……130

5.13.13 Cloning……130

i) Preparation of plasmid DNA……130

ii) Polymerase chain reaction (PCR)……130

iii) Agarose gel electrophoresis of DNA……130

iv) Restriction digest and DNA ligation……130

5.13.14 Single-gene inactivation in bacteria……131

5.13.15 Growth curve……131

5.13.16 DNA transformation……131

i) Transformation of chemically competent *E. coli*……131

ii) Transformation of electrocompetent bacteria……131

5.13.17 Individual-nucleotide resolution UV crosslinking and

immunoprecipitation (iCLIP)……132

i) Seeding cells……132

ii) Infection assays……132

iii) UV Cross-linking……132

iv) Bead preparation……132

v) Partial RNA digestion and centrifugation……132

vi) Immunoprecipitation……133

vii) 3' end RNA dephosphorylation……133

viii) L3 Linker ligation……133

ix) 5' end labelling……133

x) SDS-PAGE and nitrocellulose transfer……134

xi) RNA isolation from the membrane……134

xii) Reverse transcription……134

xiii) Gel purification……135

xiv) Ligation of the primer to the 5'end of the cDNA……135

xv) PCR amplification……136

5.13.18 Sequencing……136

i) Sanger sequencing……136

ii) Whole-transcriptome sequencing……137

iii) MiSeq……137

5.13.19 Statistical analysis……137

6 REFERENCES……138

7 CURICULUM VITAE……155

8 LIST OF PUBLICATIONS……157

Erklärung/Affidavit……159

1 INTRODUCTION

1.1 Host-pathogen interaction during bacterial infection

The interactions between a pathogen and the human host emerge from a continuous co-evolutionary struggle for survival. Humans evolved sophisticated defense strategies against bacterial colonization, and bacteria, in turn, have developed the ability to avoid host resistance mechanisms. Upon encounter, both organisms are subjected to profound changes and stress. The immune response against bacteria shapes a harsh environment necessary for the eradication of the pathogen, but it is often harmful to the host itself. Therefore, it must be precisely balanced to avoid excessive damage, and still resolve the infection. The mechanisms governing this balance are complex and interdependent. They involve adjustments at several levels including innate and adaptive immunity, stress response, barrier integrity, and homeostasis.

In the host, bacteria experience drastic environmental changes to which they have to adapt rapidly. Bacterial colonization is achieved through the expression of virulence genes and the activation of specific metabolic and stress response programs. Different bacterial pathogens have acquired the capacity to colonize successfully a specific niche by exploiting flaws in the host defense. Thus, the interaction between the bacterial pathogen and the human host is a perpetual evolutionary arms race that brings forth different strategies for colonization or elimination, respectively. Understanding bacterial pathogenesis requires the exploration of the molecular basis of host defense and that of bacterial virulence.

1.1.1 The host innate defense mechanisms

The first line of defense against a pathogen threat is the innate immune response. In the last two decades, the discovery of innate immune pathways unveiled a diversity of mechanisms that lead to the rapid discrimination of a potentially dangerous non-self. The mechanisms of innate immune recognition are considered to be a primitive form of immunity because of their wide conservation in plants, invertebrates, and vertebrates (Buchmann, 2014). Though initially considered as a non-specific response because it does not involve memory, or gene rearrangement like the adaptive immune response, the innate immune response involves several pathogen recognition receptors (PRRs) that

recognize specific pathogen associated molecular patterns (PAMPs) (Janeway and Medzhitov, 2002). Such receptors can be found ubiquitously in all immune and non-immune cells, thus conferring an immediate protection at the cellular level (Janeway and Medzhitov, 2002). Recognition of pathogen derived molecules is mediated by surface or intracellular receptors, the main types being Toll-like receptors (TLRs), NOD-like receptors (NLRs), the RIG-I-like receptors (RLRs), cytosolic DNA sensors (CDS), and the C-type lectin receptors (CLRs) (Akira et al., 2006). Some PAMPs are specifically recognized by the host PRRs because of their absence in the host, for example the Gram-negative bacteria derived lipopolysaccharides (LPS) recognized by TLR4, double-stranded RNA recognized by RLRs in the cytoplasm, or bacterial conserved proteins such as flagellin recognized by TLR5 (Fig 1.1) (Beutler, 2000; Hayashi et al., 2001; Yoneyama et al., 2004).

Innate immune receptors have a particular distribution covering the extracellular environment of the cell, the cytosol, and intracellular organelles. For instance, TLR4 is localized to the cell surface of macrophages and neutrophils and can recognize extracellular LPS alerting the presence of bacteria in a sterile environment, whereas TLR7, 8 or 9 recognize foreign nucleic acids in endosomes (Beutler, 2000; Hemmi et al., 2000). Receptor ligation leads to the activation of a pro-inflammatory transcriptional response, involving pathways such as NFκB, MAPK kinases, interferon response, and the inflammasome (Fig 1.1) (Lee and Kim, 2007; Meylan et al., 2006). These activated pathways initiate the innate immune response leading often to inflammation and the activation of the adaptive immune response (Lee and Kim, 2007). Other mechanisms of defense are also brought into play, such as the activation of the complement cascade, autophagy, production of reactive oxygen species (ROS) and antimicrobial peptides, and apoptosis (Baxt et al., 2013). The activation of the different defense pathways is dependent on the nature of the PAMP but also the sub-cellular compartment occupied by the pathogen. Extracellular pathogens are targeted by the complement and antimicrobial peptides, while intracellular pathogens are eliminated by autophagy and host cell apoptosis (Baxt et al., 2013).

Sub-cellular compartments create concentration gradients and controlled environments, the disturbance of which can be more readily detected (Fig 1.1). Notably, the disruptions of the cellular normal functions and molecules have been recognized as danger signals in their own right and are called damage-associated molecular patterns

(DAMPs) (Casadevall and Pirofski, 2003; Gallucci and Matzinger, 2001; Stuart et al., 2013). For example, cellular starvation induced by intracellular *Shigella* or *Salmonella* leads to the activation of autophagy and innate immune genes (Tattoli et al., 2012). Nucleic acids released by a necrotic cell can activate the PRRs and serve as damage-associated signals (Imaeda et al., 2009). The redox state of the cell is also an important injury-related signal, when perturbed it can activate the innate immune response (Rubartelli and Lotze, 2007). DAMP recognition is an additional layer for patrolling the cell, specifically in non-immune cells such as epithelial cells, which do not express a wide array of PRRs and thus are limited in detecting PAMPs (Stuart et al., 2013). The host innate immune system has therefore evolved diverse strategies to recognize foreign molecules or the damage caused by them at the cellular level.

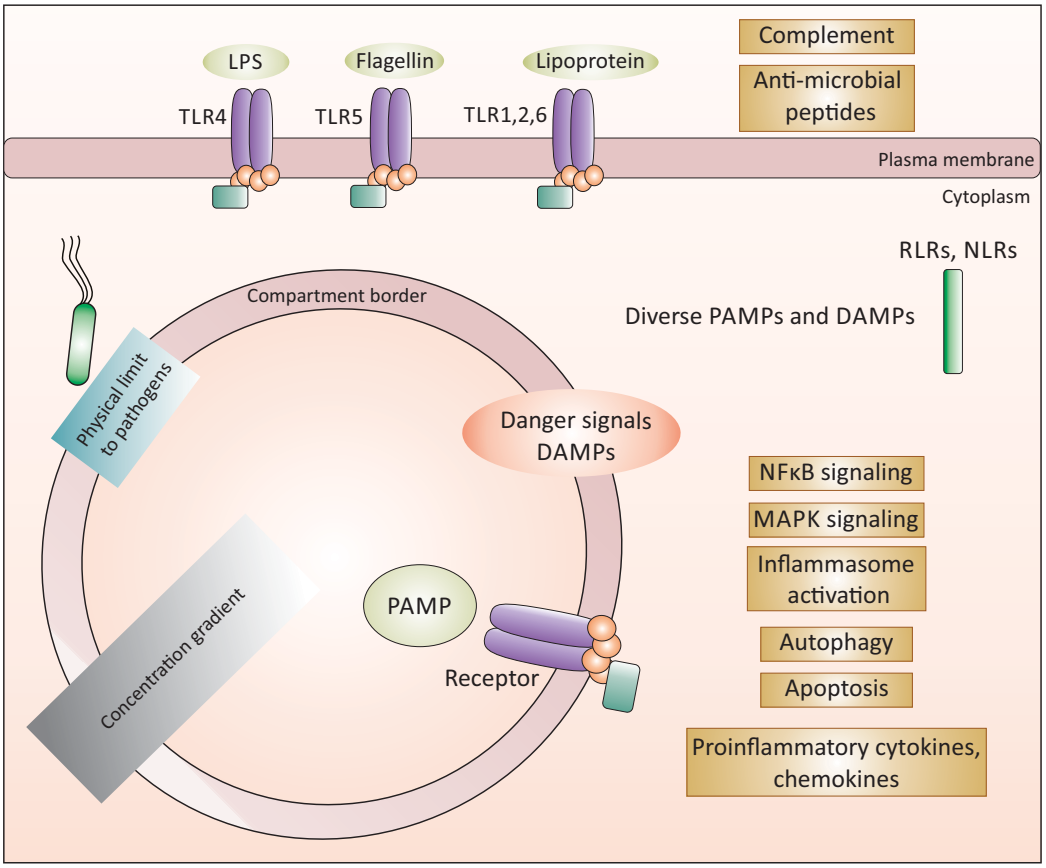

Figure 1.1 Host innate defense mechanisms

Pathogens and other cellular perturbations are recognized by pattern recognition receptors (PRRs) of the innate immune system. These receptors are expressed in different cellular compartments where they play a role in the surveillance of cellular integrity. TLR 1, 2, 4, 5, and 6 are expressed at the cell surface, and examples of their specific ligands are featured, e.g. LPS by TLR4, flagellin by TLR5 and lipoprotein by TLR1, 2, and 6. There are additional receptors in the cytoplasm such as RIG-I like receptors (RLRs) and NOD-like receptors (NLRs) that recognize cytoplasmic pathogen-associated molecular patterns (PAMPs) and damage-associated molecular patterns (DAMPs). Other receptors are found in subcellular compartments where they recognize PAMPs specific to this compartment. Sub-comparments pose a physical obstacle to pathogens, and maintain a specific concentration gradients, the perturbation of which can be more readily detected. Danger signals activate cellular immune defense, which leads to different responses (rectangles).

1.1.2 Virulence strategies in model bacterial pathogens: *Shigella flexneri* and *Salmonella enterica* serovar Typhimurium

In this dissertation, the bacterial pathogens *Shigella flexneri* and *Salmonella enterica* serovar Typhimurium have been used as model organisms for the investigation of host-pathogen interactions. The main focus of the study is on *Shigella*. *Salmonella* is used for comparison and for understanding the mechanistic differences between the strategies utilized by the two pathogens.

i) *Shigella flexneri*

Shigella genus comprises four species *S. flexneri*, *S. dysenteriae*, *S. sonnei*, and *S. boydii*. *Shigella* is a gram-negative bacterium belonging to the *Enterobacteriaceae* family. Each species contains several serotypes depending on the O-antigen variation of the LPS of different isolates; *S. flexneri* comprises 14 serotypes. *Shigella* carries one large virulence plasmid (~210-250 kb) and one chromosome, and it is phylogenetically related to *Escherichia coli* (Sims and Kim, 2011). All sequenced *Shigella* strains are non-motile due to various genetic mutations in the flagella operon; they also lack fimbriae in contrast to their *E. coli* counterparts (Yang et al., 2005). *Shigella* is the etiological agent of bacillary dysentery or shigellosis in humans, which is manifested by an exacerbated inflammation and colonic mucosal rupture. This results in diarrhea and in some cases severe dysentery and fever. The symptoms reflect the invasive nature of *Shigella* and its capacity to induce strong mucosal inflammation, an environment where *Shigella* has been shown to thrive (Marteyn et al., 2012). Shigellosis stools are marked by a high number of erythrocytes and polymorphonuclear leukocytes (PMNs), which is due to the inflammatory destruction and immune cell infiltration to the site of infection (Marteyn et al., 2012). *Shigella* is highly contagious; it is transmitted through the oral-fecal route and is a cause of fatality in infants and toddlers (DuPont et al., 1989; Kotloff et al., 1999).

The main virulence attribute of *Shigella* is the type 3 secretion system (T3SS) and its substrates, almost all of which are encoded on the virulence plasmid (Schroeder and Hilbi, 2008). The secreted virulence factors or effectors allow the bacterium to manipulate the host extensively and shape a favorable replicative niche (Killackey et al., 2016; Marteyn et al., 2012; Phalipon and Sansonetti, 2007; Schroeder and Hilbi, 2008). *Shigella* encodes ~30 T3SS substrates identified to date that have specific targets and functions within the host cell. The main steps of *Shigella* infection of cells are adhesion, invasion, intercellular spreading, and intracellular replication (Fig 1.2). These steps are dependent

on the T3SS effectors, which regulate additional processes like apoptosis, release of pro- and anti-inflammatory cytokines, and the regulation of the innate and adaptive immune response (Marteyn et al., 2012). *Shigella* resides in the cytoplasm of cells where it replicates, and displays actin-based intra- and inter-cellular motility (Ray et al., 2009). Observations suggest that *Shigella* does not invade the colon epithelial cells from the apical side *in vivo*, instead it might exploit microfold cells (M cells) to traverse the epithelium, which are specialized epithelial cells that constantly sample antigens in the lumen (Sansonetti et al., 1996; Wassef et al., 1989). *Shigella* breaches the epithelium and thereupon survives resident macrophages by inducing rapid apoptosis and release of IL-18 and IL-1β. This process is essential to mount an inflammatory response. Consequently, *Shigella* invades the epithelial cells from the baso-lateral side, where it replicates and induces the release of IL-8, which results in the recruitment of myeloid cells and the destruction of the epithelium (Fig 1.2) (Schroeder and Hilbi, 2008).

Although, *Shigella* has been widely used to study various processes, the lack of good and accessible animal models has presented an important drawback in fully understanding this bacterium pathogenesis. Adult mice are resistant to *Shigella* for unclear reasons (Marteyn et al., 2012). Other models have been in use like the rabbit ligated ileal loop, Guinea pigs, and some rare examples of mice with human colon xenographs (Marteyn et al., 2012). This notwithstanding, the accumulating knowledge on *Shigella* pathogenesis, the availability of genetic tools, and the numerous sequenced genomes make it an interesting model pathogen to promote the understanding of bacterial pathogenesis and host immunity.

ii) *Salmonella* Typhimurium

Salmonella is closely related to *Shigella* and *E. coli* forming a separate phylogenetic cluster. It is a human and animal food-borne pathogen disseminated through the fecal route. *Salmonella enterica* species comprise over 2500 serovars that differ in their flagella and LPS structure (Fierer and Guiney, 2001). Whereas the serovars Typhi and Paratyphi cause more severe diseases in humans, the most widely studied is *Salmonella enterica* serovar Typhimurium (Coburn et al., 2007). Unlike *Shigella*, *Salmonella* is motile and expresses unipolar flagella, which play an important role in infection and immune recognition (Fierer and Guiney, 2001). The initial stages of infection by *Salmonella* are reminiscent of that by *Shigella,* involving transcytosis through M cells (Fig 1.2). However, *Salmonella* is resident in macrophages, in addition to epithelial cells, which can cause

septicemia (Coburn et al., 2007). Further differences are observed at the cellular level, *Salmonella* resides in the endocytic vacuole called *Salmonella* containing vacuole (SCV) and reroutes the endo/lysosomal pathway to promote survival and replication (Fig 1.2) (Ibarra and Steele-Mortimer, 2009). Much of the symptoms caused by *Salmonella* depend on the host immune competence; it can cause an inflammatory intestinal disease, enteritis, and diarrhea, and in some cases typhoid fever and bacteremia (Coburn et al., 2007; Hansen-Wester and Hensel, 2001). Importantly, *Salmonella* can invade various types of cells, and colonize different organs like the spleen, gallbladder, and peritoneal cavity due to its access to the host circulation.

Salmonella Typhimurium acquired the virulence genes by horizontal transfer on genomic loci called pathogenicity islands. Two *Salmonella* pathogenicity islands (SPI) SPI-1 and SPI-2 encode for the main virulence factors and two T3SSs, T3SS-1 and T3SS-2 (Fabrega and Vila, 2013). Each T3SS is responsible for translocating a defined set of effector proteins, some of which are translocated through both systems (LaRock et al., 2015). The T3SS-1 is mainly responsible for the host cell invasion process, whereas the T3SS-2 is activated intracellularly and promotes intracellular replication and survival (LaRock et al., 2015).

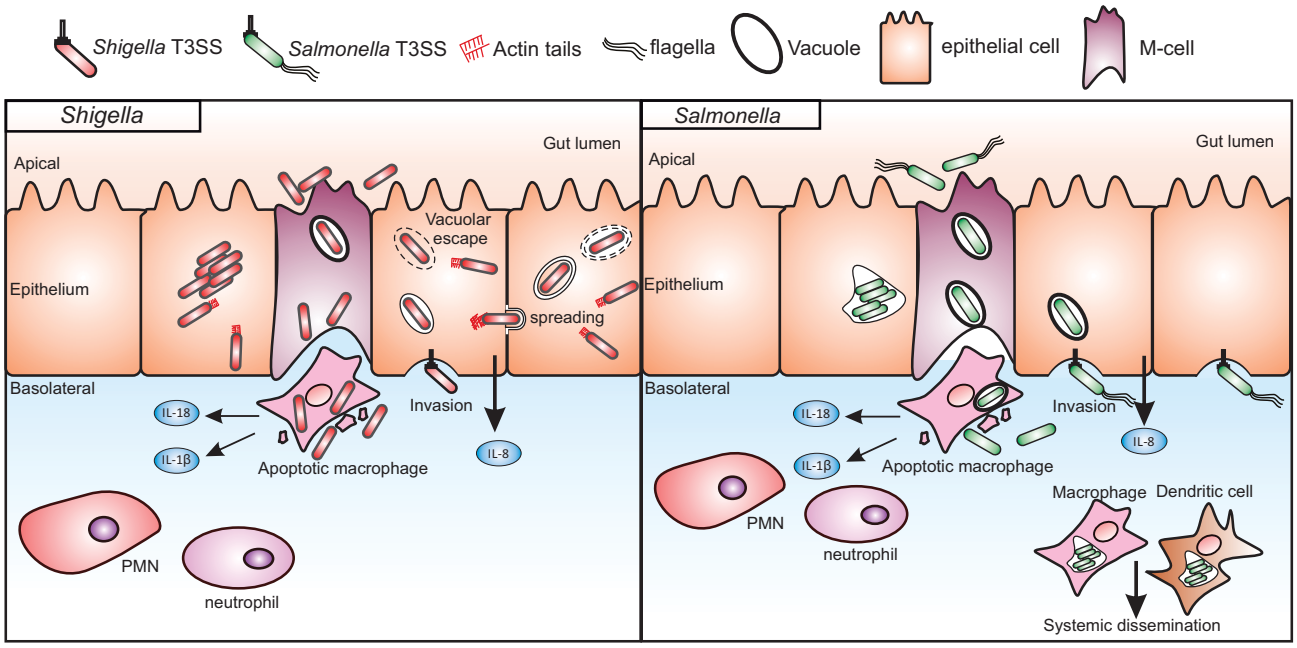

Figure 1.2 *Shigella* and *Salmonella* invasion of the gut epithelium

Shigella and *Salmonella* are food-borne pathogens that cause gastrointestinal diseases. Both pathogens breach the intestinal epithelium through specialized microfold cells (M cells) and infect resident macrophages. *Shigella* induces the rapid killing of the host macrophage and the release of IL-18 and IL-1β, which mount an inflammatory response. Subsequently, *Shigella* invades the intestinal epithelial cells through the baso-lateral side in a T3SS-dependent manner. In the cell, *Shigella* rapidly escapes the endocytic vacuole, replicates in the cytoplasm, and uses actin-based tail structures to spread to neighboring cells. Whereas *Salmonella* breaches the epithelium similarly to *Shigella*, it has a distinct intracellular lifestyle. It replicates in the endocytic vacuole that it modifies into a *Salmonella*-containing vacuole (SCV) in a T3SS-dependent manner. *Salmonella* is also resident in macrophages and other immune cells such as dendritic cells, which allow its dissemination systemically and into other organs.

1.2 The role of membranes and lipid-rafts in the defense against pathogens

Cellular membranes are an important barrier against pathogens and comprise the first physical obstacle to infection. The extracellular milieu poses a challenging environment for pathogens by exposure to immune cells, secreted anti-microbials, and competition with other commensal microbes. Thus, many pathogens have evolved to invade cells, in order to fend themselves from host defense. Invading pathogens have to establish a niche in the intracellular compartments and overcome the different innate immune recognition strategies. Invasion consists of breaching the cells physically and trespassing one or more membranes. Therefore, cell and organelle membranes are the first and most important barriers to various pathogens especially in epithelial cells, which are the first contact between the exterior and the sterile interior of the organism.

The plasma and organelle membranes are not composed of a uniform entity; rather they are formed of sub-structures made of lipids and proteins called lipid-rafts. Lipid rafts are membrane domains enriched in sphingolipids and cholesterol that mediate important pathways by sorting signaling proteins and receptors (Fig 1.3) (Lingwood and Simons, 2010; Triantafilou et al., 2002). Importantly, sphingolipid and cholesterol rafts are exploited by a large number of bacterial, viral, and protozoan pathogens to attach and enter host cells, and to manipulate cellular signaling (Manes et al., 2003; Riethmuller et al., 2006). It is proposed that pathogens require the specific topology of the membrane curvature formed by lipid-rafts, also known as caveolae, for entry (Duncan et al., 2002). Additionally, several immune and other receptors utilized by pathogens are raft-associated (Manes et al., 2003). For example, the raft-associated host receptor CD44 is essential for the adhesion and entry of *Shigella* by interacting with the bacterial protein IpaB (Lafont et al., 2002). *Salmonella* similarly requires sphingolipid-cholesterol rafts for host cell invasion (Garner et al., 2002).

The depletion of cholesterol or sphingolipids in the membrane leads to the disintegration of membrane rafts, which interferes with pathogen infection (Manes et al., 2003; Riethmuller et al., 2006). Interestingly, sphingomyelin turnover can occur in response to various stimuli through the activation of the neutral (NSM) and acid sphingomyelinases (ASM) leading to the production of ceramide, an important signaling molecule involved in many pathways such as apoptosis and innate immunity (Fig 1.3) (Stancevic and Kolesnick, 2010). For instance, NSM and ASM are activated by the tumor necrosis factor (TNF)-α, or by insults such as hydrogen peroxide, hypoxia, and infection

(Fig 1.3) (Grassme et al., 2003; Hannun and Luberto, 2000; Li et al., 2012). The NSM and ASM enzymes have been shown to be important for the infection by various pathogens. *Pseudomonas aeruginosa* infection activates ASM leading to the production of ceramide-rich platforms important for pathogen uptake and host defense (Grassme et al., 2003). Additionally, the accumulation of ceramide in the membrane mediated by the activation of NSM and ASM during infection is important for the uptake of *Neisseria gonorrhoeae* and *Neisseria meningitidis*, respectively (Faulstich et al., 2015; Simonis et al., 2014). These findings have been further supported by the use of Niemann-Pick disease models, a disease characterized by a mutation of the ASM gene *smpd1* in humans. Despite the growing importance of sphingolipid-rafts and their remodeling by the stress-responsive NSM and ASM, their role has not been characterized in the infection by important pathogens and in the corresponding host responses.

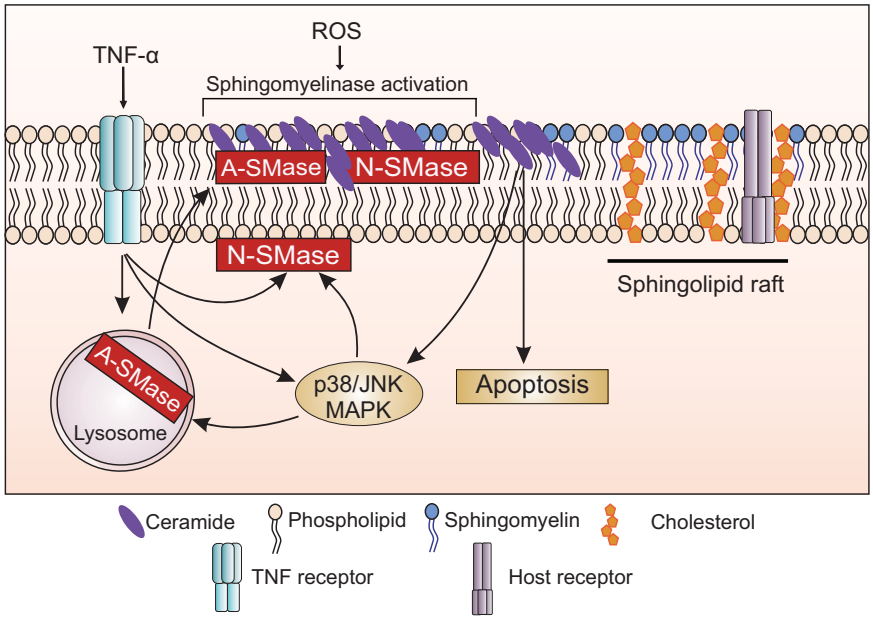

Figure 1.3 Membrane lipid rafts and the sphingomyelinase pathways

Lipid rafts are membrane domains enriched in sphingolipids and cholesterol that mediate important pathways by sorting signaling proteins and receptors. Sphingolipid-rafts can be remodeled by enzymes called sphingomyelinases, the neutral sphingomyelinase (NSM) is localized on the cytoplasmic side of the plasma membrane and the acid sphingomyelinase (ASM) is mainly localized in lysosome membranes. These enzymes can be activated by different stresses such as oxidative stress but also stimuli such as TNF-α. Upon activation, NSM is translocated to the outer leaflet of the membrane where the sphingomyelin is present, and ASM is similarly enriched in the sphingolipid rafts by the fusion of lysosomes with the plasma membrane. Both enzymes degrade the sphingomyelin and produce ceramide-rich platforms, which in turn modulate pathways such as MAPK and apoptosis signaling.

1.3 The role of stress in host defense during infection

The remodeling of membrane lipid-rafts is one example of stress induced changes in the cell. Infection by bacteria leads to an extensive perturbation of host functions. In addition to aggravations caused by the action of toxins and effectors, the thriving pathogen also rapidly depletes the available nutrients and produces harmful metabolites. Therefore, stress is a major component of any infection process but its role is only starting to become clear (Chovatiya and Medzhitov, 2014; Muralidharan and Mandrekar, 2013). Increasing evidence shows that the stress response overlaps with immune pathways suggesting that it might play an important role in the defense against bacterial colonization. In this respect, stress-response pathways could constitute an additional layer of the immune response, the elucidation of which would help establish new therapeutic approaches, and understand pathological manifestations. There are several focal points in the crosstalk between stress and immune pathways such as inflammation, oxidative stress, and stress granules (SGs). Inflammation is induced by the innate immune response, and it causes a severe environment that activates the stress-response pathways (Muralidharan and Mandrekar, 2013). Oxidative stress caused by an accumulation of ROS has been shown to activate several innate immune pathways (Bogdan et al., 2000; Tschopp and Schroder, 2010). Finally, SGs are at the interface of stress and immunity, as they constitute a major stress response and have been shown to play an important role during infection (Reineke and Lloyd, 2013).

1.3.1 Inflammation at the intersection of stress and immunity

Inflammation is one of the main consequences of the innate immune response. It plays a crucial role in the crosstalk with the adaptive immunity and the final eradication of the pathogen. Inflammation constitutes a harsh environment and recruits immune cells to the site of infection to compromise the residing pathogen. Neutrophils, mast cells, and dendritic cells are recruited to the site of perturbation, where the degranulation of mast cells leads to the activation of resident macrophages and dendritic cells play a central role in the activation of the antigen specific adaptive immunity (Karin et al., 2006). Resident macrophages expressing PRRs and other receptors mount a strong pro-inflammatory response mainly mediated by TNF-α (Sabio and Davis, 2014). Most studies have been

focused on the pro-inflammatory signaling mediated through the TNF-receptors and the IL-1R/TLR signaling (Karin et al., 2006; Sabio and Davis, 2014).

Due to the establishment of severe conditions, inflammation comes hand-in-hand with stress presenting a challenge for the host tissue, and in cases of 'sterile' or chronic inflammation it leads to important pathologies (Rock et al., 2010). Thus, it is tagged as a 'double-edged sword' because of the delicate balance that separates it from being beneficial or harmful to the host (Smith, 1994). Inflammation is not only caused by infectious agents, it can occur as a consequence of endogenous tissue damage or deviation from physiological homeostasis (Chovatiya and Medzhitov, 2014; Kono et al., 2014). Stressed cells produce various DAMPs that activate the innate immune response leading to inflammation (Chen and Nunez, 2010; Kono et al., 2014). For instance, the thioredoxin peroxidase PRDX2 is oxidized and glutathionylated in macrophages undergoing oxidative stress, forming a DAMP that leads to inflammation (Salzano et al., 2014). Thus, inflammation can be viewed as a defense mechanism or as an extension of a stress response.

There are a few examples of inflammatory stress stimuli playing an important role in host defense. Studies from inflammatory bowel disease (IBD) mouse models revealed the different stress stimuli accompanying mucosal inflammation (Colgan and Taylor, 2010). The infiltration of PMN cells and neutrophils into the intestinal mucosa results in a significant oxidative burst due to the secretion of reactive oxygen species (ROS), and a profound mucosal hypoxia is established (Colgan and Taylor, 2010). Though the gut environment is naturally found in a partial hypoxic state, the inflammatory hypoxia is much more pronounced and propagates deep into the mucosal tissue. Thus, hypoxia presents a major stress condition during gut inflammation, which activates the transcription factor hypoxia inducible factor 1 (HIF1α) that crosstalks with several innate immune pathways, such as the NFκB pathway (Colgan and Taylor, 2010; Nizet and Johnson, 2009; Taylor, 2008). Hypoxic stress influences the immediate cell environment, but also influences the surrounding tissue (Shweiki et al., 1992).

Another major stress-related defense strategy is the generation of ROS through the production of hydrogen peroxide. Gradients of H_2O_2 are established at the site of infection playing a role as chemoattractants for immune cells, and become bactericidal at high concentrations (Niethammer et al., 2009; Wittmann et al., 2012). Additionally, H_2O_2 has the capacity of propagating and activating non-affected tissue to prime host defense

(Niethammer et al., 2009). Additionally, cross-tissue propagation has been demonstrated in the case of stress-responsive MAPK signaling during *Shigella* infection, where the activation of p38, ERK, and JNK spreads to adjacent non-infected cells through GAP junctions (Kasper et al., 2010). These examples demonstrate the distinct crosstalk between stress and immune pathways, and show that stress signals contribute to the communication between cells to promote host defense.

1.3.2 Oxidative stress as a danger signal

Free radicals such as reactive oxygen species (ROS) and reactive nitrogen species (RNS) are important biological secondary metabolites. They are produced in response to internal and external stimuli in the cell in the form of hydrogen peroxide, superoxide, nitric oxide and others (Fig 1.4) (Nathan and Cunningham-Bussel, 2013). In mammalian cells, ROS is mainly produced by NADPH oxidases; other sources include the mitochondrial respiratory chain or enzymes like nitric oxide synthases (Fang, 2004; Nathan and Cunningham-Bussel, 2013). Free radicals are constantly produced and catabolized; once the production exceeds the catabolic rate, they accumulate and lead to stress (Fang, 2004).

The role of ROS in the host defense has been first described as a bactericidal oxidative burst by innate immune cells, including PMNs and neutrophils (Holmes et al., 1967). Subsequent studies demonstrated the central role of ROS in many immune-related processes such as TNF-α signaling, apoptosis, MAPK signaling, inflammasome activation, and autophagy (Fig 1.4) (Bae et al., 2011; Panday et al., 2015; Tripathi et al., 2013). The importance of ROS in innate immunity is best demonstrated by the manifestation of immune-deficiency in patients with a genetic disorder termed chronic granulomatous disease (CGD) (Bylund et al., 2005; Quinn et al., 2006). CGD is caused by mutations in NADPH enzymes such as NOX2 leading to a deficient oxidative burst and phagocytosis (Bylund et al., 2005; Quinn et al., 2006).

The study of the role and localization of ROS has been challenging because of the difficulty in distinguishing the different free radicals and the inaccuracy in their tracking. However, there are seminal studies demonstrating the role of ROS during infection. The measurements of bulk oxidative states in tissues do not always reflect the true contribution of free radicals to the outcome of infection. A study applying single-cell

methods for the detection of free radical production demonstrated a localized and cell specific respiratory burst that eliminated *Salmonella* in inflammatory lesions (Burton et al., 2014). This study showed that neutrophils and monocytes are able to kill efficiently *Salmonella* in a mouse typhoid model; the pathogen was only able to survive outside of infection foci by colonizing red pulp macrophages, which exhibit a low respiratory burst (Burton et al., 2014). Furthermore, ROS are important immune effectors not only in local immune signaling but also in inter-organ communication. A study conducted in *Drosophila* demonstrated a ROS dependent communication between the gut and the fat body, an important immune organ in flies (Wu et al., 2012). The induction of inflammation in the fly gut induces intestinal oxidative stress, which through ROS leads to the production of antimicrobial peptides in the distant fat body organ (Wu et al., 2012). Moreover, studies exploiting the transparent property of zebrafish and using H_2O_2 genetic sensors reported that extensive H_2O_2 gradients are established in response to wounding leading to the recruitment of leukocytes (Niethammer et al., 2009; Wittmann et al., 2012). Production of ROS in the form of H_2O_2 by non-immune cells during tissue wounding or infection is essential for the recruitment of immune cells; it is recognized as the epithelial hydrogen peroxide burst (Wittmann et al., 2012). Together, these examples illustrate the central role of ROS in mediating the crosstalk between innate immune and stress pathways in response to cellular perturbation.

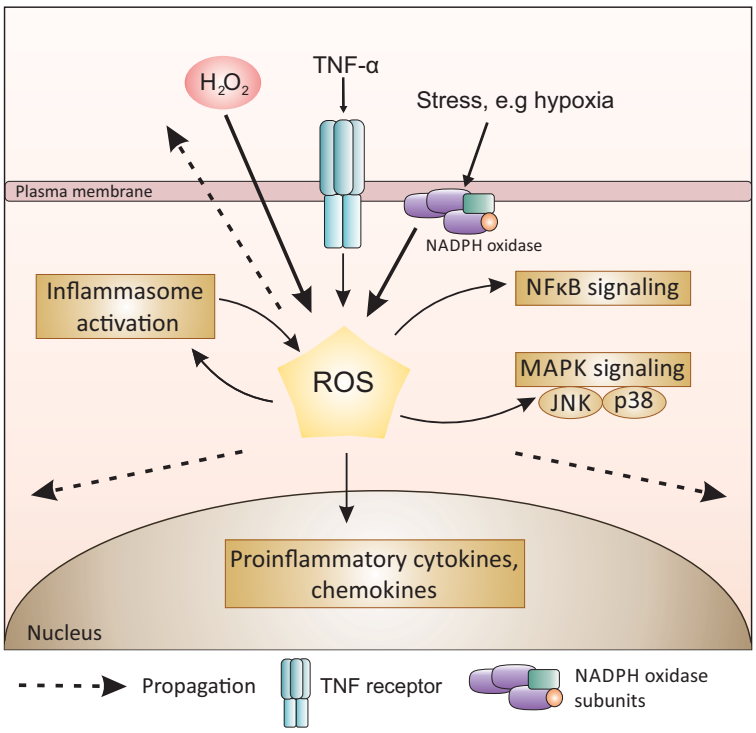

Figure 1.4 Involvement of reactive oxygen species in stress and immune signaling

Free radicals such as reactive oxygen species (ROS) are important biological secondary metabolites. They are produced in response to internal and external stimuli in the cell in different forms. Hydrogen peroxide is a main source of ROS during the immune response and stress. In mammalian cells, ROS are mainly produced by NADPH oxidases, and these enzymes are activated upon cytokine stimulation or in response to stresses such as hypoxia. ROS mediates important signaling pathways such as MAPK and NFκB signaling, and inflammasome activation. The propagative property of ROS in different forms, particularly as hydrogen peroxide, is an important defense strategy that activates immune and stress pathways in neighboring cells and tissues.

1.4 Pathogen interference with host stress granules

The aggregation of large RNA-protein complexes termed stress-granules (SGs) is a conserved response to stress in all eukaryotes. These distinct dynamic complexes form an agglomeration of important signaling molecules and cellular processes (Fig 1.5). It is now well recognized that SGs are involved in the defense against viral infections and recent studies have also demonstrated SG involvement in bacterial infections, suggesting that they are at the intersection of the stress-response and innate immunity. Another important aspect of SGs is that they are a species of a bigger family of RNA granules where RNA is subjected to extensive post-transcriptional regulation by RNA-binding proteins (RBPs). The role of RBPs in the post-transcriptional regulation of innate immunity is emerging due to several recent pioneering studies (Carpenter et al., 2014).

1.4.1 The role of stress-granules in infection

RNA granules are large ribonucleoprotein complexes conserved from unicellular eukaryotes to mammals. Stress Granules (SGs) are a class of RNA granules that are involved mainly in mRNA storage during stress conditions. They are generally composed of translation initiation factors (e.g. eIF4E, eIF4G, eIF3, and PABP-1), 40S ribosomal subunits, RNA-binding proteins (e.g. HuR, G3BP-1, TIAR, TIA-1), and RNAs (e.g. mRNAs, non-coding RNAs) (Fig 1.5) (Kedersha and Anderson, 2007). Stresses such as heat-shock, UV radiation, viral infection, and oxidative stress can lead to SG assembly, which are rapidly disassembled after the relief of stress allowing translation to resume (Buchan and Parker, 2009). SGs are very dynamic structures and are in constant exchange with the cytoplasm and other RNA-granules, namely processing bodies (P-bodies) that contain RNA nucleases and RNA silencing factors (Kedersha and Anderson, 2007). Post-stress, the mRNAs are channelled from SGs to ribosomes for translation or to P-bodies for degradation. Thus, SGs play a decisive role in the fate of mRNAs and gene expression (Anderson and Kedersha, 2008).

Though the components of translation pre-initiation are constant SG residents, other factors vary depending on the stress condition (Kedersha and Anderson, 2007). Some RNA-interacting proteins localize to SGs but do not seem to be essential for their integrity, whereas other proteins involved in splicing and mRNA transport like TIAR, TIA-1, and G3BP1 are essential for their formation (Gilks et al., 2004; Kedersha et al., 2000; Tourriere et al., 2003). Such proteins are used as markers to track the formation of SGs by

fluorescent labelling of the protein or immunofluorescence using specific antibodies against the proteins of interest (Leung et al., 2006). Fluorescence microscopy methods have allowed a detailed inspection of the dynamics and the composition of SGs under different stress responses (Kedersha et al., 2005). The assembly of SGs has been first described as a result of the phosphorylation of the eukaryotic factor EIF2α, which inhibits the EIF2/$tRNA_i^{Met}$/GTP translation initiation complex and stalls translation (Kimball et al., 2003). The phosphorylation of EIF2α is mediated by the stress-sensing kinases HRI, PKR, GCN2, and PERK that are specific to particular types of stresses (Kedersha et al., 2013). However, it has been shown that some stresses such as hydrogen peroxide induce SGs aggregation independent of EIF2α phosphorylation (Emara et al., 2012). Various other important signalling molecules have been described to localize to SGs forming important signalling hubs (Fig 1.5) (Kedersha et al., 2013). The main role attributed to SGs so far is an anti-apoptotic function. The apoptosis activator RACK1 is recruited to SGs inhibiting JNK and p38-induced apoptosis (Arimoto et al., 2008). Another study showed that the MAPK JNK pathway is activated through a non-canonical pathway upon SG-formation by the recruitment of the JNK-binding protein WDR62 to SGs (Wasserman et al., 2010). Though much remains to be understood on the role of SGs, they seem to play an important modulatory role due to the interception of many essential cellular factors within the granules.

The interest in SGs during infection has emerged upon the detection of cytoplasmic granular formations during viral infection or in other cases the inhibition of SG-aggregation. Particularly RNA viruses induce SGs through the direct recognition of the viral RNA by the dsRNA-dependent protein kinase (PKR) or through GCN2 activation, both inducing EIF2α phosphorylation (Weber et al., 2006). An inverse correlation between SG-formation, viral titer, and intensity of the antiviral IFN response has been reported by many studies, however the exact role of SGs in these processes is not well understood (Onomoto et al., 2014).

The localization of many central innate immune factors to SGs suggests that these aggregates might enhance the interaction between the molecular PAMPs and the innate immune receptors (Fig 1.5). RIG-I has been found to localize to SGs upon influenza A virus (IAV) infection, which enhances the interferon response in a PKR-dependent manner (Onomoto et al., 2012). Additionally, RNase L and OAS localize to viral-induced SGs, which in turn could cleave the viral RNAs and produce accessible ligands for PRRs (Langereis et al., 2013). On a different note, the discovery that the TNF-α receptor-associated factor 2

(TRAF2), which directs NFκB activation through TNF-α, accumulates in SGs and limits NFκB activation suggests that SGs could also have an antagonistic role (Kim et al., 2005). These findings propose an intricate balance achieved by the gathering of central signaling molecules within SGs.

The relevance of SGs in the host defense is not only based on their function as interaction platforms for innate immune effectors but also the reported interference of viruses with their formation (Reineke and Lloyd, 2013). Numerous studies have shed light on the mechanisms of interference with SGs during viral infection (Onomoto et al., 2014; Reineke and Lloyd, 2013). The non-structural protein 1 (NS1) from the influenza A virus (IAV) sterically inhibits PKR activation by viral RNAs, and the consequent phosphorylation of EIF2α (Khaperskyy et al., 2012). Poliovirus has been shown to cleave the SG-essential protein G3BP by the viral protease 3C and a similar mechanism was demonstrated for the Encephalomyocarditis Virus (SMCV) (Ng et al., 2013; White et al., 2007). Interestingly, viruses not always induce a permanent inhibition of SGs. For example, hepatitis C virus (HCV) infection induces oscillations in SG formation, which allows the persistence of the virus and survival of the cell (Ruggieri et al., 2012). These examples illustrate that viruses have evolved strategies to specifically interfere with SG aggregation suggesting an antiviral role for SGs that needs to be further demonstrated.

Recent studies have also shown an involvement of SGs in bacterial infections. The first study to show bacterial infection interfering with P-bodies, RNA granules related to SGs, demonstrated that cells infected with *Salmonella* and *Shigella* are unable to form P-bodies (Eulalio et al., 2011). A following study demonstrated that early infection by the same two pathogens induces amino acid starvation and GCN2 activation through the host membrane damage response, which leads to transient SG formation (Tattoli et al., 2012). A more recent study has shown that cells infected with *Shigella* are unable to form SGs in response to exogenous stress (Vonaesch et al., 2016). These pioneering studies suggest an extensive role for SGs in orchestrating the balance between the cellular stress response and the innate immune response during infection.

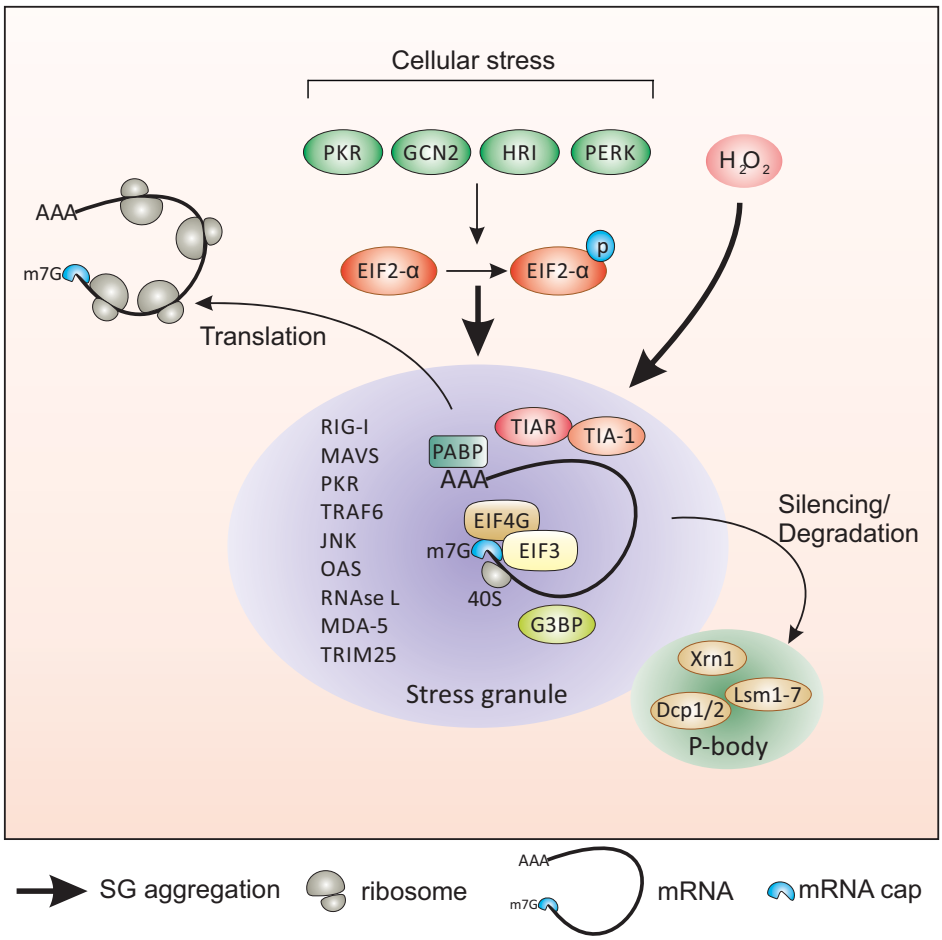

Figure 1.5 Stress granules at the crossroads of stress and innate immunity

Stress granule (SGs) are large non-membranous RNA-protein complexes that form in response to various stresses including infection. The main pathway of SG-aggregation is through the phosphorylation of EIF2α by one of the four stress sensor kinases PKR, GCN2, HRI, and PERK. However, some stresses like hydrogen peroxide can induce SG-formation independent of EIF2α phosphorylation. The main role of SGs is the storage and triage of stalled mRNAs during stress and the resilience to stress by suppressing apoptosis. Other RNA-granules such as P-bodies can dock to SGs to exchange protein factors and RNAs. Proteins like G3BP1, TIAR, and TIA-1 are essential for the formation of SGs, whereas other proteins are dispensable and they shuttle dynamically between the cytosol and the nucleated granule complex. Importantly, numerous immune and stress signaling proteins are found to associate with SGs suggesting a broader role for these structures.

1.4.2 The role of RNA-binding proteins in the post-transcriptional regulation of the innate immune response

Stress exposure is accompanied by a massive translational shutdown, but the translation of some transcripts remains efficient. Particularly, during infection many cytokines and innate immune genes are highly translated. This triage is mediated by post-transcriptional mechanisms that provide an additive layer of regulation to transcription. Interestingly, several of the SG-associated RBPs are involved in this post-transcriptional regulation. The mRNAs of several cytokines expressed in resting cells, are stored in RNA-granules and associated with RBPs. Upon stimulation of the cells, their translation is activated resulting in a rapid production of cytokines (Anderson, 2008; Kafasla et al., 2014). This particular property of the post-transcriptional regulation provides advantages including the speed of response, economy of resources and an additional surveillance layer in response to various conditions (Kafasla et al., 2014; Rodriguez-Gabriel and Russell, 2008).

RNAs are associated with proteins from transcription, through export, until decay; these proteins regulate the stability, translation, and decay of the transcripts. Cytokine mRNAs particularly contain adenine and uridine-rich stretches (AREs) in the 3' untranslated region (3'-UTR) that are bound and regulated by ARE-binding RBPs (Anderson, 2008). SG-associated RBPs, e.g. TIAR and TIA-1, bind such regions and have been shown to regulate mRNA translation and stability in coordination with additional RBPs such as TTP and HuR (Kafasla et al., 2014). The *tnfα* mRNA has been widely studied as a model to understand these processes *in vitro* and *in vivo*. TIA-1 has been shown to repress *tnfα* mRNA translation in resting mouse macrophages through binding the ARE-element (Piecyk et al., 2000). However, a complex combination between different RBPs on the mRNA substrate leads to the stabilization or decay of the transcript (Anderson, 2008). The transcripts of *tnfα* and *il-1β* are translationally silenced in mouse myeloid cells expressing HuR. This is dependent on the presence of TIA-1, arguing that both proteins act cooperatively to inhibit both transcripts (Katsanou et al., 2005). Conversely, HuR activates and TIA-1 inhibits the translation of the cytochrome c mRNA in HeLa cells (Kawai et al., 2006).

RBPs are themselves regulated by phosphorylation and other modifications like ubiquitination. Interestingly, the stress activated MAP kinases (SAPK) JNK and p38 are well established regulators of RBPs and post-transcriptional regulation processes. For

instance, the *il-2* mRNA has been shown to be stabilized by the JNK pathway (Katabami et al., 1998). Furthermore, the regulation of the translation and stability of the *tnfα* and *il-6* mRNAs is regulated by the p38 pathway in an ARE-dependent manner (Kotlyarov et al., 1999; Neininger et al., 2002). Several RBPs like HuR, TTP, AUF1, KSRP, TIAR and TIA-1 are involved in the stress-activated protein kinases (SAPK) regulation of mRNA stability (Rodriguez-Gabriel and Russell, 2008). RBPs are also involved in other processes of immune post-transcriptional regulation such as alternative splicing, regulation of translation initiation and elongation, and the regulation by non-coding RNAs such as microRNAs and long non-coding RNA (lncRNAs) (Carpenter et al., 2014). Altogether, these studies establish an important role for RBPs in the regulation of immune processes and stress.

1.5 Aims of the study

It is now established that the stress response pathways and the innate immune response are interdependent. However, the involvement of the stress response in the process of host defense is still not well understood. Understanding the contribution of the stress response and the nature of its relationship with the innate immune response whether it is cooperative, synergistic, antagonistic, or complementary remains to be deciphered. This study aims to answer a critical question: does the host stress response contribute to the defense against bacterial infection? To answer this question two aspects are investigated: i) the consequence of host cellular stress on the outcome of bacterial infection and ii) the interference of intracellular bacterial pathogens with stress-response pathways, such as stress-granules and RBPs. Identifying new mechanisms of host defense opens new perspectives for understanding pathogen success and disease propagation. Such findings would open new venues for the treatment of infections.

2 RESULTS

2.1 Cellular stress inhibits *Shigella* infection

2.1.1 Cellular stress inhibits *Shigella* infection in epithelial cells

The inflammatory conditions are a major cause of stress to the epithelial barrier and the gut environment. To investigate the effect of host-stress on the outcome of *Shigella* infection, cells were exposed to sub-lethal concentrations of sodium arsenite ($NaAsO_2$), a widely used method to induce stress in cells (Bernstam and Nriagu, 2000; Flora, 2011), and infected after the removal of the stress (Fig 2.1.1 A). Immunostaining of the SG-proteins TIAR or TIA-1 showed SG-aggregation confirming the response of the cells to the stress (Supp. Fig 4.1 A, B). The infection efficiency was monitored at early, intermediate, and late stages of infection (0.5, 3, and 6hpi, respectively) by microscopy using GFP expressing *Shigella*, and the infection was quantified by measuring the levels of *Shigella* GFP mRNA and by colony forming units assays. Interestingly, there was a strong decrease in infection in cells previously exposed to stress starting at an early time-point (0.5 hpi; >3-fold compared to control), and this decrease was maintained throughout the infection with a slight recovery at mid- and late time-points (3 and 6 hpi; >2-fold decrease) (Fig 2.1.1 B, C; Supp. Fig 4.1 C). The infection inhibition occured at early stages of infection and did not affect later stages, which is consistent with the fast reversibility of the stress induced by arsenite after its removal (Flora, 2011). *Shigella* infection was similarly inhibited in the colon cell line HCT-8 at early stages when the cells were pre-exposed to stress (Fig 2.1.1 D, E; Supp. Fig 4.1 D). This result shows that the inhibition of *Shigella* infection is a general response of epithelial cells to stress. Notably, *Shigella* growth was not affected when exposed to the same concentration of arsenite as the cells, excluding any bactericidal effects of arsenite (Supp. Fig 4.1 E). These results show that exposing epithelial cells to stress inhibits *Shigella* infection.

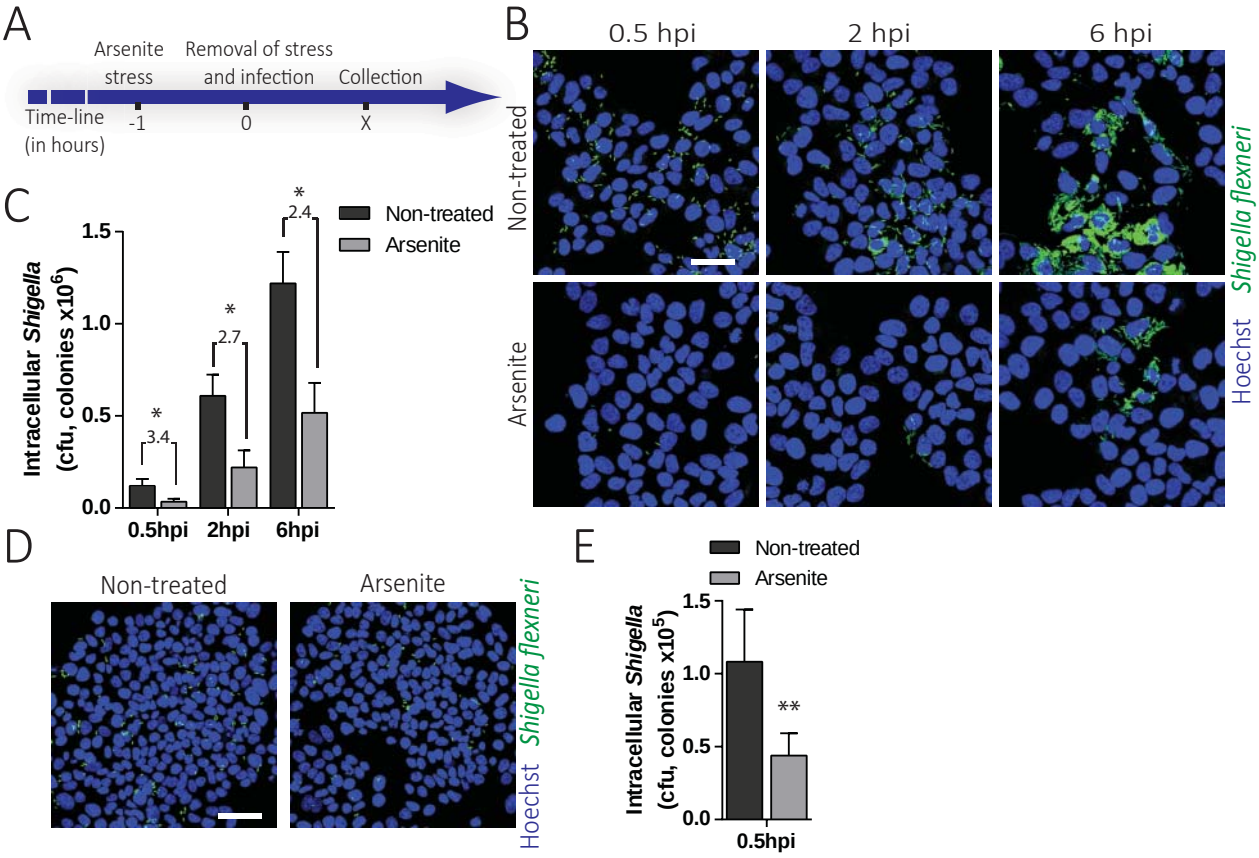

Figure 2.1.1 *Shigella* infection of arsenite stressed epithelial cells is inhibited

(A) Schematic representation of the experimental design. Cells are exposed to stress before infection, then the stress is removed and the cells are infected and analyzed at different time-points post-infection. (B) Representative images of the time-course of infection in non-stressed and arsenite stressed cells. HeLa cells were infected with *Shigella* WT expressing GFP and the nuclei were stained with Hoechst. (C) Quantification of the intracellular *Shigella* in cells infected same as in (B) using colony forming units (CFU) assays. (D) Representative images of infection at 0.5hpi in non-stressed and arsenite stressed HCT-8 cells. (E) CFU quantification of intracellular bacteria of infections performed same as in (D). Results are shown as mean ± s.e.m; n ≥ 3, *p<0.05, **p<0.01, two-tailed Student's t-test. Scale-bar 50µm.

2.1.2 *Shigella* infection of epithelial cells experiencing oxidative stress is inhibited

Arsenite induces the aggregation of SGs, the immediate result of which is translational and transcriptional shutdown (Anderson and Kedersha, 2008). To test whether this global shutdown leads to the inhibition of *Shigella* infection, cells were treated with the translational inhibitors puromycin and cycloheximide, or the transcriptional inhibitor actinomycin D. Treating cells with the individual inhibitors did not lead to a significant inhibition of *Shigella* infection, showing that there is no effect of translation or transcription on invasion (Supp. Fig 4.2 A, B, C). In addition to SG-aggregation, oxidative stress is the main response of cells exposed to arsenite (Bernstam and Nriagu, 2000). Thus, it could be a general response to oxidative stress leading to the inhibition of infection. To test this, oxidative stress was induced in the cells using different approaches. First, cells were treated with anisomycin, which is shown to induce oxidative stress leading the activation of MAPK kinases JNK and p38 (Torocsik and Szeberenyi, 2000). A short pre-treatment of cells with anisomycin inhibited early infection by *Shigella* (Fig 2.1.2 A, B; Supp Fig 4.2 D). Additionally, stimulation of cells with the inflammatory cytokine TNF-α leads to the production of ROS and induces oxidative stress (Ardestani et al., 2013; Kim et al., 2010). Consistently, short treatment of cells with TNF-α also lead to a decrease in *Shigella* infection (Fig 2.1.2 A, B; Supp Fig 4.2 D).

Exposure to stress and oxidative insults is common to the inflammatory environment, which is a hallmark of *Shigella* infection (Marteyn et al., 2012). The results suggest that an environment inducing oxidative stress in epithelial cells inhibits *Shigella* infection. Common cues encountered during inflammation in addition to cytokine stimulation are ROS production and hypoxia (Colgan and Taylor, 2010). The exposure of cells to hydrogen peroxide or hypoxia was tested for the inhibition of infection with *Shigella*. Consistently, H_2O_2 and hypoxia both strongly inhibited *Shigella* infection in Hela cells (Fig 2.1.2 C, E, F; Supp Fig 4.2 E, G). Exposure of HCT-8 cells to H_2O_2 also lead to a strong inhibition of *Shigella* infection (Fig 2.1.2 D; Supp Fig 4.2 F). Of note, HCT-8 cells did not tolerate exposure to hypoxia that led to their detachment, thus this condition was only tested in HeLa cells. The induction of the stress was monitored by staining for SG-proteins; both H_2O_2 and hypoxia exposed cells formed SGs as reported previously (Supp Fig 4.2 H, I) (Arimoto et al., 2008; Emara et al., 2012). These results show that common inflammatory stress cues, such as cytokines, H_2O_2, and hypoxia, inhibit the infection of epithelial cells by *Shigella*.

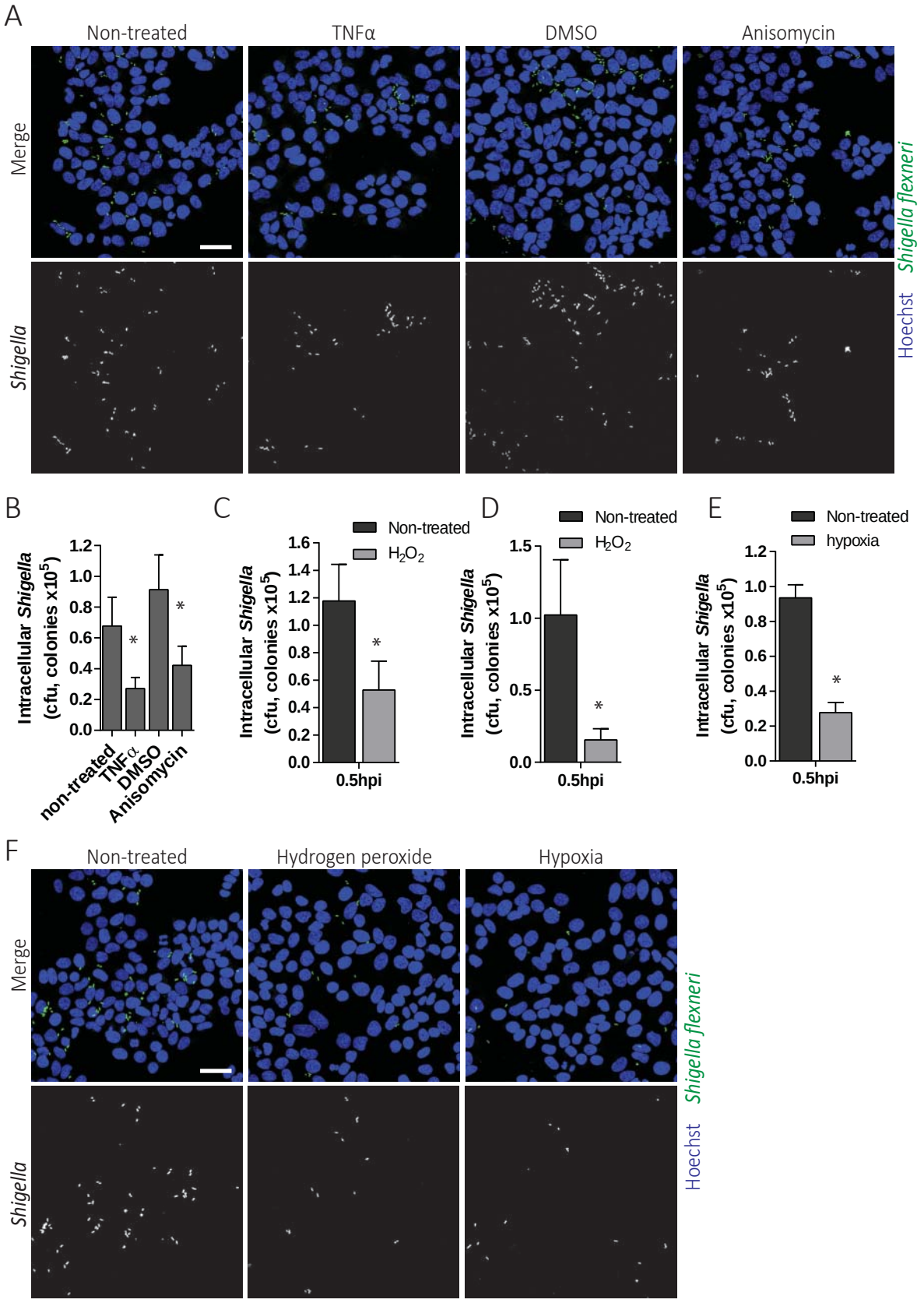
A
Non-treated
TNFα
DMSO
Anisomycin
Merge
Shigella
Shigella flexneri
Hoechst
B
Intracellular Shigella (cfu, colonies x10^5)
non-treated
TNFα
DMSO
Anisomycin
C
Non-treated
H2O2
0.5hpi
D
Non-treated
H2O2
0.5hpi
E
Non-treated
hypoxia
0.5hpi
F
Non-treated
Hydrogen peroxide
Hypoxia
Merge
Shigella
Shigella flexneri
Hoechst

Figure 2.1.2 *Shigella* infection of epithelial cells experiencing oxidative stress is inhibited

(A) Representative images of infections in control HeLa cells or treated with TNF-α for 15 min or with anisomycin for 20min. Cells were fixed and stained with Hoechst at 0.5hpi (B) CFU quantification of *Shigella* infection at 0.5hpi in HeLa treated with TNF-α (compared to mock-treated), or anisomycin (compared to DMSO). (C, D) CFU analysis of *Shigella* infection at 0.5hpi in HeLa (C) or HCT-8 (D) treated with H_2O_2 for 3h. (E) Same as in (C) except HeLa were exposed to hypoxia for 15h. (F) Representative images of the infections in HeLa cells same as in (C) and (E). Results are shown as mean ± s.e.m; $n \geq 3$, $^*p<0.05$, two-tailed Student's t-test. Scale-bar 50μm.

2.1.3 *Shigella* adhesion to stressed host cells is inhibited

Shigella infection of epithelial cells consists of several stages starting from adhesion to the cell surface, T3SS-dependent induction of actin ruffles for invasion, disruption of the endocytic vacuole, rapid replication in the cytoplasm, and intercellular spreading using actin tail structures (Fig 1.2) (Marteyn et al., 2012). Infection of stressed cells can be inhibited at any of these stages leading to a decrease in bacterial counts. The analysis of the time-course of infection in cells exposed to arsenite-stress showed a major decrease in bacterial counts as early as 0.5 hpi (Fig 2.1.1 C). No further decrease of infection at later time-points was observed, but rather a slight recovery probably due to replication and spreading (Fig 2.1.1 C). This result shows that the infection is mainly inhibited at early stages and there is no inhibitory effect on later stages. Therefore, the inhibition can occur at the stages of adhesion, invasion, or both. Adhesion assays with wild-type *Shigella* showed a strong decrease in bound bacteria to stressed cells compared to control cells (6.7-fold for *Shigella* WT; Fig 2.1.3 A, B; Supp Fig 4.2 J). This result shows that *Shigella* adhesion to stressed cells is strongly inhibited, but does not exclude an effect on bacterial entry. To test whether entry is affected, a T3SS-deficient *Shigella* mutant *ΔipaB,* which is incapable of inducing ruffles and uptake but able to adhere efficiently, was used (Menard et al., 1996). Adhesion assays with *Shigella ΔipaB* showed a similar decrease in bound bacteria to WT albeit to a lesser extent (3.7-fold), which could be due to the hyperadhesive phenotype of the *ΔipaB* mutation, or to minor effects on the uptake of WT *Shigella* (Figure 2.1.3 A, B; Supp Fig 4.2 J) (Brotcke Zumsteg et al., 2014; High et al., 1992). Additionally, staining of the cytoskeleton using a fluorophore conjugated Phalloidin showed that actin ruffles induced by *Shigella* WT were intact in both stressed and non-stressed cells, which excludes an effect of stress on ruffle formation that is necessary for uptake (Fig 2.1.3 A, white arrowheads). Together, these results show that *Shigella* infection of stressed host cells is mainly inhibited at the adhesion step.

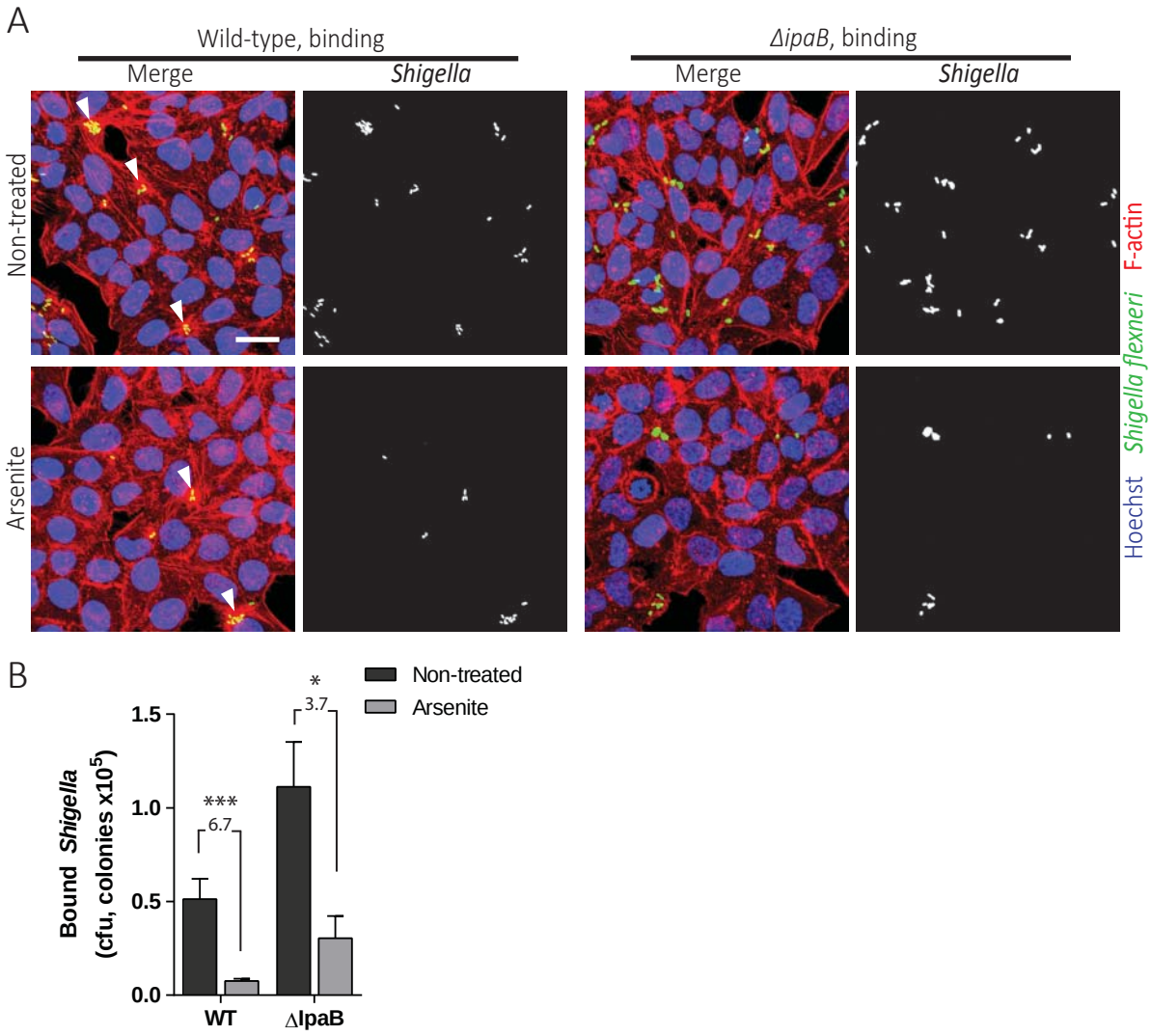

Figure 2.1.3 *Shigella* adhesion to stressed host cells is inhibited

(A) Representative images of adhesion assays in non-stressed and arsenite stressed HeLa cells with *Shigella* WT and the *ΔipaB* mutant. *Shigella* was stained with a specific antibody (green), and the F-actin network of the cells was stained using Phalloidin (red). The *Shigella*-induced actin ruffles can be observed during *Shigella* WT adhesion (white arrowheads) but are absent with *Shigella ΔipaB*. (B) CFU analysis of the adhesion assays in (A), numbers represent the fold-change compared to control. Results are shown as mean ± s.e.m; n ≥ 3. *p<0.05, ***p<0.001 two-tailed Student's t-test. Scale-bar 25µm.

2.1.4 Depletion of sphingolipid-rafts by sphingomyelinases in stressed cells inhibits *Shigella* adhesion

Given that *Shigella* adhesion to the cell surface is inhibited during host stress and that the response is very rapid (e.g. 15 minutes of TNFα stimulation), the postulated hypothesis was that the membrane undergoes rapid modifications under stress conditions. Membrane composition is crucial for the adhesion and entry of *Shigella* into host cells, specifically sphingolipid-rafts have been shown to be essential for successful *Shigella* infection (Lafont et al., 2002). Sphingomyelinases are enzymes involved in sphingomyelin turnover and membrane microdomain remodeling (Marchesini and Hannun, 2004). To investigate whether the activation of sphingomyelinases is inhibiting the adhesion of *Shigella* to host cells, their activity was blocked using specific inhibitors. Two types of sphingomyelinases are responsive to stress and are important for membrane sphingomyelin turnover: NSM present in the plasma membrane; and ASM, which is normally associated with lysosomal membranes but is delivered to the plasma membrane upon activation (Marchesini and Hannun, 2004). First, ASM was blocked using a specific inhibitor amitryptilin in combination with arsenite or anisomycin. Amitryptilin treatment partially reverted the inhibitory effect of arsenite (~3-fold) and fully reverted inhibition by anisomycin (Fig 2.1.4 A, C, E; Supp Fig 4.3 C, D, E). Treating cells with GW4869, the specific inhibitor of NSM, did not have an effect on the infection inhibition by arsenite or anisomycin (Fig 2.1.4 B, D, E; Supp Fig 4.3 C, D, E). However, when cells were treated with both amitryptilin and GW4869, a significant additive effect reverting the inhibition with arsenite was observed (~4-fold) but not with anisomycin, where a full recovery was already achieved with amitryptilin alone (Fig 2.1.4 B, D, E; Supp Fig 4.3 C, D, E). Treatment of cells with amitryptilin or GW4869 alone in the absence of stress, did not influence *Shigella* infection significantly; combining both inhibitors led to an increase in infection, but this increase does not account for the ~3-fold recovery observed with arsenite (Supp. Fig 4.3 A, B). These results demonstrate that ASM and to a lesser extent NSM are involved in the inhibition of *Shigella* infection in stressed cells.

There are four genes expressing sphingomyelinases in humans, *smpd1*, *smpd2*, *smpd3*, and *smpd4* encoding for ASM, NSM-1, NSM-2, and a putative sphingomyelinase, respectively. ASM and NSM-1 are expressed in HeLa and HCT-8 cells, whereas NSM-2 is not expressed in these cell lines and accordingly the *smpd3* mRNA could be detected by qRT-PCR (data not shown). To confirm the involvement of ASM and NSM-1 specifically in

the inhibition of *Shigella* infection, cells were transfected with specific siRNAs for *smpd1* or *smpd2* or both, then treated with arsenite and infected. The knockdown of both genes had no significant effect on *Shigella* infection in the absence of stress (Supp. Fig 4.3 F, G). The knockdown of ASM alone reverted the inhibition of *Shigella* infection by arsenite significantly (3-fold), similar to the result obtained with amytriptilin (Fig 2.1.4 F, G, H). The knockown of NSM-1 did not have any significant effect on the inhibition of infection by arsenite similarly to the result obtained with GW4869 (Fig 2.1.4 F, G, H). However, combining both siRNAs reverted the inhibition to the same extent as with the knockdown of ASM alone, and did not show an additive effect similar to the one obtained with amitryptilin and GW4869 together (Fig 2.1.4 F, G, H). The knockdown of the individual genes was achieved with 50nM of siRNA, but with the combination of both siRNAs only 25nM of each was used leading to a variable knockdown efficiency, which could explain the lack of an additive effect when using both siRNAs (Supp Fig 4.3 H, I). These results show that ASM is directly responsible for the inhibition of infection in stressed cells.

Upon activation, ASM and NSM translocate to the outer leaflet of the plasma membrane and accumulate in membrane sphingolipid microdomains giving rise to ceramide-rich platforms upon breaking-down of the sphingomyelin (Simonis et al., 2014; Yabu et al., 2008). To monitor the activation of ASM and NSM, the enzyme activity in the membrane fraction was measured. A modest but significant increase in ASM activity was observed in the membrane fractions of cells treated with arsenite (Fig 2.1.4 I). For anisomycin and TNFα treatments, a slight increase of ASM activity was detected, albeit not significant, probably due to limitations in the sensitivity of the enzymatic assays (Fig 2.1.4 I). Similarly, the increase in the activity of NSM detected for the various stresses was statistically not significant (Fig 2.1.4 J). Additionally, to validate the activation of the sphingomyelinases, the accumulation of ASM and ceramide in membrane foci was visualized by confocal microscopy, as observed previously (Simonis et al., 2014). The lack of a specific NSM-1 antibody did not allow the analysis of the accumulation of this enzyme in the membrane by microscopy. A strong accumulation of ceramide was observed when cells were treated with arsenite, TNFα, and anisomycin compared to the control in both HeLa and HCT-8 cells (Fig 2.1.5 A; data not shown for HCT-8). Similarly, ASM staining with a specific antibody showed that it formed platform-like foci in cells treated with all three stressors compared to control, where the signal was more diffuse (Fig 2.1.5 B). The ASM staining specificity was confirmed using the ASM siRNA: upon ASM knockdown a

considerable decrease of ASM foci was observed in arsenite treated cells, and a decrease of the ASM protein levels was observed by Western blot (Supp Fig 4.3 K, L). Ceramide levels in response to arsenite also decreased upon ASM or ASM/NSM-1 knockdown (Supp. Fig 4.3 J). The 3D reconstruction of cells stained for ceramide or ASM and a whole-cell dye showed the clear increase of the enzyme or the product in the membrane domains in response to arsenite (Fig 2.1.5 C, D). Taken together, these results show that the adhesion of *Shigella* during cellular stress is limited by the depletion of sphingolipid-rafts. This depletion is caused by the activation and translocation of the ASM to the membrane, with a minor contribution from NSM, leading to the formation of ceramide-rich platforms.

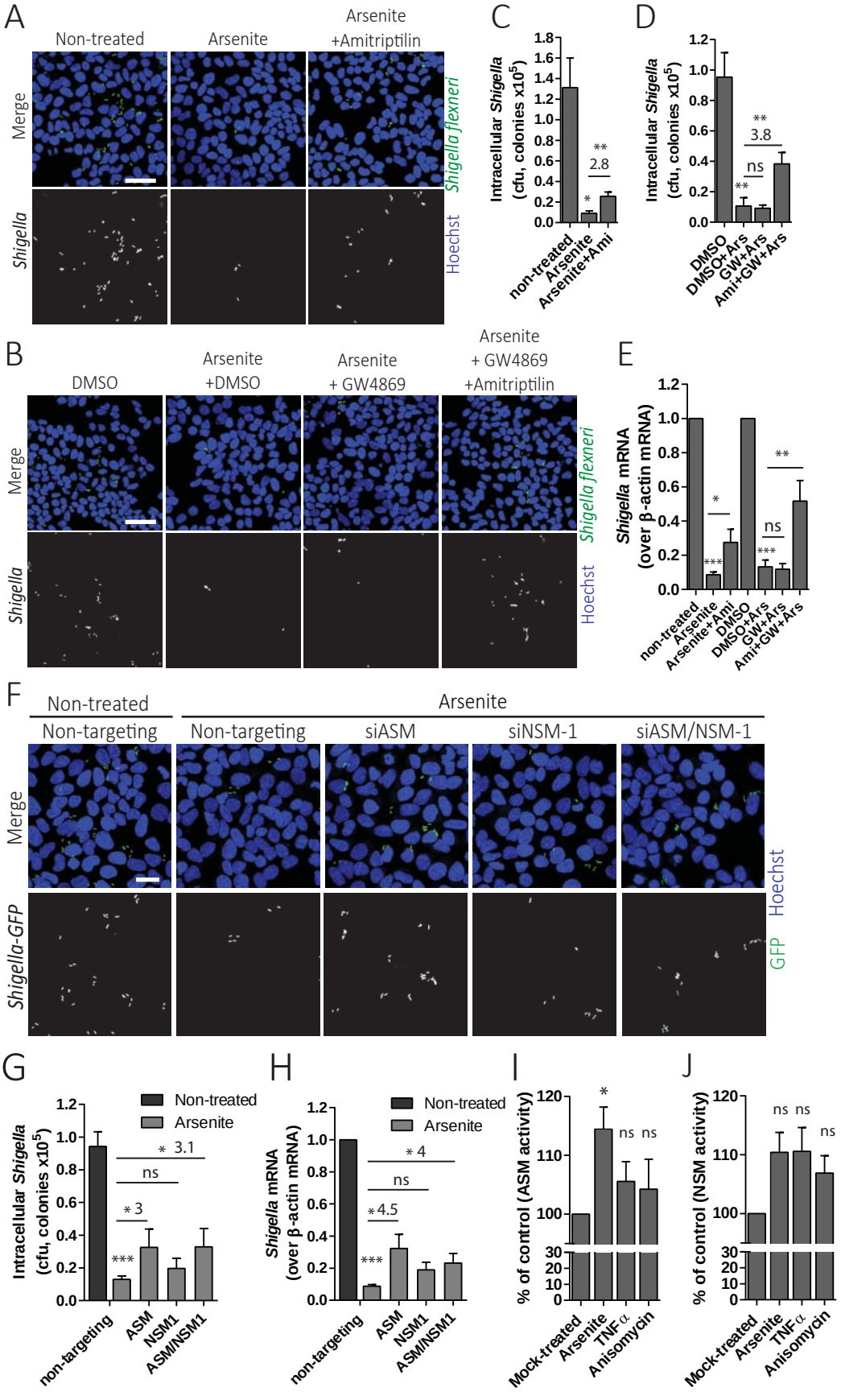
A
Non-treated
Arsenite
Arsenite +Amitriptilin
Merge
Shigella
Shigella flexneri
Hoechst
C
Intracellular Shigella (cfu, colonies x10^5)
non-treated
Arsenite
Arsenite+Ami
2.8
D
Intracellular Shigella (cfu, colonies x10^5)
DMSO
DMSO+Ars
GW+Ars
Ami+GW+Ars
3.8
ns
B
DMSO
Arsenite +DMSO
Arsenite + GW4869
Arsenite + GW4869 +Amitriptilin
E
Shigella mRNA (over β-actin mRNA)
F
Non-treated
Arsenite
Non-targeting
Non-targeting
siASM
siNSM-1
siASM/NSM-1
Shigella-GFP
GFP
G
Non-treated
Arsenite
3.1
3
ASM
NSM1
ASM/NSM1
H
4
4.5
I
% of control (ASM activity)
Mock-treated
TNFα
Anisomycin
J
% of control (NSM activity)

Figure 2.1.4 Sphingolipid-rafts depletion by the stress-activated ASM and NSM inhibits *Shigella* infection

(A) Representative images of *Shigella*-GFP infection at 0.5hpi in control cells, cells treated with arsenite, or treated with arsenite in combination with amitryptilin. (B) Representative images of infections at 0.5hpi in cells treated with the vehicle DMSO, or arsenite combined with DMSO, GW4869, or amitryptilin and GW4869. (C, D) CFU analysis of infections in (A) and (B), respectively. Numbers represent fold-change compared to control. (E) Quantification of *Shigella* infections same as in (C) and (D) by qRT-PCR. (F) Representative images of infections at 0.5hpi in cells transfected with different siRNAs and treated with arsenite. (G) CFU quantification and (H) qRT-PCR quantification of infections same as in (F). Numbers represent fold-change compared to control. (I, J) the activity of ASM (I) and NSM (J) was measured in the membrane fractions of control or treated cells. Percent activation is shown compared to the mock-treated control (100% activity). Results are shown as mean ± s.e.m. n ≥ 3, *p<0.05, **p<0.01, ***p<0.001 ns: non-significant; two-way ANOVA. Scale-bar 25μm.

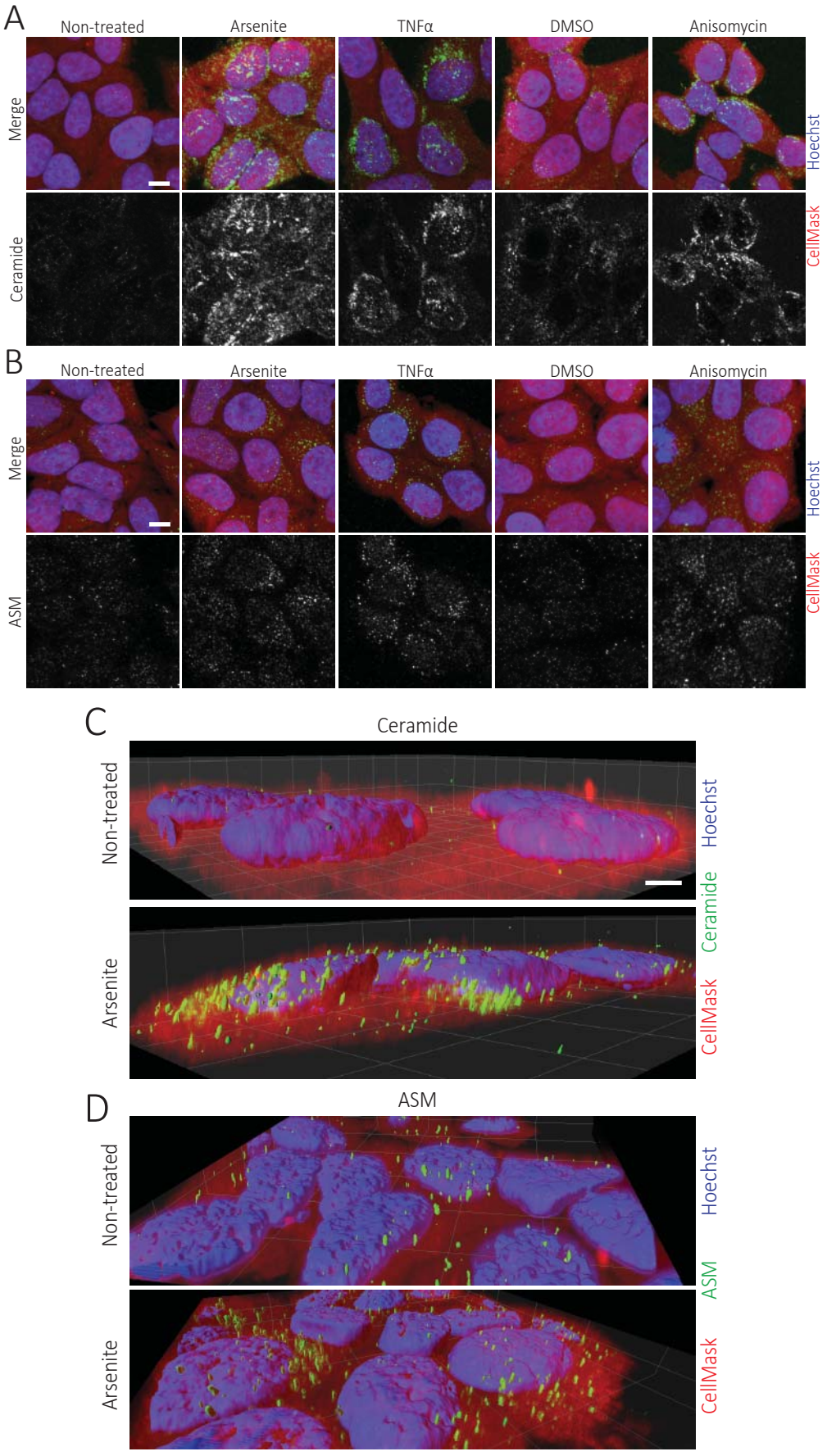
A
Non-treated
Arsenite
TNFα
DMSO
Anisomycin
Merge
Ceramide
Hoechst
CellMask
B
Non-treated
Arsenite
TNFα
DMSO
Anisomycin
Merge
ASM
Hoechst
CellMask
C
Ceramide
Non-treated
Arsenite
Hoechst
Ceramide
CellMask
D
ASM
Non-treated
Arsenite
Hoechst
ASM
CellMask

Figure 2.1.5 Stress-activated ASM localizes to the cell membrane and forms ceramide-rich platforms

(A) Representative images of ceramide staining (green) in differently treated HeLa cells (cell body staining with CellMask (red)), Scale-bar 10μm. (B) Representative images of ASM (green) accumulation in the membrane upon stress in HeLa cells; cells were stained with CellMask (red), Scale-bar 10μm. (C) 3D reconstruction of images same as in (A). Ceramide (green) and nuclei (blue) were surface converted by voxel distance. Scale-bar 5μm. (D) 3D reconstruction of images same as in (B). ASM (green) and nuclei (blue) were surface converted by voxel distance. Scale-bar 5μm.

2.1.5 P38 MAPK is required for the inhibition of infection in stressed cells

The results show that sphingomyelinase activation during cellular stress leads to a decrease in *Shigella* infection. Previous studies have shown a strong correlation between the activation of sphingomyelinases and that of p38 MAPK during stress (Bianco et al., 2009). Oxidative stress leads to the activation of sphingomyelinases and the production of ceramide, which in turn leads to the phosphorylation of p38 and JNK MAPKs (Chen et al., 2008). A positive feedback loop has been suggested between p38 and NSM/ASM (Clarke et al., 2007). Thus, p38 could be an important player in the activation of the sphingomyelinases during cellular stress, and in the inhibition of *Shigella* infection. A specific p38 inhibitor SB203580 was used in combination with arsenite or anisomycin to inhibit p38 activation in response to stress. Inhibiting p38 reverted the decrease in infection partially for arsenite, and fully for anisomycin (Fig 2.1.6 A, B, C, D). Using the p38 inhibitor alone in the absence of stress did not affect *Shigella* infection (Fig 2.1.6 E). Furthermore, the activation of p38 in HeLa cells by arsenite, anisomycin, and TNF-α, was observed by detecting the phosphorylated p38 on Western blot (Fig 2.1.6 F, G). The SB203580 inhibitor efficiently inhibited the phosphorylation of p38 in response to stress (Fig 2.1.6 H). These results demonstrate that the inhibition of *Shigella* infection during stress is dependent on the activation of p38 MAPK.

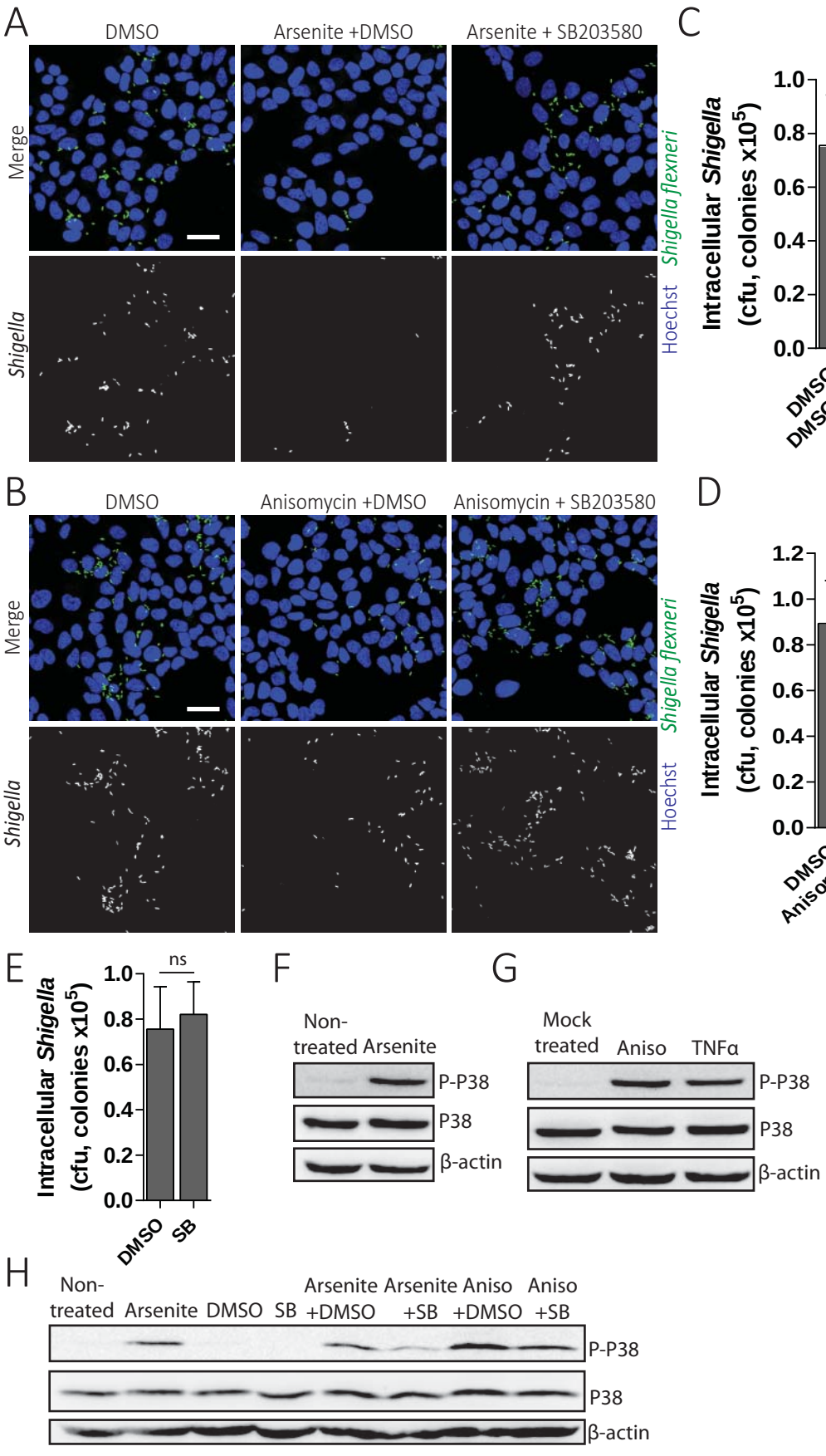
A
DMSO
Arsenite +DMSO
Arsenite + SB203580
Merge
Shigella
Hoechst
Shigella flexneri
C
Intracellular Shigella (cfu, colonies x10^5)
1.0
0.8
0.6
0.4
0.2
0.0
*
2.3
*
DMSO
DMSO+Ars
Ars+SB
B
DMSO
Anisomycin +DMSO
Anisomycin + SB203580
Merge
Shigella
Hoechst
Shigella flexneri
D
Intracellular Shigella (cfu, colonies x10^5)
1.2
1.0
0.8
0.6
0.4
0.2
0.0
*
1.7
*
DMSO
Anisomycin
Aniso+SB
E
Intracellular Shigella (cfu, colonies x10^5)
ns
1.0
0.8
0.6
0.4
0.2
0.0
DMSO
SB
F
Non-treated
Arsenite
P-P38
P38
β-actin
G
Mock treated
Aniso
TNFα
P-P38
P38
β-actin
H
Non-treated
Arsenite
DMSO
SB
Arsenite +DMSO
Arsenite +SB
Aniso +DMSO
Aniso +SB
P-P38
P38
β-actin

Figure 2.1.6 The inhibition of *Shigella* infection in stressed cells is dependent on MAPK p38 activation

(A) Representative images of *Shigella* infections at 0.5hpi in control cells, cells treated with arsenite, or cells treated with arsenite in combination with SB203580, the specific inhibitor of p38. (B) same as in (A) except cells were treated with anisomycin instead of arsenite. (C) CFU analysis of infections same as in (A). (D) CFU analysis of infections same as in (B). (E) CFU analysis of *Shigella* infections at 0.5hpi in cells treated with vehicle (DMSO) or SB203580 alone. (F) Western blot analysis of p38 activation by phosphorylation in HeLa cells treated with (F) arsenite or (G) anisomycin and TNF-α. (H) Western blot showing the inhibition of p38 phosphorylation by SB203580. The total levels of p38 protein are shown and β-actin is used as loading control. Results are shown as mean ± s.e.m; n ≥ 3. *p<0.05, ns: non-significant; two-way ANOVA. Scale-bar 50μm.

2.1.6 *Salmonella* motility compensates for the depletion of sphingolipid-rafts in stressed cells

Membrane lipid-rafts are required for the adhesion and the invasion of various bacterial pathogens (Manes et al., 2003). Thus, the finding that the depletion of sphingolipid-rafts during stress inhibits *Shigella* adhesion should apply to other pathogens requiring these membrane domains. *Salmonella* Typhimurium, a closely related pathogen to *Shigella*, similarly requires sphingolipid/cholesterol-rich membrane rafts to invade cells (Garner et al., 2002). Surprisingly, *Salmonella* infection was not significantly decreased upon treatment with arsenite or TNFα; only a slight decrease was observed with anisomycin treatment (Fig 2.1.7 A, B; Supp Fig 4.4 A, B). Notably, the pattern of infection was different in treated cells compared to control, specifically fewer infected cells but more bacteria per cell were observed under stress conditions (Fig 2.1.7 C, Supp Fig 4.4 C). To verify this observation, adhesion assays with *Salmonella* WT were performed with cells treated with arsenite or anisomycin, and the number of attached bacteria per cell was counted using microscopy. Indeed, a significant increase was observed in the number of bacteria adhering per cell when cells were exposed to arsenite or anisomycin (Fig 2.1.7 D, F; Supp Fig 4.4 D). To confirm that specifically adhesion of *Salmonella* is affected, an invasion-deficient mutant *Δ4* lacking four effector proteins (SopE, SopE2, SopA, and SipB) essential for invasion was used (Raffatellu et al., 2005). Performing adhesion assays and counting the bound bacteria to the cell surface showed that the *Salmonella Δ4* mutant accumulates in specific sites on the cells resulting in a higher number of bacteria per cell similar to what was observed with WT (Fig 2.1.7 E, F; Supp Fig 4.4 D). These results indicate that there are fewer cells infected by *Salmonella* during stress, but the number of bacteria per cell is strikingly higher and results in a similar total bacterial load as in non-stressed cells.

The pattern of *Salmonella* adhesion to stressed cells suggests that it is able to accumulate and adhere at the remaining rafts after stress-induced membrane remodeling. A possible explanation for this phenomenon is that *Salmonella* is a motile pathogen, whereas *Shigella* is non-motile. Thus, *Salmonella* motility could compensate for the lack of lipid-rafts by swarming towards the remaining sites. To test this hypothesis, the *Salmonella* motility-deficient mutant *ΔfliC* was used (Supp Fig 4.4 G). *Salmonella ΔfliC* lacks a phase-variable filament protein FliC affecting the motility of a part of the population, where only bacteria expressing the other filament protein FljB maintain

motility (Bonifield and Hughes, 2003). Additionally, a fully non-motile mutant *ΔflhC* lacking the flagella operon master regulator was used (Supp Fig 4.4 G) (Kutsukake et al., 1988). Strikingly, both *Salmonella ΔfliC* and *ΔflhC* adhesion to cells treated with arsenite or anisomycin was strongly inhibited, similar to what was observed for *Shigella* (Fig 2.1.7 G, H; Supp Fig 4.4 E, F). Complementing *ΔfliC* by ectopic expression of FliC from a native promoter was able to restore WT levels of adhesion to stressed cells (Fig 2.1.7 G, H; Supp Fig 4.4 E, F). As expected, the adhesion of the *Salmonella Δ4* mutant was not significantly affected by the stress treatment, since it has similar motility to WT (Fig 2.1.7 G; Supp Fig 4.4 E). Furthermore, motility assays confirmed the swarming capacity of the strains showing a deficiency in the motility of *ΔfliC* compared to *Salmonella* WT and the complemented strain, and a complete lack of motility for *Salmonella ΔflhC* and *Shigella* (Supp Fig 4.4 G). The *Salmonella* motility mutants phenocopied the infection of *Shigella* in stressed cells, showing that the lack of motility strongly compromises the infection when adhesion sites are scarce.

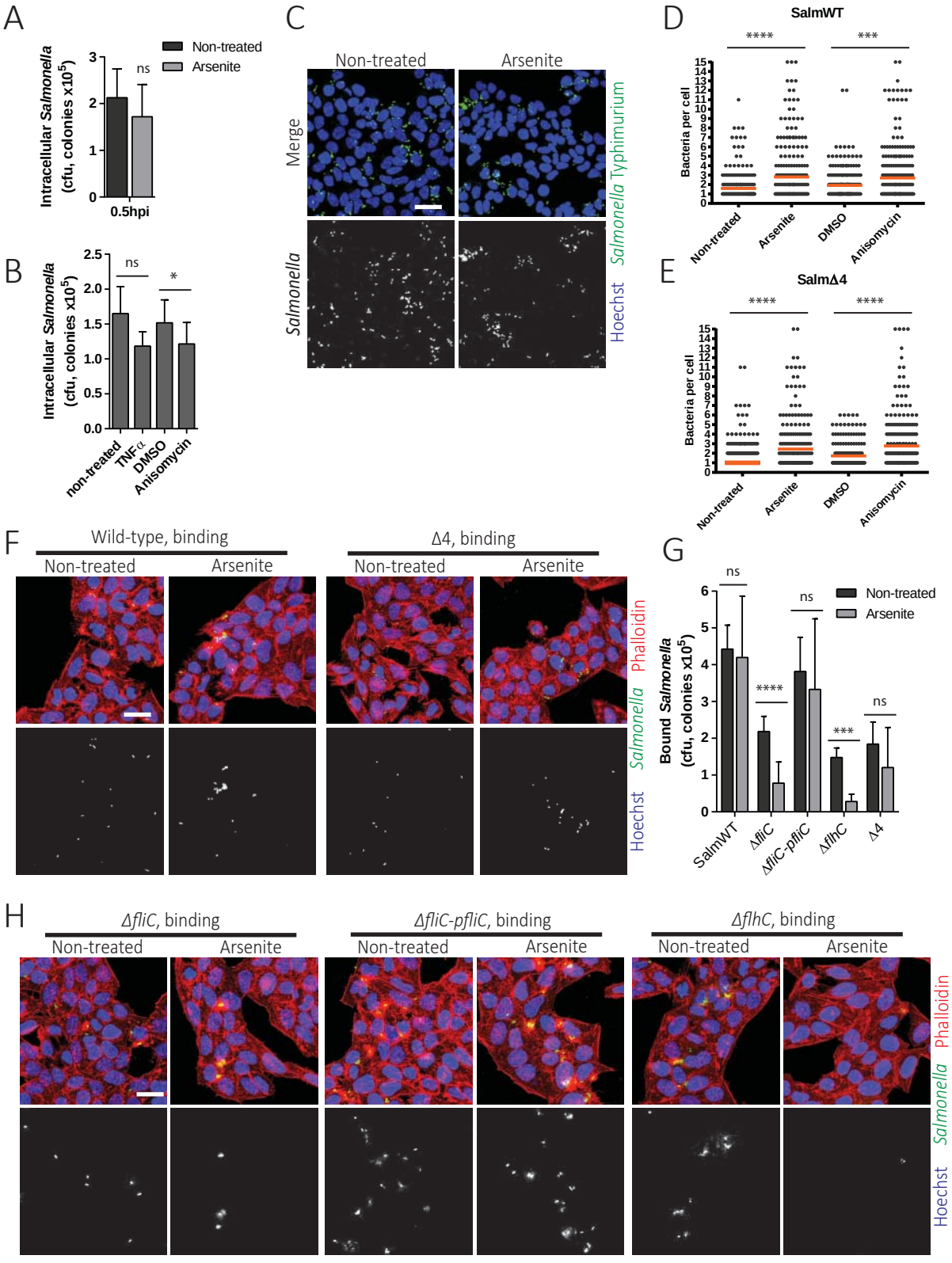
A
Intracellular Salmonella (cfu, colonies x10^5)
Non-treated
Arsenite
ns
0.5hpi
B
Intracellular Salmonella (cfu, colonies x10^5)
ns
*
non-treated
TNFα
DMSO
Anisomycin
C
Non-treated
Arsenite
Merge
Salmonella
Salmonella Typhimurium
Hoechst
D
SalmWT
****
***
Bacteria per cell
Non-treated
Arsenite
DMSO
Anisomycin
E
SalmΔ4
****
****
Bacteria per cell
Non-treated
Arsenite
DMSO
Anisomycin
F
Wild-type, binding
Δ4, binding
Non-treated
Arsenite
Non-treated
Arsenite
Phalloidin
Salmonella
Hoechst
G
Bound Salmonella (cfu, colonies x10^5)
ns
ns
ns
****
***
Non-treated
Arsenite
SalmWT
ΔfliC
ΔfliC-pfliC
ΔflhC
Δ4
H
ΔfliC, binding
ΔfliC-pfliC, binding
ΔflhC, binding
Non-treated
Arsenite
Non-treated
Arsenite
Non-treated
Arsenite
Phalloidin
Salmonella
Hoechst

Figure 2.1.7 *Salmonella* motility compensates for the depletion of lipid-rafts in stressed cells

(A) CFU quantification of intracellular *Salmonella* at 0.5hpi in control cells or cells treated with arsenite. (B) CFU quantification of intracellular *Salmonella* at 0.5hpi in control cells, or cells treated with anisomycin or TNF-α. (C) Representative images of *Salmonella*-GFP infections at 0.5hpi. Scale-bar 50μm. (D, E) Counts of bound bacteria per cell for (D) *Salmonella* WT and (E) *Salmonella Δ4* in adhesion assays in cells treated with different conditions. 150 cells from representative images were counted for each condition; the median for each group is represented (orange line). (F) Representative images of adhesion assays with *Salmonella* WT and *Δ4* expressing GFP in non-stressed or arsenite treated cells. The cell F-actin network was stained with Phalloidin (red) and the nuclei with Hoechst. Scale-bar 25μm. (G) CFU analysis of adhesion assays with *Salmonella* WT, *ΔfliC*, *ΔfliC* complemented strain by ectopic expression of FliC, *ΔflhC*, and *Δ4* in non-treated or arsenite treated cells. (H) Representative images of adhesion assays performed same as in (G). Scale-bar 25μm. Results are shown as mean ± s.e.m. n ≥ 3; two-way ANOVA ns: non-significant; *p<0.05; ***p<0.001; ****p<0.0001.

2.1.7 *Shigella* replication in cells inhibits re-infection by extracellular bacteria

Results from this study show that cells experiencing oxidative stress, cytokine stimulation, and the activation of p38 MAPK restrict the infection by *Shigella*. Similarly, the intracellular replication of *Shigella* causes cellular stress that results in oxidative stress, cytokine secretion, and MAPK activation (Carneiro et al., 2009; Kasper et al., 2010; Pedron et al., 2003). Thus, cells with replicating *Shigella* should lead to the inhibition of extracellular bacterial adhesion, and ultimately infection. To test this, cells primarily infected for 3h with replicating *Shigella*-mCherry or mock infected cells were re-infected with *Shigella* expressing GFP (Fig 2.1.8 A). The secondary infection with *Shigella*-GFP was decreased in cells with replicating *Shigella*-mCherry compared to mock-infected cells (>2-fold; Fig 2.18 B, D; Supp Fig 4.5 A). Interestingly, no decrease in *Shigella*-GFP infection was observed in cells primarily infected with the invasive but T3SS-deficient mutant *ΔipaB/Inv*, which remains in the endocytic vacuole and does not replicate (Isberg et al., 1987; Menard et al., 1996) (Fig 2.1.8 B, D; Supp Fig 4.5 A). This latter result demonstrated that *Shigella* replication in the cytoplasm is required to cause the inhibition of re-infection. Consistent with the previous results that cellular stress restricts non-motile bacteria, infection with *Salmonella* WT-GFP was not decreased in cells with replicating *Shigella*-mCherry nor with *ΔipaB/Inv* compared to the mock-infected cells (Fig 2.1.8 C, E; Supp Fig 4.5 B). Additionally, the re-infection assays were performed in HCT-8 cells, where *Shigella*-GFP re-infection was inhibited in cells containing replicating *Shigella*-mCherry, whereas *Salmonella*-GFP re-infection was not decreased (Supp Fig 4.5 E-L). Of note, the decrease in *Shigella* was only observed for the secondary infection; the primary infection with *Shigella*-mCherry or *ΔipaB*/Inv did not change in the different conditions in Hela and in HCT-8 cells (Supp Fig 4.5 C, D, M, N).

To test whether the motility of *Salmonella* circumvents the restriction by infected cells, the motility mutants were tested in the re-infection experiments. The infection with *Salmonella ΔfliC* was decreased in cells containing replicating *Shigella*-mCherry, and this decrease was compensated by the ectopic expression of FliC (Fig 2.1.9 A, B, C). Similarly, the re-infection with the *Salmonella* mutant *ΔflhC* lacking the flagella operon expression was strongly inhibited (Fig 2.1.9 A, B, C). There was no change in the levels of the primary *Shigella*-mCherry infection in combination with the different *Salmonella* strains (Supp Fig 4.6 A). These results indicate that *Shigella* replication in epithelial cells inhibits the adhesion of extracellular non-motile bacteria.

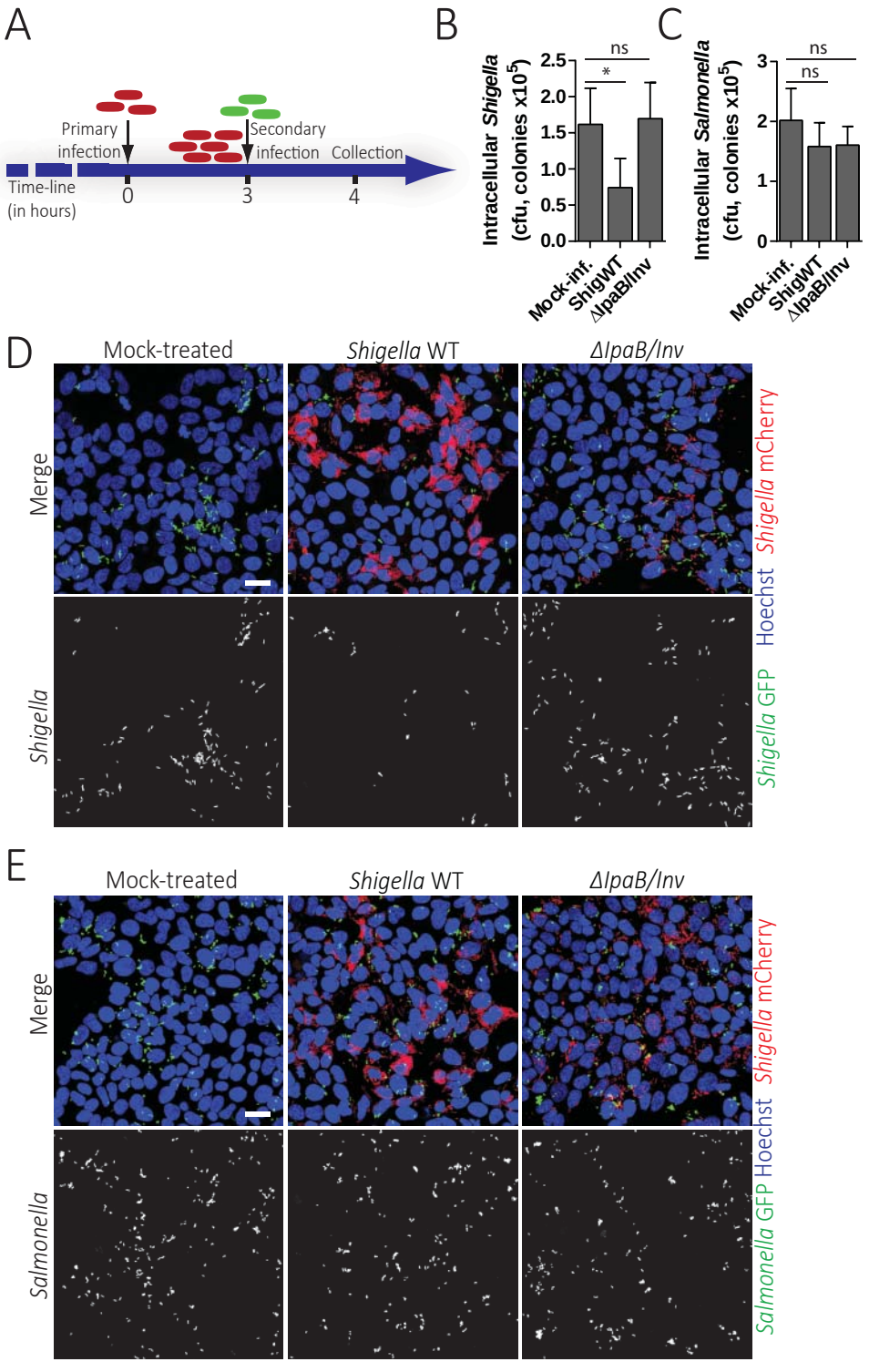
A
Primary infection
Secondary infection
Collection
Time-line (in hours)
0
3
4
B
Intracellular Shigella (cfu, colonies x10^5)
ns
*
2.5
2.0
1.5
1.0
0.5
0.0
Mock-inf.
ShigWT
ΔIpaB/Inv
C
Intracellular Salmonella (cfu, colonies x10^5)
ns
ns
3
2
1
0
Mock-inf.
ShigWT
ΔIpaB/Inv
D
Mock-treated
Shigella WT
ΔIpaB/Inv
Merge
Shigella
Hoechst Shigella mCherry
Shigella GFP
E
Mock-treated
Shigella WT
ΔIpaB/Inv
Merge
Salmonella
Salmonella GFP Hoechst Shigella mCherry

Figure 2.1.8 *Shigella* replication in cells inhibits re-infection by extracellular bacteria

(A) Schematic representation of the experimental design for the re-infection assays. Cells are infected with mCherry labelled *Shigella*, and at 3hpi re-infected with GFP labelled *Shigella*. The secondary *Shigella*-GFP infection is collected at 0.5hpi (4hpi for the primary *Shigella*-mCherry infection). (B) CFU quantification of intracellular *Shigella*-GFP in re-infection assays with mock-infected, *Shigella* WT-mCherry infected, and *Shigella ΔipaB*/invasin-mCherry infected cells. (C) CFU quantification of intracellular *Salmonella*-GFP in re-infection assays. (D) Representative images of *Shigella*-GFP re-infection assays with mock-infected, *Shigella* WT-mCherry infected, and *Shigella ΔipaB*/invasin-mCherry infected cells. (E) Representative images of *Salmonella*-GFP re-infection assays. Scale-bar 50μm. Results are shown as mean ± s.e.m. two-way ANOVA, n ≥ 3. ns: non-significant; *p<0.05.

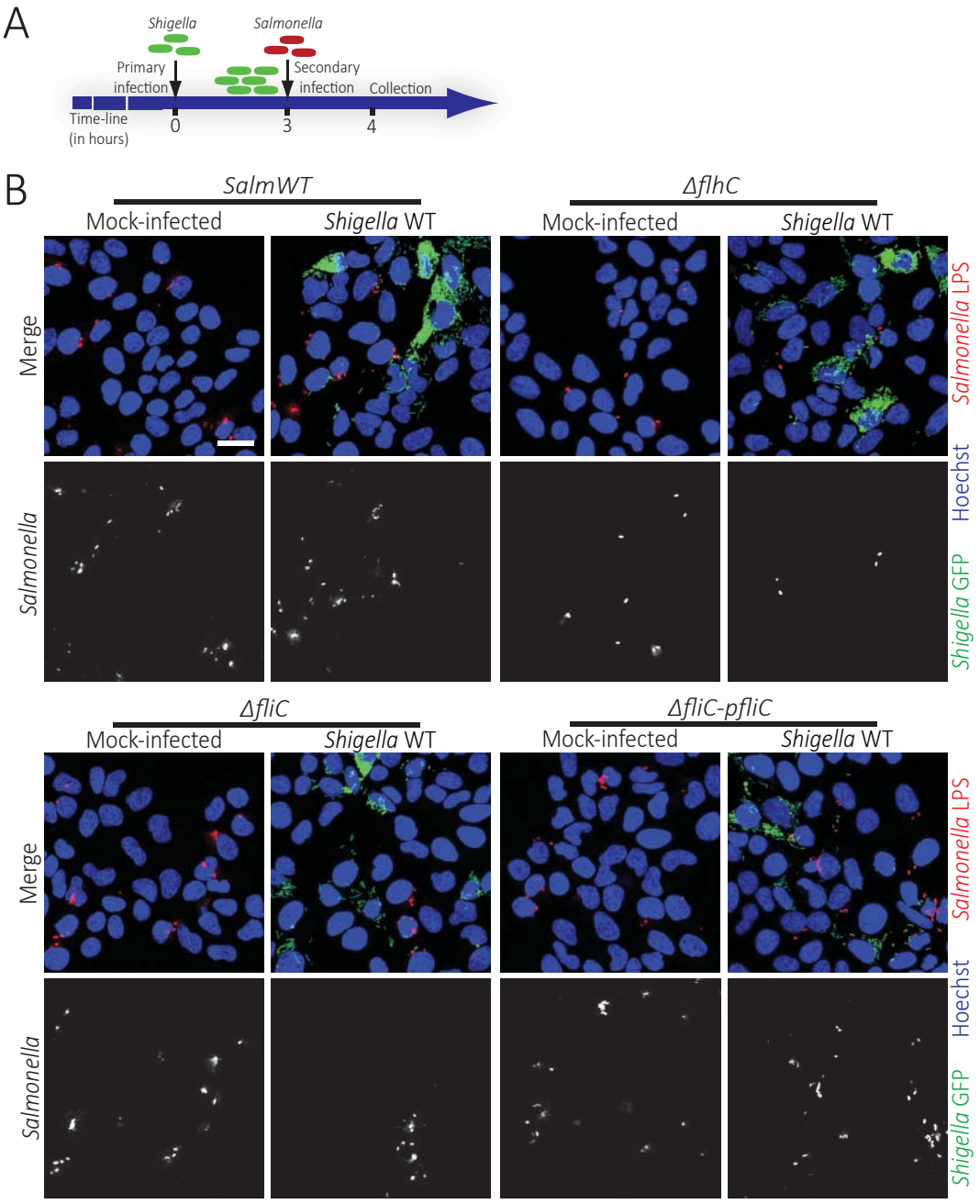
A
Shigella
Salmonella
Primary infection
Secondary infection
Collection
Time-line (in hours)
0
3
4
B
SalmWT
ΔflhC
Mock-infected
Shigella WT
Mock-infected
Shigella WT
Merge
Salmonella
Salmonella LPS
Hoechst
Shigella GFP
ΔfliC
ΔfliC-pfliC
Mock-infected
Shigella WT
Mock-infected
Shigella WT
Merge
Salmonella
Salmonella LPS
Hoechst
Shigella GFP
C
Intracellular Salmonella (cfu, colonies x10^5)
3.5
3.0
2.5
2.0
1.5
1.0
0.5
0.0
ns
***
ns
*
Mock-infected
ShigWT
SalmWT
ΔfliC
ΔfliC-pfliC
ΔflhC

Figure 2.1.9 *Salmonella* motility compensates for the inhibition caused by infected cells

(A) Schematic representation of the experimental design for the re-infection assays. Cells are infected with GFP labelled *Shigella*, and at 3hpi re-infected with *Salmonella*-GFP. The secondary *Salmonella*-GFP infection is collected at 0.5hpi (4hpi for the primary *Shigella*-mCherry infection). (B) Representative images of *Salmonella* re-infection with mock-infected or *Shigella* WT-GFP infected cells. *Salmonella* was stained with a specific LPS antibody (red). (C) CFU quantification of intracellular *Salmonella* WT, *ΔfliC*, *ΔfliC*-pFliC, and *ΔflhC* in re-infection assays with mock-infected, or *Shigella* WT infected cells. Scale-bar 25μm. Results are shown as mean ± s.e.m. n ≥ 3; two-way ANOVA, ns: non-significant; *p<0.05; ***p<0.001.

2.1.8 *Shigella* intracellular replication remodels the cell membrane through the activation of ASM and NSM

To test whether the inhibition of re-infection is caused by the stress-induced membrane remodeling, ASM and NSM activity was inhibited in cells infected with *Shigella*. The specific inhibitors of NSM and ASM were added to *Shigella*-mCherry infected cells at 2hpi, and the cells were re-infected with *Shigella*-GFP after 1h of treatment (Fig 2.1.10 A). Indeed, amitryptilin reversed the inhibitory effect exerted by the intracellular *Shigella*-mCherry on the adhesion of extracellular *Shigella*-GFP (Fig 2.1.10 B, D, F). Whereas GW4869 did not have an effect alone, an additive effect was observed when it was combined with amitryptilin leading to a full recovery of the re-infection with *Shigella*-GFP (Fig 2.1.10 C, E, G). No effect was observed for amitriptilin or GW4869 on the primary (*Shigella*-mCherry) nor the secondary (*Shigella*-GFP) infection alone (Supp Fig 4.6 B-E). An increase in the *Shigella*-GFP secondary infection was observed when cells were treated with both amitryptilin and GW4869, but this increase does not account for the recovery observed during re-infection (Supp Fig 4.6 C). These results demonstrate that the inhibition of the re-infection is dependent on the activity of ASM and NSM. Moreover, a clear accumulation of ceramide was observed by immunostaining in *Shigella*-mCherry infected cells compared to the control (Fig 2.1.10 H). *Shigella* infection also lead to the accumulation of ASM in membrane foci similar to what was observed in cells experiencing stress (Fig 2.1.10 I). Furthermore, enzymatic assays were performed on membrane fractions from cells infected with different multiplicity of infection (MOI) of *Shigella*-mCherry at 3hpi. A modest but significant increase was observed in the activity of both NSM and ASM at MOI 100 and 250; no increase in activity was measured at MOI 10 possibly due to the low percentage of infected cells at this MOI and the sensitivity of the enzymatic assays (Fig 2.1.10 J, K). These results show that *Shigella* intracellular replication leads to the ASM and NSM mediated remodeling of the membrane and the formation of ceramide-rich platforms.

To show that the inhibition of extracellular bacterial adhesion by infected cells is specifically induced by ASM and NSM-1, cells were transfected with siRNAs against each gene or both combined, and re-infection assays were performed. The knockdown of ASM or NSM-1 lead to a partial recovery of the secondary infection by *Shigella*-GFP during re-infection, when compared to cells transfected with a non-targeting siRNA (Fig 2.1.11 A-C). When both siRNAs were combined, re-infection by *Shigella*-GFP was recovered to

same extent as with ASM siRNA alone (Fig 2.1.11 A-C). An additive effect was not observed when both siRNAs were combined possibly due to the insufficient knockdown achieved at 25nM of each siRNA compared to 50nM for the individual knockdown (Supp Fig 4.3 H, I). Knockdown of ASM and NSM-1 individually or in combination did not affect the primary infection by *Shigella*-mCherry (Supp Fig 4.6 G, I). The knockdown of only ASM lead to an increase in the secondary infection by *Shigella*-GFP, however it did not account for the recovery observed during re-infection (Supp Fig 4.6 F, H). Collectively, the results demonstrate that *Shigella* intracellular replication in epithelial cells leads to the activation of ASM and NSM resulting in the depletion of sphingolipid-rafts in the membrane, which restrains infection by extracellular *Shigella*.

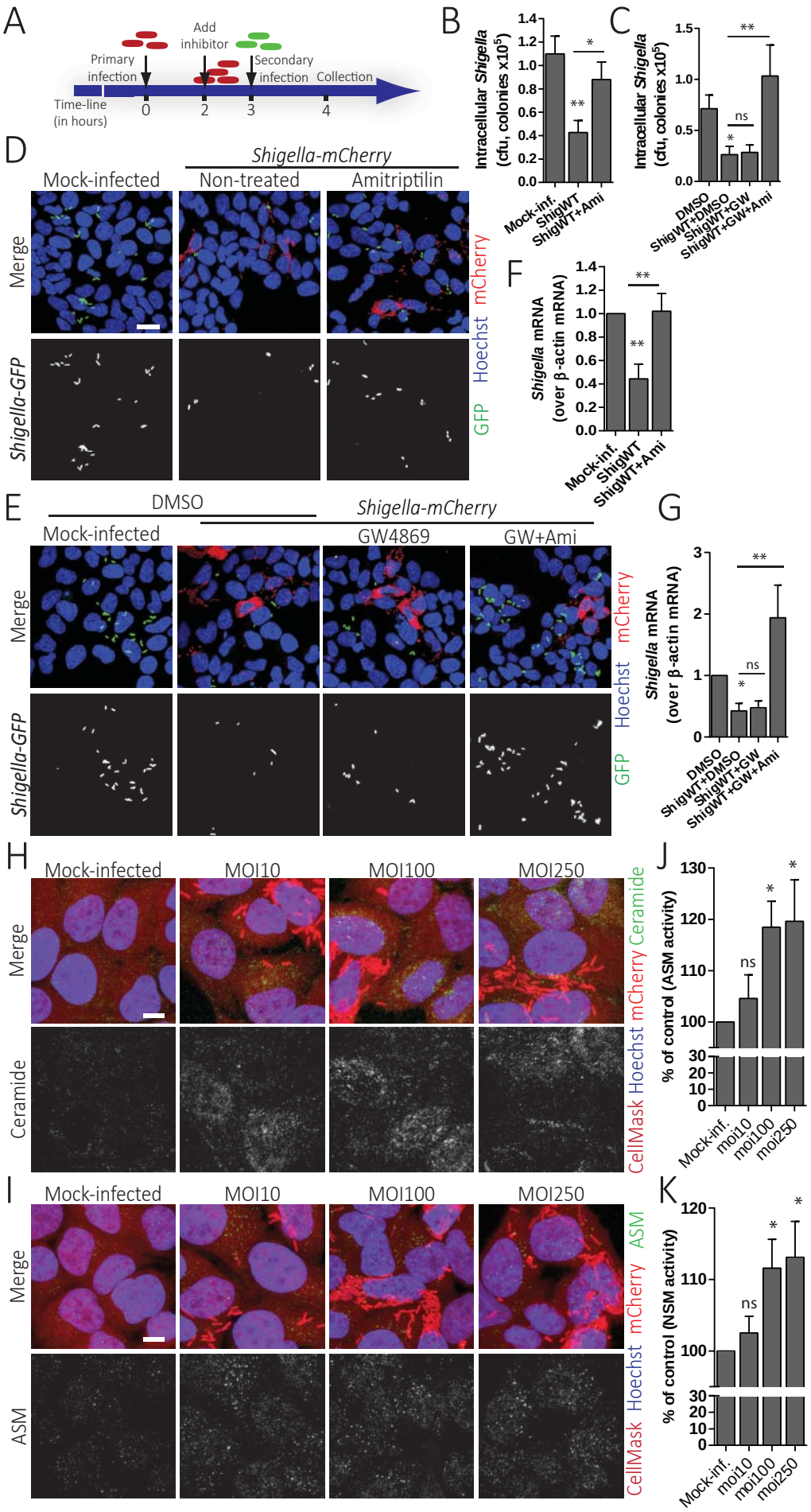
A
Add inhibitor
Primary infection
Secondary infection
Collection
Time-line (in hours)
0
2
3
4
B
Intracellular Shigella (cfu, colonies x10^5)
Mock-inf.
ShigWT
ShigWT+Ami
C
Intracellular Shigella (cfu, colonies x10^5)
DMSO
ShigWT+DMSO
ShigWT+GW
ShigWT+GW+Ami
D
Shigella-mCherry
Mock-infected
Non-treated
Amitriptilin
Merge
Shigella-GFP
Hoechst mCherry
GFP
F
Shigella mRNA (over β-actin mRNA)
Mock-inf.
ShigWT
ShigWT+Ami
E
DMSO
Shigella-mCherry
Mock-infected
GW4869
GW+Ami
G
Shigella mRNA (over β-actin mRNA)
DMSO
ShigWT+DMSO
ShigWT+GW
ShigWT+GW+Ami
H
Mock-infected
MOI10
MOI100
MOI250
Merge
Ceramide
CellMask Hoechst mCherry Ceramide
J
% of control (ASM activity)
Mock-inf.
moi10
moi100
moi250
I
Mock-infected
MOI10
MOI100
MOI250
Merge
ASM
CellMask Hoechst mCherry ASM
K
% of control (NSM activity)
Mock-inf.
moi10
moi100
moi250

Figure 2.1.10 *Shigella* replication in cells induces host-cell membrane remodeling

(A) Schematic representation of the experimental design of the re-infection assays. Cells are infected primarily with *Shigella*-mCherry. ASM and NSM inhibitors are added at 2hpi for 1h, and the cells are re-infected at 3hpi with *Shigella*-GFP. (B, C) CFU quantification of intracellular *Shigella*-GFP after re-infection in the presence of amitryptilin (B) or GW4869 or both (C). (D, E) Representative images of the re-infection assays with *Shigella*-GFP in the presence of (D) amitryptilin or (E) GW4869 or both. Scale-bar 25μm. (F) Quantification of intracellular *Shigella* by qRT-PCR in the re-infection assays in the presence of (F) amitryptilin or (G) GW4869 or both. The results were normalized to β-actin mRNA, and fold-change is reported compared to the corresponding control, (F) mock-infected or (G) mock-infected DMSO treated. (H, I) Representative images of (H) ceramide or (I) ASM staining (green) in HeLa cells mock-infected or infected with increasing MOIs of *Shigella*-mCherry (cell body staining with CellMask (purple)). Scale-bar 10μm. (J, K) the activity of (J) ASM and (K) NSM was measured in the membrane fractions of mock or *Shigella* infected cells. Percent activation is shown compared to the mock-infected control (100% activity). Results are shown as mean ± s.e.m. n ≥ 3. two-way ANOVA, ns: non-significant; *p<0.05; **p<0.01.

2.1.9 Concluding remarks

Stress is a prevalent condition during bacterial infection; it involves specific stress-response pathways and crosstalks with innate immunity. As determined by this study, epithelial cells exposed to different kinds of stress conditions such as oxidative stress, hypoxia, TNF-α stimulation, or intracellular replicating *Shigella* inhibit bacterial adhesion. This inhibition occurs due to the remodeling of the cell surface through the activation of the sphingomyelinases ASM and NSM-1. These sphingomyelinases translocate to the cell surface upon stress and degrade sphingomyelin, which leads to the depletion of sphingolipid-rafts and the production of ceramide-rich platforms. The activation of these enzymes is positively regulated by p38 MAPK, which is phosphorylated during stress and *Shigella* infection. Interestingly, the depletion of lipid-rafts in stressed cells is highly restrictive to non-motile bacteria, whereas motile bacteria are able to circumvent this restriction. The findings in this study suggest a novel innate defense strategy intrinsic to epithelial cells in response to stress cues.

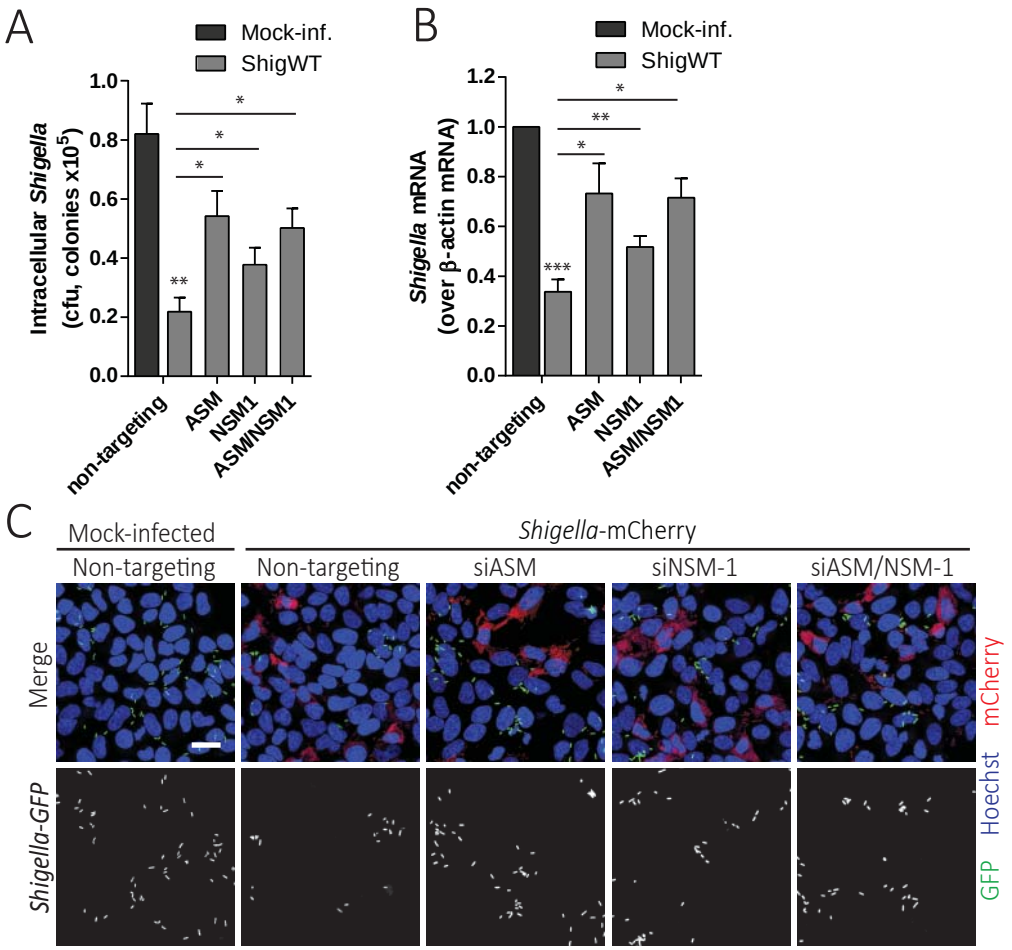

Figure 2.1.11 ASM knockdown reverts the inhibition of extracellular *Shigella* by infected cells

(A) CFU and (B) qRT-PCR quantification of *Shigella*-GFP re-infection at 0.5hpi in cells transfected with siRNAs. (C) Representative images of re-infection with *Shigella*-GFP at 0.5hpi in cells transfected with different siRNAs. Results are shown as mean ± s.e.m. n ≥ 3, *p<0.05, **p<0.01, ***p<0.001 ns: non-significant; two-way ANOVA. Scale-bar 25µm.

2.2 Intracellular bacterial replication inhibits SG-formation and affects TIAR/TIA-1 localization

2.2.1 *Shigella* replication inhibits generic SG-aggregation

Shigella infection is characterized by an intense inflammation and a damaged colonic mucosal lining (Marteyn et al., 2012). The acute inflammatory environment subjects the epithelial cells and tissue to stresses such as heat, oxidative stress, hypoxia, and cytokine stimulation (Karin et al., 2006). One major cellular stress response to exogenous and endogenous stresses is the formation of stress granules (SGs), a highly conserved response across eukaryotes (Decker and Parker, 2012). The long-standing evidence that SGs play a role in host-defense particularly in viral infection suggests that this stress response might be also important during bacterial infection. To investigate the role of SGs during *Shigella* infection, the integrity of SGs was evaluated in different cell lines. HeLa, Caco-2, HT-29, U2OS, and 293T cells were infected with *Shigella* WT and treated 5hpi with sodium arsenite for 1h to induce SG-formation. In all cell lines, cells infected with *Shigella* failed to efficiently form SGs, whereas in the non-infected bystander cells the granules were large and visible (Fig 2.2.1 A). Immunostaining of essential proteins for SG-aggregation such as EIF3 and G3BP-1 showed that these proteins did not aggregate in heat-shock induced SGs in infected cells (Fig 2.2.1 B). Similar results were obtained for both TIAR and TIA-1 proteins in response to arsenite stress (Fig 2.2.1 C). The interference of *Shigella* with SG-aggregation was manifested by a decrease in the size of granules or their entire disappearance compared to very large granules formed in non-infected cells (Figure 2.2.1 C, white arrowheads). These results show that SG-inhibition in infected cells is a generic effect independent of the stress or the individual proteins.

To analyze at what stage of *Shigella* infected cells fail to form SGs, cells were infected and SGs induced with arsenite at 0.5, 1, 2, 3, 4, and 6hpi. Interestingly, during early infection at 0.5, 1, and 2hpi SGs formation was similar in infected and non-infected cells; SG morphology started to change at intermediate times post-infection (>3hpi) and complete impairment of formation was observed at late time-points (6hpi) in infected cells (Figure 2.2.2 A). These results suggest that the interference with SGs depends on the replication of intracellular *Shigella* and/or on the number of bacteria per cell.

SG-aggregation is induced canonically by the phosphorylation of EIF2α by sensor kinases and the composition of granules varies depending on the stress type (Anderson and Kedersha, 2008). However, some stresses, such as H_2O_2 and pateamine A, induce SGs

independent of EIF2α phosphorylation (Figure 2.2.2 B) (Dang et al., 2006; Emara et al., 2012). To verify whether *Shigella* infection interferes with the canonical SG-formation downstream EIF2α phosphorylation or happens independently of this pathway, infected cells were stressed with H_2O_2. SGs induced by this type of stress were also inhibited in infected cells (Figure 2.2.2 C). These results demonstrate that *Shigella* infection blocks the generic SG-aggregation process independent of the initiating signaling cascade through EIF2α phosphorylation.

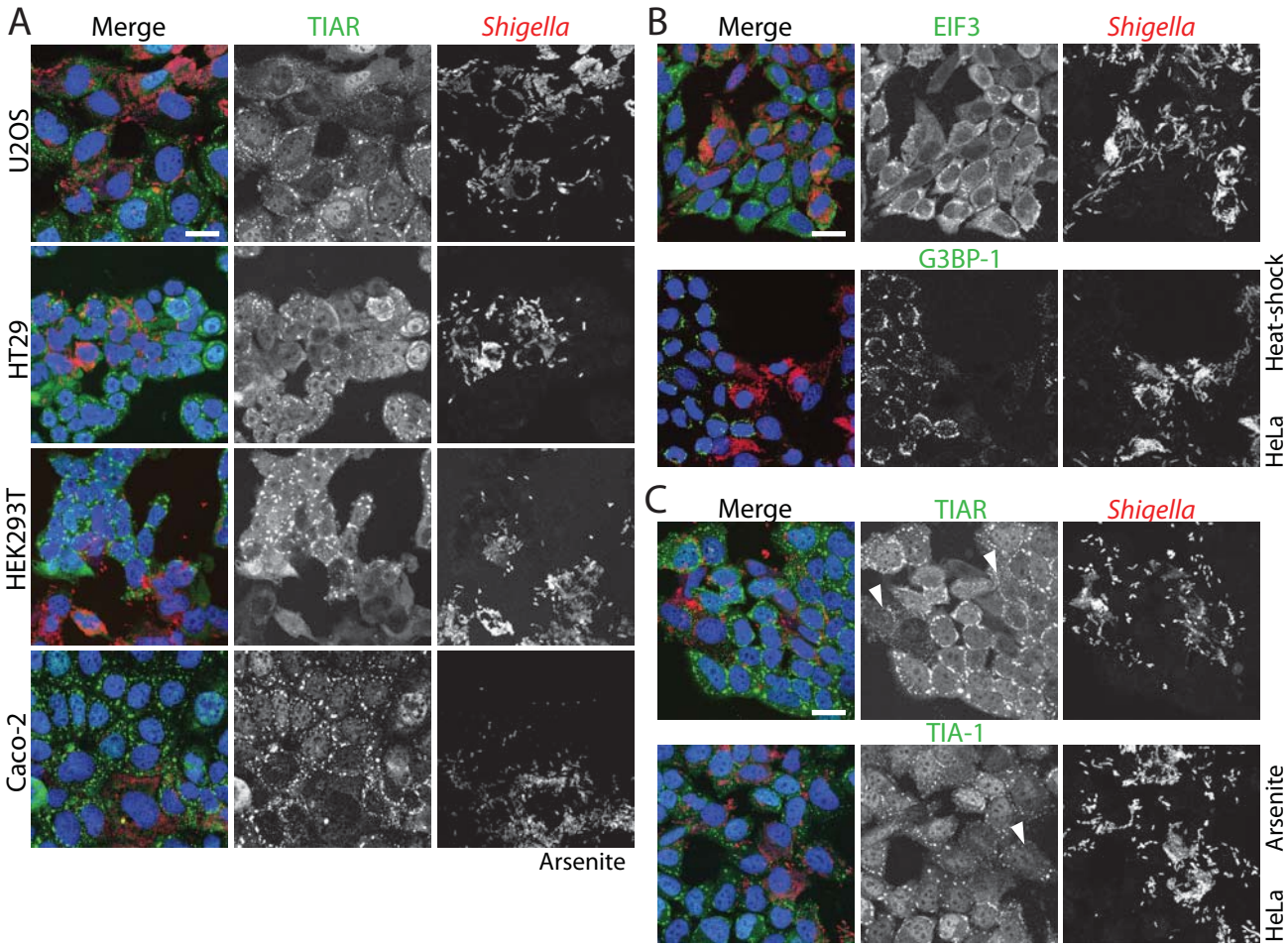

Figure 2.2.1 *Shigella* infected cells inhibit SG-aggregation in response to stress

(A) U2OS, HT-29, HEK293, and Caco-2 cells were infected with *Shigella* WT at MOI10. SGs were induced with 0.5 µM arsenite at 5hpi, and were fixed for immunostaining at 6hpi. SGs were detected using an antibody specific for the SG-protein TIAR (green), *Shigella* was stained using a specific antibody (red), and the cell nuclei were stained with Hoechst (blue). (B) HeLa cells were infected as in (A) and exposed to 45˚C for heat-shock at 5hpi. The cells were fixed for immunostaining and SGs were detected using EIF3 or G3BP1 specific antibodies (green), *Shigella* and the nuclei were stained as in (A). (C) HeLa cells were infected and treated same as in (A) and SGs were detected using specific antibodies against TIAR and TIA-1. White arrowheads show smaller granules in infected cells. Scale-bar 25µm.

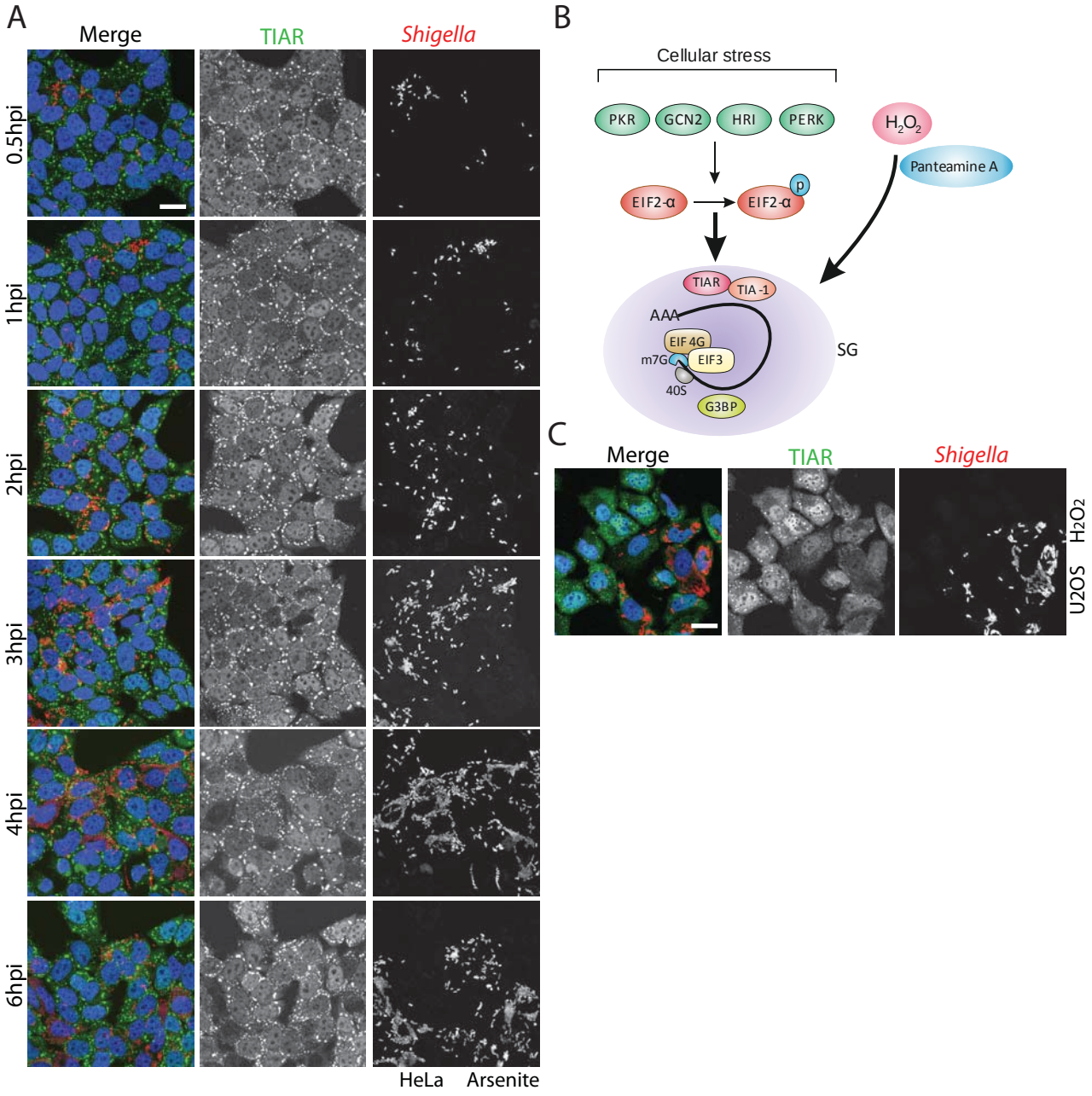

Figure 2.2.2 *Shigella* intracellular replication inhibits generic SG-aggregation

(A) Hela cells were infected with *Shigella* WT at MOI10, and SGs were induced with 0.5 µM arsenite for 1h. Cells were fixed at 0.5, 1, 2, 3, 4, and 6hpi and SGs were detected by staining TIAR. (B) A schematic illustrating the canonical and non-canonical pathways of SG-aggregation. Hydrogen peroxide and panteamine A induce SGs independently of EIF2-α phosphorylation. (C) U2OS cells were infected with *Shigella* WT at MOI10, and SGs were induced with 3mM H2O2 for 2h. TIAR was stained to detect SGs (green). Scale-bar 25µm.

2.2.2 Intracellular cytosolic replication inhibits SG-aggregation

The results show that *Shigella* replication and/or the number of bacteria per cell interfere with SG-aggregation (Fig 2.2.2 A). To test whether the invasion of cells and the localization of bacteria intracellularly is sufficient to induce this phenotype, an invasive but non-virulent *Shigella* strain was used. *Shigella ΔipaB*/invasin lacks the *ipaB* gene essential for T3SS function making it avirulent and carries a plasmid expressing ectopically the *Yersinia* invasin protein, which is sufficient to induce uptake by cells (Fig 2.2.3 A) (Isberg et al., 1987; Menard et al., 1996). This strain is able to invade the cells, but unlike *Shigella* WT, it is incapable of escaping the endocytic vacuole or replicating (Fig 2.2.3 A). Intriguingly, high numbers of intracellular *ΔipaB*/invasin did not interfere with SG-formation in response to arsenite (Fig 2.2.3 B). This result suggests two possible hypotheses: i) a functional T3SS or the T3SS effectors are responsible for the inhibition of SGs, ii) the escape into the cytosol and replication inhibit SGs. To test these hypotheses, single knock-out mutants for each of the 30 known effectors were generated and compared to *Shigella* WT for their capacity to inhibit SGs (Table 4.1). Cells were infected at the same MOI as WT and treated with arsenite at 5hpi, and SG-inhibition in infected cells was compared to WT. All of the 26 single-mutants that are able to invade the cells were able to inhibit SG-formation similar to WT, and the remaining 4 mutants *ΔipaB*, *ΔipgD*, *Δspa15*, and *ΔipaH4.5* were defective in invasion (Table 4.1; data not shown). Particularly, the *Shigella ΔvirG* mutant that loses the ability to spread from cell-to-cell using actin tails, inhibited SGs similar to WT showing that intercellular spreading is not responsible for SG-inhibition (Table 4.1; Fig 2.2.3 C) (Bernardini et al., 1989). These results show that there is no single effector responsible for the inhibition of SG-aggregation.

The mechanism of vacuolar rupture by *Shigella* is dependent on the entire T3SS apparatus, which is also necessary for replication (Du et al., 2016). Ideally, a strain capable of escaping into the cytoplasm but not replicate would inform on whether cytosolic sensing of the bacteria or the replication process itself is responsible for the inhibition of SGs. Given that such a strain is not available, an independent approach was undertaken to understand which bacterial lifestyle affects SG-formation. *Listeria monocytogenes* a Gram-positive pathogen having a similar intracellular lifestyle to *Shigella*, including cytosolic replication and actin-dependent intercellular spreading, was tested for its ability to interfere with SGs (Tilney and Portnoy, 1989). Strikingly, *Listeria* infected cells were

unable to form SGs in response to arsenite compared to non-infected bystanders similar to *Shigella* WT (Fig 2.2.3 D). This result suggests that cytoplasmic replication is sufficient to inhibit SGs independent of the bacterial pathogen. To further validate this result, *Salmonella* Typhimurium a *Shigella*-related bacterium having a distinct intracellular lifestyle was tested. *Salmonella* enters the cells similarly to *Shigella* but remains in the vacuole where it replicates (de Jong et al., 2012). As reported previously, cells with intracellular replicating *Salmonella* were able to form SGs comparable to the non-infected bystander cells (Fig 2.2.3 E) (Eulalio et al., 2011). Results from *Listeria* and *Salmonella* infected cells support that replication alone is not sufficient to inhibit SGs, rather cytosolic localization is necessary. To validate this hypothesis, the *Salmonella ΔsifA* mutant, which escapes the vacuole and hyper-replicates in the cytoplasm (Beuzon et al., 2000), was tested for its ability to inhibit SG formation. Indeed, *Salmonella ΔsifA* infected cells were unable to form SGs, whereas SGs in bystander cells were formed efficiently (Fig 2.2.3 F). Collectively, these results show that cytosolic bacterial replication inhibits SG-formation in response to stress independently of the bacterial species.

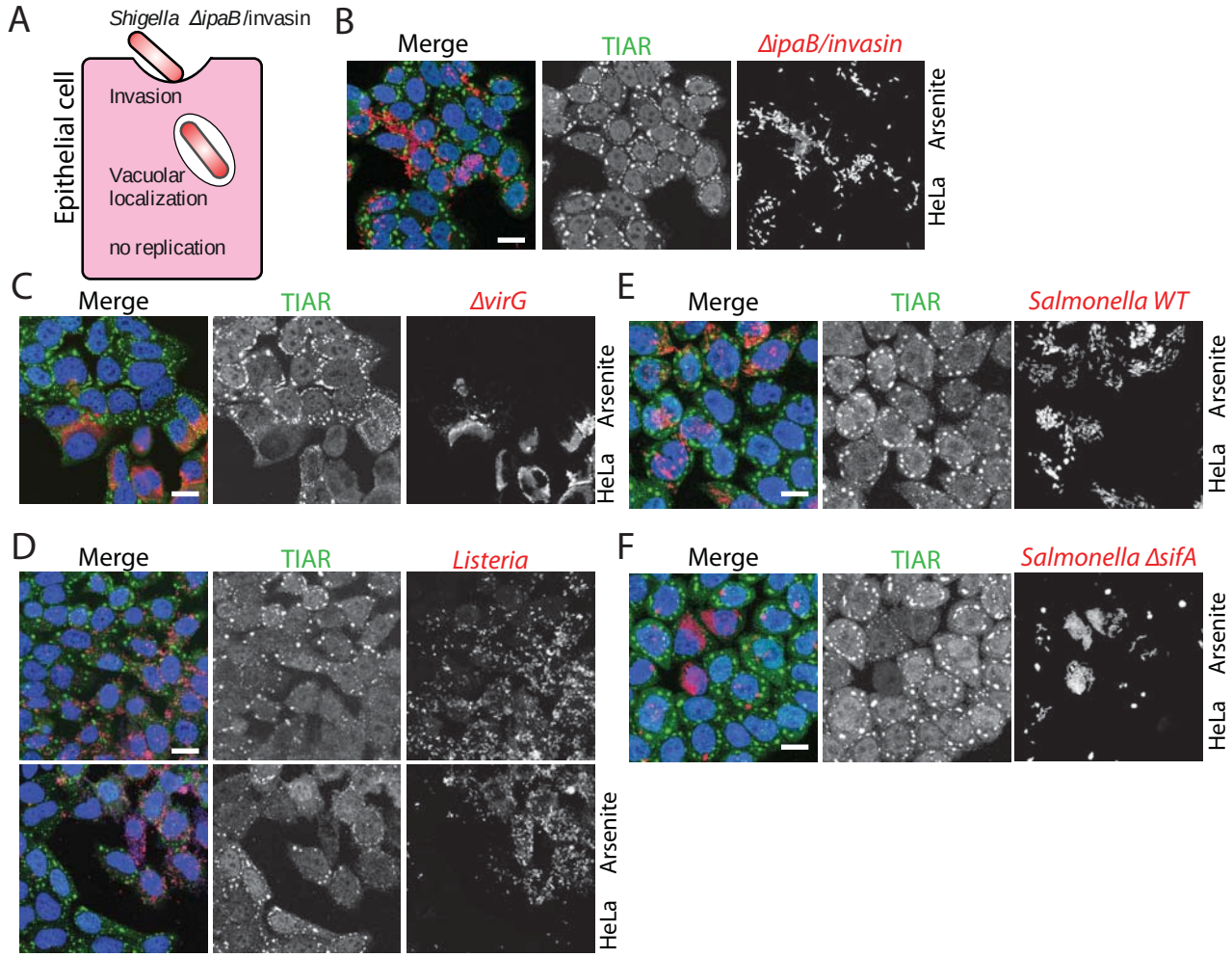

Figure 2.2.3 Replication in the cytoplasm inhibits SG-formation independently of the bacterial pathogen

(A) An illustration depicting the infection of an epithelial cell by *Shigella ΔipaB*/invasin. The *Shigella ΔipaB* mutant has a deficient T3SS, thus it is non-invasive. The expression of the invasin protein from *Yersinia* is sufficient to induce the uptake of the *ΔipaB* mutant by the cells. However, this strain remains in the endocytic vacuole and does not replicate. (B) HeLa cells were infected with *Shigella ΔipaB*/invasin at MOI 350, SGs were induced with arsenite at 5hpi and fixed at 6hpi. TIAR was stained for the detection of SGs (green), *Shigella* was stained with a specific antibody (red), and the nuclei were stained with Hoechst. (C) HeLa cells were infected with the spreading-deficient *Shigella ΔvirG* mutant at MOI 50 and fixed at 3hpi, SGs were induced with arsenite (D) HeLa cells were infected with *Listeria* WT at MOI 50, and fixed at 20hpi. SGs were induced with arsenite, and *Listeria* was stained with a specific antibody. (E, F) HeLa cells were infected with (E) *Salmonella* WT for 20h or (F) *Salmonella ΔsifA* for 8h at MOI25, SGs were induced with arsenite. Scale-bar 25µm.

2.2.3 *Shigella* replication in the host cytoplasm promotes nuclear/cytosolic re-localization of the RBPs TIAR and TIA-1

The results show that *Shigella* cytosolic replication interferes with the SG-aggregation process independent of the upstream signaling. SG-assembly depends on self-oligomerizing proteins, for example G3BP-1, TIAR, and TIA-1. The absence of these proteins prevents SG-formation (Kedersha et al., 1999; Tourriere et al., 2003). TIA-1 and TIAR have a prion related domain (PRD) that is responsible for the nucleation of the granule, its absence inhibits aggregation, whereas the over-expression of the protein leads to spontaneous aggregation in the absence of stress (Kedersha et al., 1999). To test whether the inhibition of SG formation during *Shigella* infection is caused by a change in proteins essential for SG-aggregation, the levels of EIF3, G3BP-1, TIAR, and TIA-1 were assessed in unstimulated total cell lysates by Western blot. There was no difference in the level of these proteins in infected and mock-infected cells (Fig 2.2.4 A-D).

The localization of the different essential SG-proteins was also examined by immunostaining in stress-exposed and resting cells. G3BP-1 and EIF3 localize to the cytoplasm where they display a diffuse signal, and form large foci corresponding to SGs upon stress (data not shown). TIAR and TIA-1 are distributed between the nucleus and the cytoplasm, and in presence of stress they form SG foci in the cytoplasm (Fig 2.2.1 C; Fig 2.2.4 E) (Zhang et al., 2005). Remarkably, the nuclear signal of both proteins decreased in *Shigella* infected cells, independent of any exogenous stress (Fig 2.2.4 F-I). Because the total levels of TIAR and TIA-1 are unchanged in infected cells compared to the control, their nuclear depletion leads to cytosolic accumulation (Figure 2.2.4 C, D). Interestingly, the nuclear/cytosolic translocation of both proteins also seemed to be dependent on the number of bacteria per cell, consistent with what was observed for SGs (Figure 2.2.4 F, G; white arrowheads). Due to the cell-to-cell spreading of *Shigella*, infected cells contain a heterogeneous number of bacteria per cell. A way to synchronize the replication process is to use the *Shigella ΔvirG* mutant, which is unable to spread. The cells invaded by *ΔvirG* have a more heterogenous number of bacteria per cell after replication compared to *Shigella* WT. Visualization of TIAR and TIA-1 distribution in *ΔvirG* infected cells showed a consistent nuclear depletion of both proteins in all infected cells (Fig 2.2.4 H, I).

To validate the change of the ratio of both proteins in the nuclear and the cytosolic compartments, cells were fractionated and analyzed by WB (Fig 2.2.4 J, K). The

fractionated cells are a mixed population of infected and non-infected bystander cells and the re-localization of the proteins occurs in infected cells, thus a high percentage of infection needs to be achieved to visualize the changes in protein ratios in the total population. For this purpose, an MOI of 350 was used for *Shigella ΔvirG* to achieve a ~60% of infected cells exhibiting a clear re-localization of the proteins in all infected cells (Fig 2.2.4 H, I). Actinomycin D treated cells, which display a strong nuclear depletion and cytosolic accumulation of TIAR and TIA-1, were used as a positive control (Fig 2.2.4 E) (Zhang et al., 2005). Indeed, WB results revealed that the levels of both proteins strongly decreased in the nucleus and increased in the cytoplasm upon actinomycin D treatment (Figure 2.2.4 J, K). In mock-infected cells, both proteins were equally distributed between both compartments with a slight skew towards the nuclear fraction particularly for TIA-1 (Fig 2.2.4 J, K). In *ΔvirG* infected cells, a clear depletion of the nuclear fraction was observed compared to the mock-infected control for both TIAR and TIA-1 (Fig 2.2.4 J, K). These data demonstrate that *Shigella* infection leads to a notable nuclear/cytoplasmic re-distribution of the two essential SG-proteins TIAR and TIA-1.

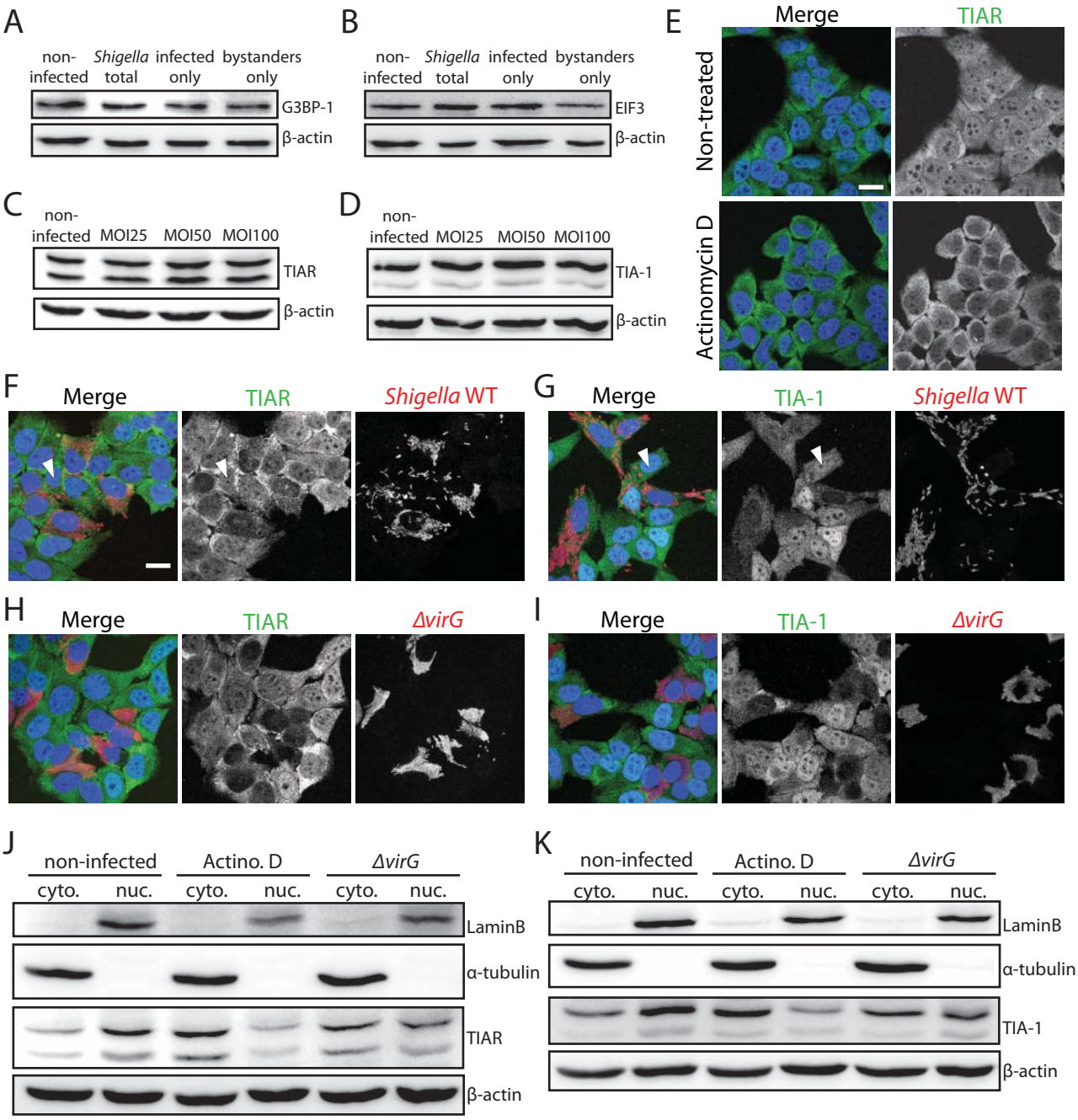
A
non-infected
Shigella total
infected only
bystanders only
G3BP-1
β-actin
B
non-infected
Shigella total
infected only
bystanders only
EIF3
β-actin
C
non-infected
MOI25
MOI50
MOI100
TIAR
β-actin
D
non-infected
MOI25
MOI50
MOI100
TIA-1
β-actin
E
Merge
TIAR
Non-treated
Actinomycin D
F
Merge
TIAR
Shigella WT
G
Merge
TIA-1
Shigella WT
H
Merge
TIAR
ΔvirG
I
Merge
TIA-1
ΔvirG
J
non-infected
Actino. D
ΔvirG
cyto.
nuc.
LaminB
α-tubulin
TIAR
β-actin
K
non-infected
Actino. D
ΔvirG
cyto.
nuc.
LaminB
α-tubulin
TIA-1
β-actin

Figure 2.2.4 *Shigella* infection induces nuclear depletion and cytosolic accumulation of TIAR and TIA-1

(A, B) Hela cells were infected with *Shigella* WT at MOI10 for 12h, and sorted into infected and non-infected bystanders. The levels of SG proteins (A) G3BP1 and (B) EIF3 was analyzed by Western blot in non-infected, total population of infected cells, and sorted cells. β-actin was used as loading control. (C, D) HeLa cells were infected with *Shigella* WT at MOI 25, 50, and 100 for 6h, and the level of (C) TIAR and (D) TIA-1 was analyzed in the total population of infected cells by Western blot. β-actin was used as loading control. (E) Non-treated or actinomycin D treated cells were fixed and stained for TIAR. (F, G) HeLa cells were infected with *Shigella* WT at MOI 10 for 6hpi, fixed, and stained for (F) TIAR or (G) TIA-1. White arrowheads indicate cells infected with few bacteria. (H, I) same as (F, G) except cells were infected with *Shigella ΔvirG* at MOI 50 for 3h. Scale-bar 25μm. (J, K) HeLa cells were mock-infected, treated with actinomycin D for 1h, or infected with *Shigella ΔvirG* at MOI 350 for 3h. (J) TIAR and (K) TIA-1 levels were analyzed in the nuclear and cytosolic fractions by Western blot, lamin B and α-tubulin were used to assess the purity of the nuclear and the cytosolic fractions, respectively; β-actin was used as loading control.

2.2.4 TIAR and TIA-1 RNA targets are upregulated during *Shigella* infection

TIAR and TIA-1 are major RNA-binding proteins with, at least partially, redundant functions. They contain three RNA recognition motifs (RRMs) and a C-terminal PRD domain (Kawakami et al., 1992). These proteins bind pre-mRNAs in the nucleus and regulate alternative splicing; it is also suggested that they regulate translation of mRNAs (Del Gatto-Konczak et al., 2000; Lopez de Silanes et al., 2005). Whereas their function in the nucleus as splicing regulators is well studied, their function in the cytoplasm is inferred from the study of a few mRNA ligands like the *tnf-α* mRNA (Gueydan et al., 1999; Piecyk et al., 2000). Although they shuttle between the nucleus and the cytoplasm, they lack a nuclear localization signal (Zhang et al., 2005). The removal of one of the RRMs restricts the protein to one or the other compartment suggesting an RNA-driven localization of the proteins (Zhang et al., 2005). However, this observation requires further investigation to establish the mechanisms of localization and functions of both proteins.

To investigate whether the RNA ligands of TIAR and TIA-1 are inducing their cytoplasmic localization during infection, a transcriptome-wide analysis was performed. On the one hand, the transcriptome of *Shigella* infected HeLa cells was analyzed by deep-sequencing to determine altered gene expression during infection. ~500 transcripts were upregulated (≥2-fold; cutoff >10 reads), and ~200 genes were downregulated (≥2-fold; cutoff >10 reads) in the total population of *Shigella* infected cells at 6hpi. On the other hand, the transcripts enriched by TIAR and TIA-1 in resting HeLa cells were analyzed using a dataset obtained from a prior study using the UV-crosslinking and immunoprecipitation (iCLIP) approach (Wang et al., 2010). Interestingly, when investigating the changes affecting TIAR and TIA-1 targets specifically, ~300 TIAR and ~230 TIA-1 targets were upregulated in *Shigella* infected cells (≥1.5-fold; enriched ≥8-fold; delimited by the magenta and green lines) (Fig 2.2.5 A, B; Table 4.2.1). Furthermore, among the genes downregulated during infection only ~100 transcripts were TIAR or TIA-1 ligands using the determined thresholds in the analysis (≥1.5-fold; ≥10-fold enrichment; delimited by the dashed-magenta and green lines) (Fig 2.2.5 A, B; Table 4.2.2). The results from these analyses show that among the upregulated transcripts during *Shigella* infection many are TIAR and TIA-1 ligands. This observation suggests that the upregulation of RNA targets during infection sequesters the proteins to the cytoplasm where they exhibit their regulatory function.

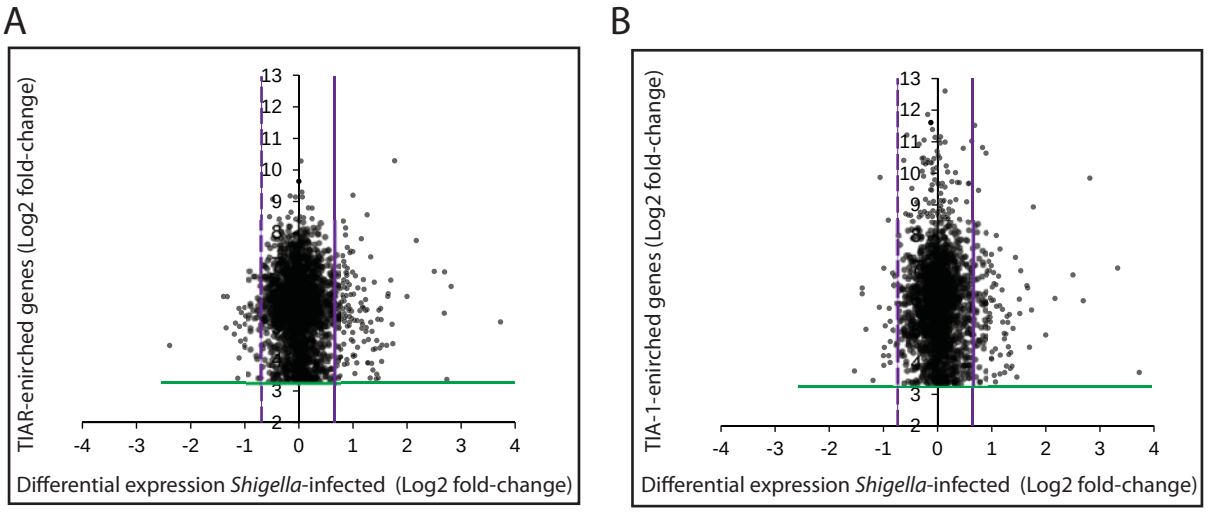

Figure 2.2.5 TIAR and TIA-1 RNA targets are upregulated during *Shigella* infection

(A, B) Scatter plot for the (A) TIAR or (B) TIA-1 enriched RNA targets (≥10-fold; green line) and genes differentially expressed during *Shigella* infection (≥2-fold, magenta line).

2.2.5 Concluding remarks

This study presents evidence for the role of SGs and the host RBPs TIAR and TIA-1 in bacterial infection. SGs play an important role in viral infection and anti-viral defense, but their role is not clear in bacterial infections. Findings from this study show that the cytosolic replication of bacterial pathogens interferes with SG-aggregation. Particularly, *Shigella* infection leads to the nuclear depletion and cytosolic accumulation of the SG-associated RBPs TIAR and TIA-1. A preliminary analysis suggests that *Shigella* infection induces an upregulation of TIAR/TIA-1 RNA targets, which is possibly the cause for the change in the localization of these proteins. Further work is required to establish the role of TIAR and TIA-1 during *Shigella* infection. For this purpose, the TIAR and TIA-1 interactome capture has been performed in infected cells, and the analysis is still ongoing. Future work on the TIAR and TIA-1 interactome will reveal the role of these proteins in the cytoplasm, in the regulation of RNA targets, and in the innate immunity of the host.

3 DISCUSSION

3.1 Stress-pathways as defense strategies against bacterial infection

3.1.1 Host stress-response contributes to the reinforcement of the epithelial barrier to *Shigella* intrusion

Profound mucosal inflammation is a hallmark of the infection by the enteric pathogen *Shigella*. It is part of the host innate immune response to the bacterial invasion of the mucosa, but it is believed to contribute to the thriving of *Shigella* (Sansonetti, 2001). Inflammation mounts the necessary defense programs, and in healthy individuals it eventually leads to the eradication of the pathogen and tissue repair, but at the same time it causes extensive stress in the tissues (Karin et al., 2006). These different aspects of inflammation are still not fully characterized, particularly whether the stress and its consequences are harmful or beneficial, and how it contributes to the outcome of infection. Results from this work present evidence that inflammatory stress cues could play a beneficial role in the host defense against *Shigella* infection. Indeed, this defense property was demonstrated in a minimal cell culture model, and was identified as an intrinsic response to stress in epithelial cells.

The exposure of epithelial cells to different inflammatory stress cues was sufficient to activate a stress response that lead to a striking decrease in *Shigella* adhesion to the cell surface. The simulation of an inflammatory environment experimentally consisted in mimicking the different conditions encountered by the epithelial cells during inflammation. Oxidative burst is the main inflammatory feature caused by immune cells such as neutrophils and monocytes; it consists in the release of large amount of ROS, for instance in the form of H_2O_2 (Wittmann et al., 2012). Other cues consist of hypoxia and cytokine stimulation such as with TNF-α (Colgan and Taylor, 2010). Results from this work demonstrate consistently that all these individual stress cues lead to the protection of cells against bacterial adhesion (Fig 3.1.1). Additionally, the intracellular replication of *Shigella* also induced a similar stress-response in cells, which inhibited re-infection by extracellular bacteria (Fig 3.1.2). This suggests that it is a general response to stress caused by infection or inflammation, which primes the cells against potential danger. It has been proposed that oxidative stress is perceived as a danger signal and can activate innate immune pathways, and here is the first demonstration showing that this type of stress enhances the defense of epithelial cells against colonization.

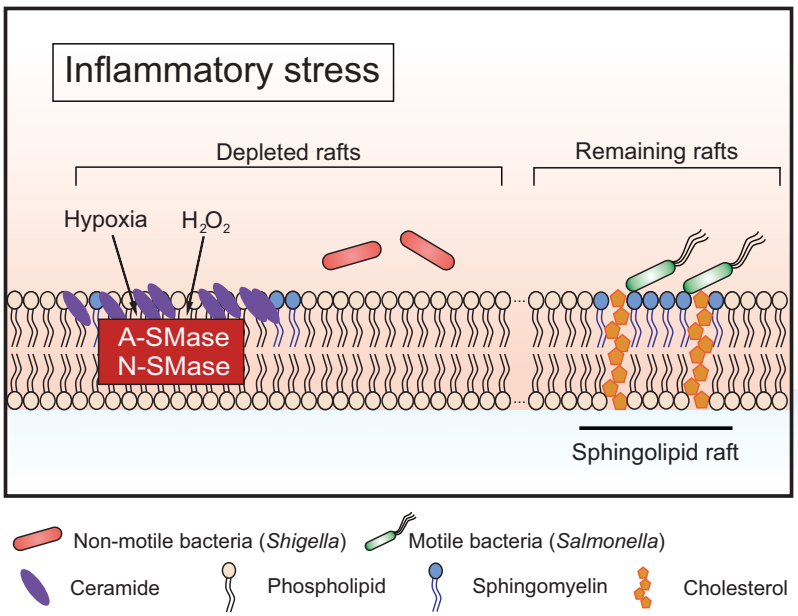

Figure 3.1.1 Model for the inhibition of bacterial infection by inflammatory stress cues

The stress response contributes to pathogen sensing and the activation of the innate and adaptive immune pathways. In this dissertation a new mechanism is established by which epithelial stress-response limits *Shigella flexneri* infection. The findings here demonstrate that response to stress such as hypoxia and hydrogen peroxide reinforces the barrier formed by epithelial cells to extracellular bacteria. ASM and NSM accumulate in membrane raft-domains in response to cellular stress and produce ceramide-rich platforms depleting anchorage sites on the cell surface, thus drastically hindering *Shigella* adhesion. However, motile pathogens such as *Salmonella* are able to bypass this limitation by swarming towards remaining docking sites.

3.1.2 Cellular stress leads to sphingolipid-raft depletion and impedes bacterial adhesion

Membrane raft domains mainly consist of sphingolipids and cholesterol defining specialized platforms for protein-protein and protein-lipid interactions (Lingwood and Simons, 2010). These platforms are essential for the regulation of signaling pathways important for all cellular processes (Simons and Toomre, 2000). Therefore, lipid-rafts are highjacked by different pathogens for adhesion, invasion, and other processes of pathogenesis (Manes et al., 2003). Adhesion to the epithelial surface is a defining step for virtually all enteric pathogens. The close entanglement with the epithelium or its invasion is the ultimate goal for pathogens to gain access to nutrient supplies and evade elimination, and this requires successful adhesion (Pizarro-Cerda and Cossart, 2006). Pathogens such as *Vibrio cholera*, enteropathogenic *Escherichia coli* (EPEC), and enterohaemorrhagic *E. coli* (EHEC) colonize the epithelial surface by establishing a broad association with epithelial cells (Croxen and Finlay, 2010; Ritchie and Waldor, 2009). Other bacteria evolved an intracellular lifestyle by invading epithelial cells such as *Shigella spp.*, *Salmonella spp,* and *Listeria monocytogenes* (Kumar and Valdivia, 2009; Ray et al., 2009). Interestingly, for all these strategies of colonization adhesion is an essential common step, which highlights the importance of the findings obtained in this study. Data from this work demonstrate that epithelial cells react intensively to stress cues, and remodel the cell membrane by depleting sphingomyelin. This finding opens new perspectives on the capacity of epithelial cells to limit pathogen intrusion in response to stress. The results here show that the adhesion of *Shigella* and *Salmonella* is inhibited by the stress-induced modification of the membrane, and this could possibly apply to other pathogens. Many pathogens require cellular receptors and surface proteins like integrins that are associated with sphingolipid-rafts (Manes et al., 2003). Additionally, sphingolipid-rafts form caveolae, which are structures important for the docking of bacteria to the cell surface (Hoffmann et al., 2010). Many studies have demonstrated that the disruption of membrane microdomains interferes with pathogen colonization (Lafont et al., 2004; Riethmuller et al., 2006).

Shigella lacks fimbriae and flagella, and only two T3SS effectors VirG and IpaB have been proposed to function as adhesins (Brotcke Zumsteg et al., 2014; Yang et al., 2005). However, it has been shown that *Shigella* utilizes the cellular filopodia to achieve higher

success rate of capture and cell surface association (Romero et al., 2011). Though this strategy is the main mechanism that increases *Shigella* association with the cells, it is still dependent on the availability of lipid rafts on the cell surface as shown by the results in this study. Whereas oxidative stress and TNFα exposure of cells has been shown to actually induce filopodia formation (Decourt et al., 2009; Wojciak-Stothard et al., 1998), the data here shows an inhibition of adhesion under these conditions. This suggests that despite inducing capture and retraction by filopodia, *Shigella* fails to adhere to the cell surface of stressed cells. Notably, *Shigella* requires the CD44 surface receptor and α5β1 integrins to adhere and invade cells; these proteins are known to be widely associated and dependent on membrane lipid-rafts (Ponta et al., 2003; Wary et al., 1998; Watarai et al., 1996).

Although *Salmonella* is weakly adhesive and relies on the T3SS for successful cell invasion similar to *Shigella*, it uses different strategies for adhesion (Bishop et al., 2008; van Asten and van Dijk, 2005). *Salmonella* has not been reported to interact with filopodia, additionally it expresses pili, fimbriae, and flagella, all structures involved in adhesion that are missing in *Shigella* (Swidsinski et al., 2007; Yang et al., 2005). Interestingly, non-motile *Salmonella* mutants were equally restricted from adhering to stressed cells, showing that *Salmonella* also requires the same membrane lipid-rafts. Though *Shigella* and *Salmonella* adopt distinct adhesion mechanisms, the abolishment of *Salmonella* motility was the only factor differentiating its capacity for adhering to stressed cells. This demonstrates that both bacteria share a similar requirement for membrane sphingolipid-rafts to adhere successfully. This supports the fact that despite the different strategies of bacterial adhesion, membrane microdomains are universally required. Furthermore, stress is a condition accompanying most enterobacterial infections, suggesting membrane remodeling could be a common strategy of defense for epithelial cells against pathogens.

Another possible role for the stress-induced barrier remodeling is the restriction of commensal bacteria translocation through the epithelium. Because the mucus layer is reduced during inflammation, there are more bacteria sampling the epithelial surface (Swidsinski et al., 2007). It is possible that the depletion of sphingolipid-rafts limits the docking of such bacteria and their potential translocation. Interestingly *Campylobacter jejuni* has been shown to induce the translocation of non-invasive *E.coli* during infection (Kalischuk et al., 2009). Additionally, this phenomenon of cooperative invasion has been observed for *Salmonella* (Lorkowski et al., 2014). Thus, the depletion of docking sites

when the epithelium is challenged might restrict excessive translocation of 'cargo-like' commensals.

3.1.3 A defense strategy involving membrane remodeling by stress-activated sphingomyelinases

The regulation of the levels of sphingolipids, particularly sphingomyelin one of the major components of lipid-rafts, is achieved through the activation of sphingomyelinases (Marchesini and Hannun, 2004). The activation of sphingomyelinases is a rapid response leading to immediate changes in the membrane; a few minutes of stimulation by the cytokine TNF-α leads to a significant depletion of sphingomyelin (this study; (Wiegmann et al., 1994). There are four putative genes (*smpd1-4*) in humans encoding for sphingomyelinases, with a demonstrated function for three *smpd1-3*. *Smpd1* encodes for the acid sphingomyelinase (ASM), and *smpd2* and *3* encode for the neutral sphingomyelinases (NSM-1 and NSM-2, respectively). Most of the studies so far focused on ASM since a mutation in the *smpd1* gene encoding ASM in humans causes the Niemann-Pick syndrome, a grave and fatal disease (Schuchman and Wasserstein, 2015). A susceptibility to bacterial infections has been observed for Niemann-Pick patients and animal models (Ng and Griffin, 2006; Schuchman, 2010). Specifically, ASM-knockout mice or macrophages are more susceptible to infection with *Listeria*, *E.coli*, and *Salmonella* (Falcone et al., 2004; McCollister et al., 2007; Utermohlen et al., 2003). No clear explanation is provided, but it is suspected to be due to lysosomal dysfunction in macrophages due to the role of ASM in lysosomal function (Marchesini and Hannun, 2004). Whereas in the case of *Salmonella* it could be a plausible explanation because it requires the endo/lysosomal network for replication; in the case of *Listeria* it is unlikely because it resides in the cytoplasm and efficiently avoids autophagy (Mitchell et al., 2015; Yoshikawa et al., 2009). The findings here propose an alternative explanation that the absence of ASM could be leading to a higher susceptibility to *Listeria* by being unable to restrict bacterial adhesion and entry. Importantly, *Listeria* similar to *Shigella* is non-motile in the human host because it represses the flagellar operon at 37°C (Kathariou et al., 1995). Furthermore, the internalization of *Yersinia enterocolitica* has been shown to be reduced in Caco-2 cells exposed to hypoxia in a lipid-raft dependent manner (Zeitouni et al., 2016). Notably, *Yersinia* represses the flagella operon at 37°C as well (Badger and

Miller, 1998). Thus, the findings in this dissertation suggest that sphingomyelinases might play a role in protecting against the infection by various non-motile pathogens.

Some pathogens might have evolved to utilize this response to stress for their own benefit. *Pseudomonas aeruginosa* infection benefits from a deregulated ASM activity in cystic fibrosis patients (Becker et al., 2010a; Grassme et al., 2003). Studies have shown that cystic fibrosis patients and mice models are more susceptible to *P. aeruginosa* due to a defective activation of ASM during infection and the massive production of ceramide. Ceramide production in the respiratory epithelial cells contributes to pathogen internalization and induction of strong inflammation, which are beneficial for the pathogen (Becker et al., 2010b; Grassme et al., 2003; Teichgraber et al., 2008; Yu et al., 2009). The use of ASM inhibitors like amitryptiline to counteract ceramide production strongly hindered *P. aeruginosa* infection (Becker et al., 2010c). Surprisingly, the same cystic fibrosis mice models were not susceptible to *Streptococcus pneumoniae*, another pathogen prevailing in lung infections (Teichgraber et al., 2008). This example illustrates that *P. aeruginosa* benefits from the activation of ASM and the production of ceramide, whereas this pathway serves as a defense against *S. pneumoniae*.

The epithelial cell model used in this study are non-polarized cells from colon and cervical origin. Lipid-rafts in non-polarized cells are distributed and constitute around 40-50% of the membrane, whereas in polarized epithelial cells the rafts cluster mainly at the apical pole (Schuck and Simons, 2004). It is possible that the depletion of sphingolipid-rafts in polarized cells is more rapid and effective because the translocation of sphingomyelinases is guided to one pole of the cells. Intestinal epithelial cells are highly polarized forming a distinct apical side and a basolateral side (Simons and Ikonen, 1997). The apical side is particularly rich in sphingolipids and cholesterol exhibiting lipid raft clustering (Cao et al., 2012; Schuck and Simons, 2004). It has been long known that during mucosal inflammation pathogen invasion of the epithelium specifically from the apical side is hindered (Sansonetti, 2004), findings obtained here provide a mechanistic explanation to how this inhibition might occur. Notably, the activation of sphingomyelinases in response to stress has been demonstrated in many different cell types like T-cells, macrophages, cardiomyocytes, endothelial cells, hepatocytes, and neuronal cells (Marchesini and Hannun, 2004). Whether the findings from this study apply to infection of other tissues beyond the epithelium remains to be verified.

3.1.4 To be motile or not to be

In this study, the comparison of *Shigella* and *Salmonella* revealed that the infection of stressed cells was compromised in the absence of motility. *Salmonella* requires similar membrane domains to *Shigella* for adhesion, but it is able to compensate for the lack of adhesion-sites by swarming. On the one hand, *Shigella* has acquired mutations abrogating the expression of flagella, despite motility providing strong advantages for the extracellular population; but flagella is a potent antigen that activates the extracellular TLR5 and intracellular PRRs (Janeway and Medzhitov, 2002). On the other hand, adhesion-site depletion seems not to affect *Salmonella* significantly because of flagellar motility, but TLR5 activation is crucial for *Salmonella* clearance (Feuillet et al., 2006; Gewirtz et al., 2001). Thus, *Shigella* reduces surface eradication by TLR5 signaling and promotes its intracellular lifestyle, whereas *Salmonella* preferentially promotes the invasion process. This observation similarly applies to pathogens that shutoff flagella expression in the host, such as *Listeria* and *Yersinia*, probably to promote the intracellular lifestyle, but in consequence compromise the extracellular population. Thus, findings from this work demonstrate a host defense mechanism that limits the extracellular population and presents a clear disadvantage to non-motile pathogens.

3.1.5 A defense strategy involving the propagation of the danger signal into adjacent cells

The conditions inducing NSM and ASM activation have an intriguing aspect that involves propagation. For instance, TNFα signaling is known to spread through a paracrine route and stimulate surrounding cells (Lee et al., 2009). Additionally, hypoxia and oxidative stress during colonic inflammation can propagate to the neighboring tissues (Colgan and Taylor, 2010). Finally, p38 and JNK signaling has been shown to propagate from *Shigella* infected to non-infected cells in a gap-junction dependent manner (Kasper et al., 2010). Indeed, many studies suggest a capacity of cells to propagate the stress response to bystander non-stressed cells (Chovatiya and Medzhitov, 2014). The results here show that the infection of the epithelial cell layer with *Shigella* leads to the production of ceramide in all the cells and particularly in bystander cells. This demonstrates that the activation of the sphingomyelinases happens in adjacent cells,

which indicates the propagation of the stimulus. Strikingly, cells with replicating bacteria exhibited lower ceramide production and ASM activation than the neighboring bystanders. This can be explained by the dependence of the sphingomyelinase activation on p38, which is inhibited in the invaded cell by the secretion of the *Shigella* effector OspF (Li et al., 2007). *Shigella* seems to counteract sphingomelinase activation through blocking p38 activation, but not in bystander cells. This shows that cells have evolved a way to propagate the danger signal into the non-infected bystanders where the bacterial proteins cannot counteract the immune signaling. Thus, the propagation of the MAPK signaling not only induces IL-8 production in bystander cells (Kasper et al., 2010), but also leads to sphingomyelinase activation and membrane remodeling as shown in this study.

In the experimental settings of this study, the total population of cells challenged with *Shigella* was able to hinder re-infection by extracellular bacteria. This phenomenon is likely to impose a strong bottleneck on the extracellular bacteria *in vivo*, where only intercellular propagation is possible. An interesting observation supporting this interpretation is the observed confinement of *Shigella* infection in the large bowel, predominantly in the rectosigmoid area (Speelman et al., 1984), whereas *Salmonella* can propagate more extensively and become systemic (de Jong et al., 2012), probably due to its ability to overcome the restriction imposed by the propagation of epithelial membrane modification.

3.1.6 Conclusion and perspectives

It has been long known that mucosal inflammation hinders pathogen invasion of the epithelium specifically from the apical side (Sansonetti, 2004). The findings described in this dissertation provide mechanistic evidence to how this inhibition occurs, by unraveling a strategy involving physical modification of the cell surface. These findings reveal an intrinsic property of the epithelial tissue that provides rapid and extensive protection against the transgression of the first barrier against pathogen colonization. This opens new perspectives on our understanding of innate immune mechanisms, which thus far have been considered to depend exclusively on specific receptors and the consequent activation of immune genes. In this study, the danger signal received is both immune stimulation by a cytokine, and stress stimulation. This further supports the emerging recognition of DAMPs as immune stimulators, which lead to protective responses.

The significance of these findings for the overall outcome of infection *in vivo* remains to be elaborated. The lack of good animal models reproducing the disease caused by *Shigella* in humans is a drawback in this pursuit. The available animal models, such as the ligated rabbit ileal loop or the guinea pig, are effective but are still not ideal for genetic modifications. Nevertheless, with the emergence of new genome editing technologies such as the CRISPR/Cas system there is a prospect for the successful translation of the *in vitro* findings to the more informative *in vivo* models. With the currently available animal models, one can verify the accumulation of ceramide, the activation of the sphingomyelinases, and the activation of p38 in the epithelial intestinal tissue of infected animals with *Shigella* using immunohistochemistry staining. Such data would be first evidence of the occurrence of these changes during *Shigella* infection, and might suggest the relevance of this phenomenon in the infection process.

The comparison of *Shigella* and *Salmonella* provides insight on how related enteric pathogens evolve different strategies to circumvent one or the other host defense mechanism. Though motility has been known to provide advantage for *Salmonella in vivo*, this study demonstrates an additional unrecognized advantage for the motile pathogen. This strategy could apply to other pathogen such as *Pseudomonas aeruginosa* or *Clostridium difficile*. The defense strategy delineated by the findings here suggests a general obstacle for non-motile pathogens showing that the evolutionary choice of pathogens favors evading one strategy while becoming susceptible to another defense strategy. Finally, the realm of innate immunity still conceals various defense strategies that need to be identified to better understand the evolutionary arms race between the pathogens and their host. This will allow further understanding of the infection process leading to improved approaches for the struggle against infectious diseases.

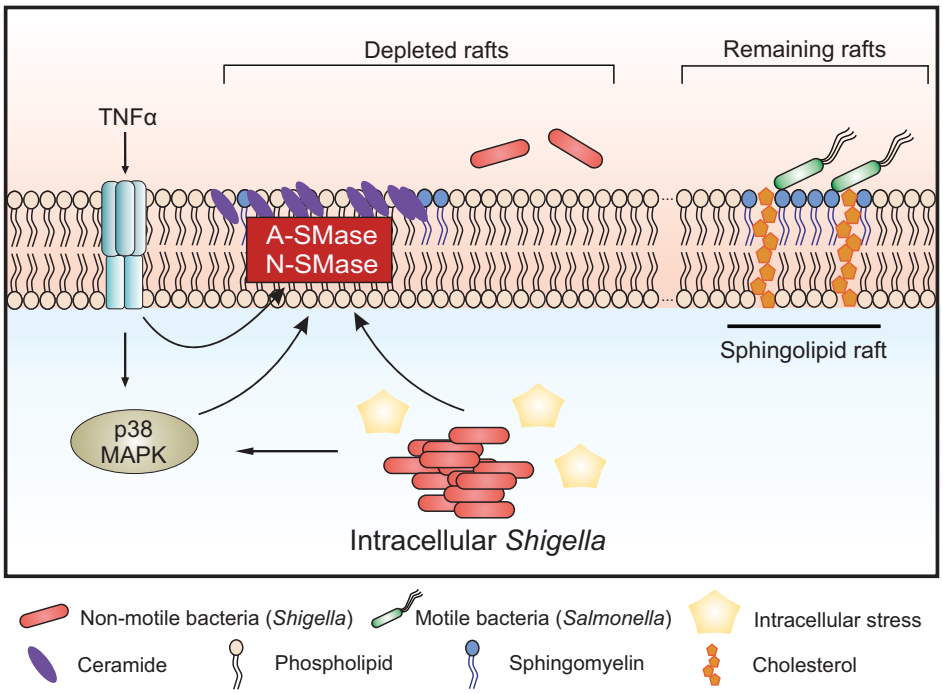

Figure 3.1.2 Model for the inhibition of re-infection by intracellular bacterial replication

Intracellular replication of *Shigella* induces membrane-raft remodeling and inhibition of re-infection by extracellular bacteria. This results from the activation of ASM and NSM in response to cellular stress induced by the replicating *Shigella*.TNF-α secretion and p38 activation by infected cells promote the activation of ASM and NSM. this leads to a strong inhibition of the non-motile pathogen *Shigella* but not the motile pathogen *Salmonella*, which is able to anchor at remaining sites.

3.2 Involvement of SGs and TIAR/TIA-1 in the infection by cytosolic bacteria

3.2.1 *Shigella* infection inhibits the aggregation of SGs in response to exogenous stress

SG-assembly is a widely conserved response to cellular stress in eukaryotes. Studies have established an evident role for SGs in infection processes, particularly in viral infections. Various mechanisms of interference with SGs have been described for a wide number of viruses (Reineke and Lloyd, 2013). Interestingly, a few recent studies have demonstrated a possible role for SGs in bacterial infections (Eulalio et al., 2011; Tattoli et al., 2012; Vonaesch et al., 2016). Results from this study are consistent with a recent report, showing that *Shigella* infection interferes with generic SG-assembly (Vonaesch et al., 2016). SG-formation was inhibited in infected cells in response to variable stresses and could be observed with many classical SG-markers like EIF3, G3BP-1, TIAR, and TIA-1. One of the stresses tested is H_2O_2, in response to which SGs assemble independently of the canonical pathway involving EIF2α phosphorylation (Emara et al., 2012). SGs in response to H_2O_2 were similarly inhibited in infected cells suggesting that the inhibition occurs downstream the EIF2α pathway, possibly affecting the aggregation process directly (Fig 3.2.1). In some cases granules of small size could still be observed in infected cells suggesting that smaller complexes are able to form but the nucleation of larger granules is inhibited. This is in line with the recent study showing that *Shigella* infection inhibited pateamine A-induced SGs, which is also independent of EIF2α phosphorylation (Vonaesch et al., 2016). In fact, it has been shown that *Shigella* induces amino starvation in infected cells leading to an increase in the phosphorylation of EIF2α by GCN2 (Tattoli et al., 2012; Vonaesch et al., 2016).

There are several possibilities for the inhibition of SGs aggregation downstream EIF2α. The nucleation of SGs into larger complexes requires active transport on the microtubule network (Nadezhdina et al., 2010), and there are ~100 factors required for SG assembly (Ohn et al., 2008). Disruption of microtubules with nocodazole for instance (Nadezhdina et al., 2010), cleavage of G3BP by the poliovirus 3C proteins (White et al., 2007), or the sequestration of G3BP by Chikungunya virus protein Nsp3 (Fros et al., 2012), all lead to SG-inhibition. These examples illustrate the diversity of ways how SG assembly can be affected. Vonaesch *et al* showed an increase in tubulin acetylation during *Shigella* infection and proposed a microtubule-related mechanism for the inhibition of

SGs. However, not enough evidence has been provided for the latter hypothesis, thus the mechanism of interference remains to be elucidated.

3.2.2 Intracellular cytoplasmic replication of bacterial pathogens interferes with SG-assembly

Only invasive *Shigella* leads to the inhibition of SGs; non-invasive or hyper-adhesive strains are not able to induce the phenotype (Vonaesch et al., 2016). However, solely invasion by *Shigella ΔipaB*/invasin in the absence of a functional T3SS was not sufficient to inhibit SGs. *Shigella* virulence is entirely dependent on the plethora of effector proteins secreted by the T3SS, which manipulate numerous host functions. Nevertheless, the phenotype of SG-inhibition could not be attributed to any of the 30 effectors of *Shigella*. It is however possible that a yet unidentified effector or one of the effectors essential for T3SS function is responsible for the phenotype. Additionally, it is common that effectors execute redundant functions, thus the absence of one could be compensated by another. For example, *Salmonella* can induce its uptake by cells through the action of 3 effectors SopE, SopE2, and SopB, which exhibit a redundant function to activate Rho GTPases (Hardt et al., 1998; Stender et al., 2000).

From another angle, the results demonstrated a dependence of the inhibition of SGs on bacterial replication in the cytoplasm (Fig3.2.1). This was not dependent on the bacterial species, considering that *Shigella*, *Listeria*, and a *Salmonella* cytosolic mutant all induced this phenotype. Due to the divergence of these pathogens particularly the Gram-positive *Listeria*, it is likely that the mechanism is conserved among various bacterial species. The data obtained does not differentiate between the mere presence of bacteria in the cytosol or the replication itself as a cause for SG-inhibition. The phenotype could be induced by the sensing of universal PAMPs from cytosolic bacteria like DNA, RNA, or bacterial metabolites such as cyclic-di-GMP (Burdette et al., 2011). This assumption suggests that the inhibition is a host response rather than a pathogen-exerted process. The evident explanation for such a host response is related to the main role of SGs, which is providing resilience to stress and promoting cell survival (Takahashi et al., 2013). Indeed, a study showed recently that a combination of ER-stress with an acute oxidative stress lead to the oxidation of TIA-1 inhibiting SGs, and consequently promoting apoptosis (Arimoto-Matsuzaki et al., 2016). It is possible that the detection of a pathogen in the

cytosol promotes programmed cell death by inhibiting SGs particularly that this phenotype occurs in infected cells only and not in bystander cells, where SGs form favorably.

3.2.3 *Shigella* infection favors the cytosolic function of TIAR and TIA-1

Further investigation of the mechanisms of interference with SGs by looking at various essential SG-proteins showed that the distribution of both RBPs TIAR and TIA-1 is altered in *Shigella* infected cells (Fig3.2.1). These two proteins reside in both the nucleus and the cytoplasm where they exert distinct functions. The function of TIAR and TIA-1 as alternative splicing regulators in the nucleus is well established and the RNA ligands as well as the binding-sites have been profiled (Forch et al., 2000; Le Guiner et al., 2001; Wang et al., 2010). Some evidence exists on the function of these proteins in the cytoplasm suggesting a role in translation regulation and stability of target mRNA transcripts, but this knowledge is based on a few model transcripts (Carrascoso et al., 2014; Gueydan et al., 1999; Mazan-Mamczarz et al., 2006).

TIAR and TIA-1 are 80% similar proteins containing three RRM domains and a PRD aggregation C-terminal domain (Kawakami et al., 1992). Characterization of the RNA sequence determinants of TIAR and TIA-1 *in vitro* and *in vivo* showed that they bind to AU-rich elements (AREs) in the 3'UTR and U-rich sequences in introns (Gueydan et al., 1999; Wang et al., 2010). Additionally, RRM3 has been shown to preferentially bind C-rich sequences (Cruz-Gallardo et al., 2014; Kim et al., 2007). Most of the studies investigating TIAR and TIA-1 ligands have analyzed the total protein population not distinguishing between the interactions in the different compartments. Interestingly, the analysis of global RNA ligands and sequence determinants for alternative splicing for both proteins by iCLIP revealed that 60% of the cDNA reads mapped to introns and only 22% mapped to 3'UTRs and non-coding RNAs, but the highest cDNA density was found at the latter sites, exceeding genome average (Wang et al., 2010). This shows that there is a high enrichment of 3'UTRs by these proteins despite the greater number in pre-mRNA targets, which might indicate a higher affinity for ARE-containing 3'UTRs (Wang et al., 2010). The same study showed that both protein have overlapping specificities and RNA targets. Taken together, these observations suggest a major and redundant role for these two proteins in the cytoplasm by binding to the 3'UTR; this however remains to be elucidated

in detail. In this work, the observation that both TIAR and TIA-1 accumulate in the cytoplasm in *Shigella* infected cells suggests that these proteins engage in the regulation of translation and stability of the cytoplasmic mRNA targets (Fig 3.2.1). This possibly leads to consequences on the global post-transcriptional gene regulation in the infected cell.

It has been shown that TIAR and TIA-1 nuclear/cytosolic shuttling is guided by the RRMs, which suggests an RNA-dependent distribution (Zhang et al., 2005). For instance, the treatment of cells with a transcription inhibitor actinomycin D leads to the nuclear depletion and the strong accumulation of both proteins in the cytoplasm (Zhang et al., 2005). This suggests that upon transcriptional shutoff and the decrease of pre-mRNA targets in the nucleus the proteins are driven into the cytosol by mRNAs having longer half-lives. Furthermore, such cytoplasmic accumulation of TIAR and TIA-1 has been reported previously during Herpes simplex virus 1 infection, but no mechanism has been proposed (Esclatine et al., 2004). Here, during *Shigella* infection many TIAR and TIA-1 mRNA targets have been found to be highly upregulated, it is possible that the corresponding mRNAs accumulate in the cytoplasm sequestering the proteins. This proposes an explanation for the change in the partition of these proteins during *Shigella* infection. This study presents the first attempt at characterizing the TIAR and TIA-1 RNA-target profile during infection and the function of the proteins in the cytoplasm.

Few studies have investigated the role of TIAR and TIA-1 in the cytoplasm. TIAR has been shown to repress the translation of a few mRNA targets in an ARE-dependent manner such as *tnf-α*, *cox-2*, and the beta(2)-adrenergic receptor (Cok et al., 2003; Gueydan et al., 1999; Kandasamy et al., 2005). A study has provided further details on this function by the analysis of purified TIAR RNP complexes and the characterization of a few targets involved in translational control eIF4A, eIF4E, eEF1B, and c-Myc (Liao et al., 2007; Mazan-Mamczarz et al., 2006). The translation of these targets was upregulated in the absence of TIAR in resting or UV-exposed cells. In the same study, an increase of the association of TIAR with these mRNAs has been observed during stress and in consequence a stronger translational repression even after the disassembly of SGs. Additionally, it has been proposed that the nuclear-cytoplasmic shuttling of RBPs, including TIAR and TIA-1, is necessary for the regulation of gene expression during stress, and that SGs are involved in this trafficking (Yang et al., 2014). With this knowledge, it is clear that TIAR and TIA-1 regulate their targets at the post-transcriptional level in the cytoplasm and that this role becomes more extensive during stress. In contrast, a study

showed that the TIAR RRM3 C-rich targets dissociate from the protein upon UV-stress (Kim et al., 2007). The different affinities of the different RRMs might lead to different target association during variable conditions of stress or infection for instance, and thus affect the localization of these proteins. Therefore, it remains to be elucidated whether these proteins influence the gene expression outcome during *Shigella* infection. Interestingly, the levels of some mRNA targets of TIAR and TIA-1 were found to be decreased upon knockdown of these proteins suggesting that they might not only regulate the translation but also affect the stability of target mRNAs (data not shown).

3.2.4 Conclusion and perspectives

In this dissertation, the interference of *Shigella* infection with the host stress response was investigated. *Shigella* infection was found to inhibit SG-assembly at the level of larger complex-nucleation stage. This inhibition was dependent on the cytosolic replication of the bacteria (Fig 3.2.1). Interestingly, this phenomenon is independent of the bacterial species found in the cytoplasm strongly suggesting that it is part of the host response. The hypothesis proposed by this finding is that the detection of bacterial PAMPs in the cytoplasm inhibits SGs to promote host cell death and pathogen restriction.

The inhibition of SGs could be driven by the sequestration of the SG-associated RBPs TIAR and TIA-1 by the upregulation of their RNA targets during infection (Fig 3.2.1). TIAR and TIA-1 have been shown to be essential for SG-assembly, thus the alteration of the ligands of these proteins might affect SG formation (Gilks et al., 2004; Kedersha et al., 1999). Finally, some preliminary data from this work along with other studies suggest a role for TIAR and TIA-1 in the cytoplasm that involves the regulation of translation and stability of target mRNAs.

These findings show that during *Shigella* infection there are major alterations of the host stress response. It remains to be fully elucidated how these alterations benefit the host and reflect on the infection process. Data obtained here shed light on the importance of the long studied TIAR and TIA-1 proteins in the post-transcriptional regulation of the stress response and the innate immune response.

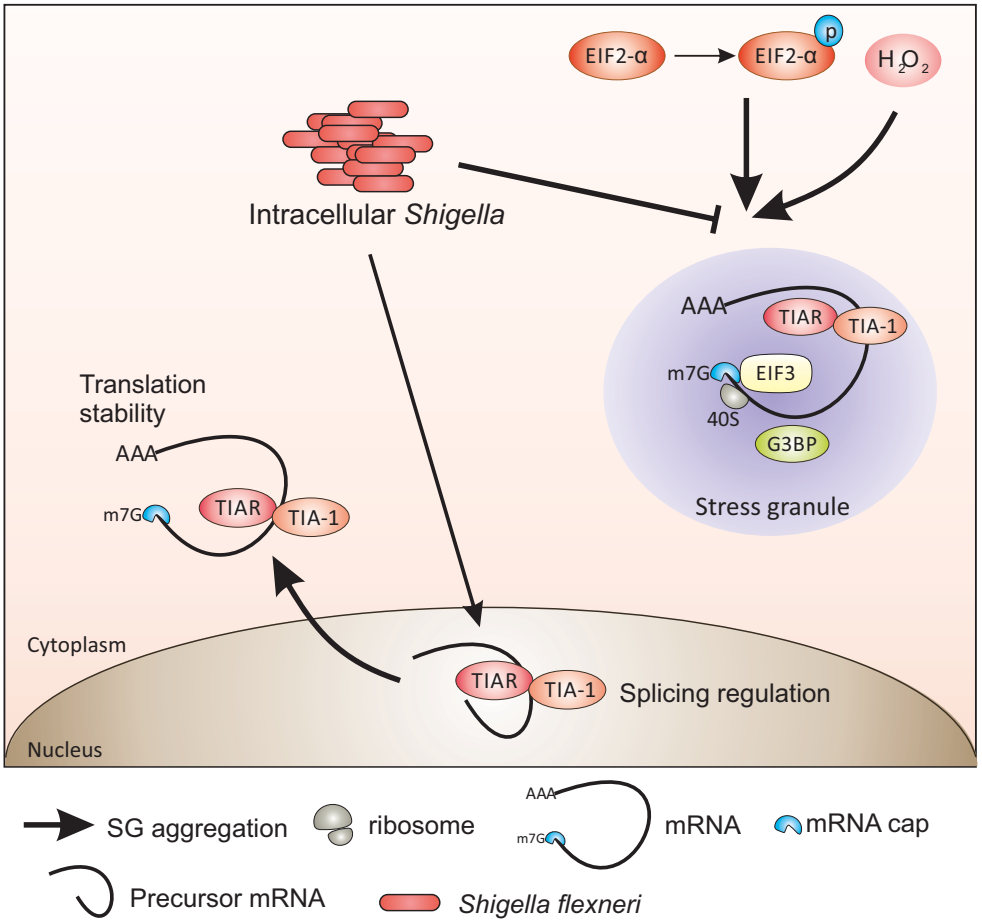

Figure 3.2.1 Model for the inhibition of SG-aggregation and induction of TIAR/TIA-1 cytoplasmic accumulation by intracellular *Shigella*

Intracellular *Shigella* replication inhibits generic SG-aggregation by interfering with the nucleation of large granules downstream EIF2α phosphorylation. *Shigella* induces the cytoplasmic accumulation of the SG-RBPs TIAR and TIA-1. In the nucleus, TIAR and TIA-1 play a role in splicing regulation, and in the cytoplasm these proteins regulate translation and stability of their RNA targets. These RBPs might play an important role in the post-transcriptional regulation of genes involved in the defense against *Shigella* infection.

4 APPENDIX

Supplementary figures

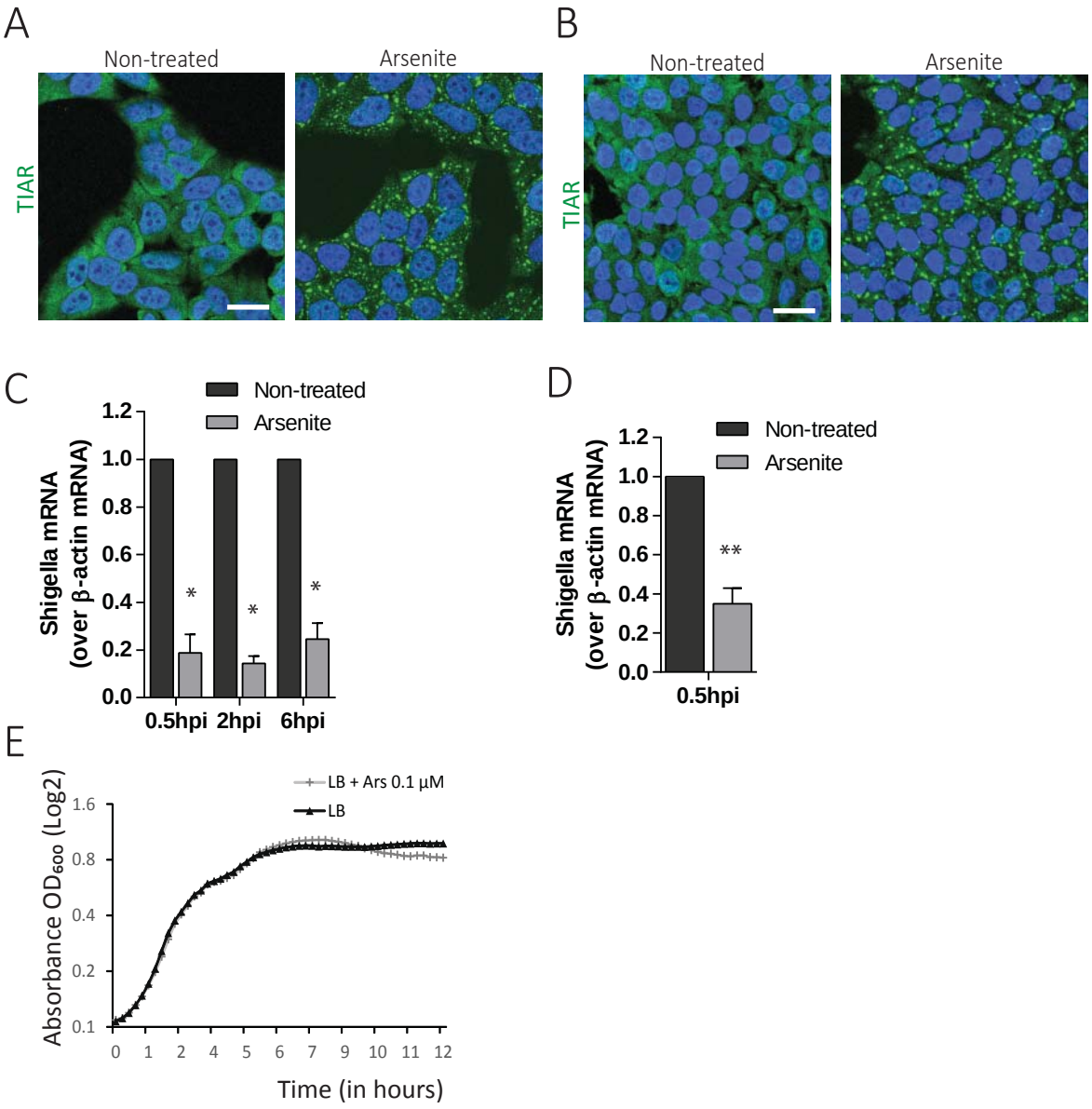

Figure 4.1 *Shigella* infection of arsenite stressed epithelial cells is inhibited

SGs were detected in (A) HeLa or (B) HCT-8 cells using a specific anti-TIAR antibody (green). Nuclei were stained with Hoechst. (C) Quantification of the intracellular *Shigella* by qRT-PCR in HeLa cells. The GFP mRNA was quantified for bacterial load and β-actin was used as a control for cell number. (D) Same as in (B) in HCT-8 cells (E) Growth curves of *Shigella* WT in LB or LB with arsenite. Results are shown as mean ± s.e.m; n ≥ 3, *p<0.05, **p<0.01, two-tailed Student's t-test. Scale-bar 25µm.

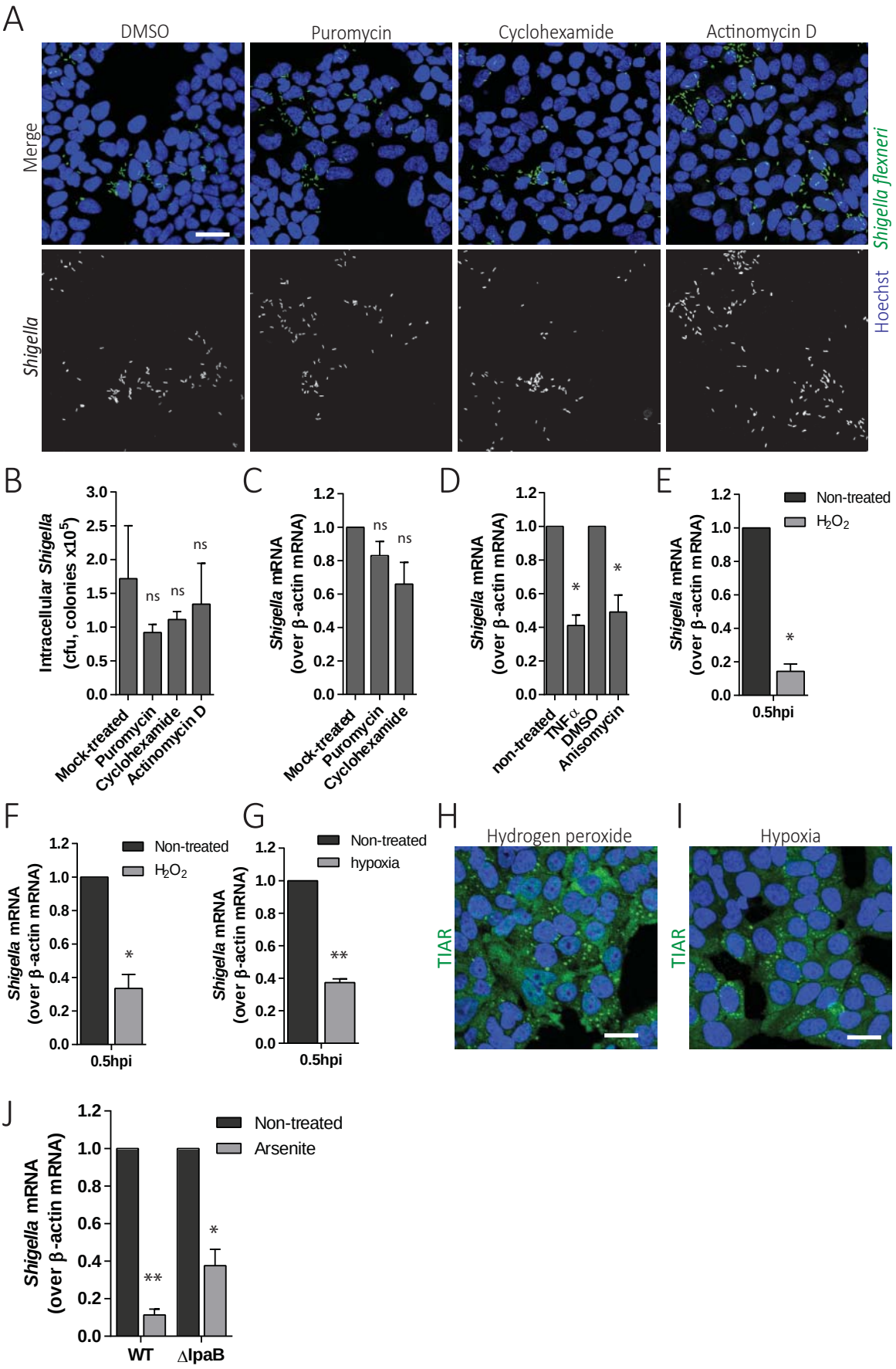
A
DMSO
Puromycin
Cyclohexamide
Actinomycin D
Merge
Shigella
Shigella flexneri
Hoechst
B
Intracellular Shigella (cfu, colonies x10^5)
ns
Mock-treated
Puromycin
Cyclohexamide
Actinomycin D
C
Shigella mRNA (over β-actin mRNA)
ns
Mock-treated
Puromycin
Cyclohexamide
D
Shigella mRNA (over β-actin mRNA)
non-treated
TNFα
DMSO
Anisomycin
E
Non-treated
H2O2
0.5hpi
F
Non-treated
H2O2
0.5hpi
G
Non-treated
hypoxia
0.5hpi
H
Hydrogen peroxide
TIAR
I
Hypoxia
TIAR
J
Non-treated
Arsenite
WT
ΔIpaB

Figure 4.2 *Shigella* infection of epithelial cells experiencing oxidative stress is inhibited

(A) Representative images of infections in control (DMSO) HeLa cells or treated with puromycin, cyclohexamide, or actinomycin D. Cells were fixed and stained with Hoechst at 0.5hpi. Scale-bar 50 μm. (B) CFU quantification and (C) qRT-PCR quantification of the infections in (A). Actinomycin D treatment (C) was excluded because of its global effect on cellular RNA abundance. (D) qRT-PCR quantification of *Shigella* infection at 0.5hpi in HeLa treated with TNF-α (compared to mock-treated), or anisomycin (compared to DMSO). (E, F) qRT-PCR quantification of infections in (E) HeLa or (F) HCT-8 treated with H_2O_2 for 3h. (G) qRT-PCR quantification of infections in HeLa cells after exposure to hypoxia for 15h. (H, I) SGs stained with an anti-TIAR antibody (green) in (H) HCT-8 treated with H_2O_2 for 3h or (I) HeLa exposure to hypoxia for 15h. Scale-bar 25 μm. (J) qRT-PCR quantification of bacteria bound to cells in control or arsenite treated cells. Results are shown as mean ± s.e.m; n ≥ 3, *p<0.05, **p<0.01, ns: non-significant; two-tailed Student's t-test.

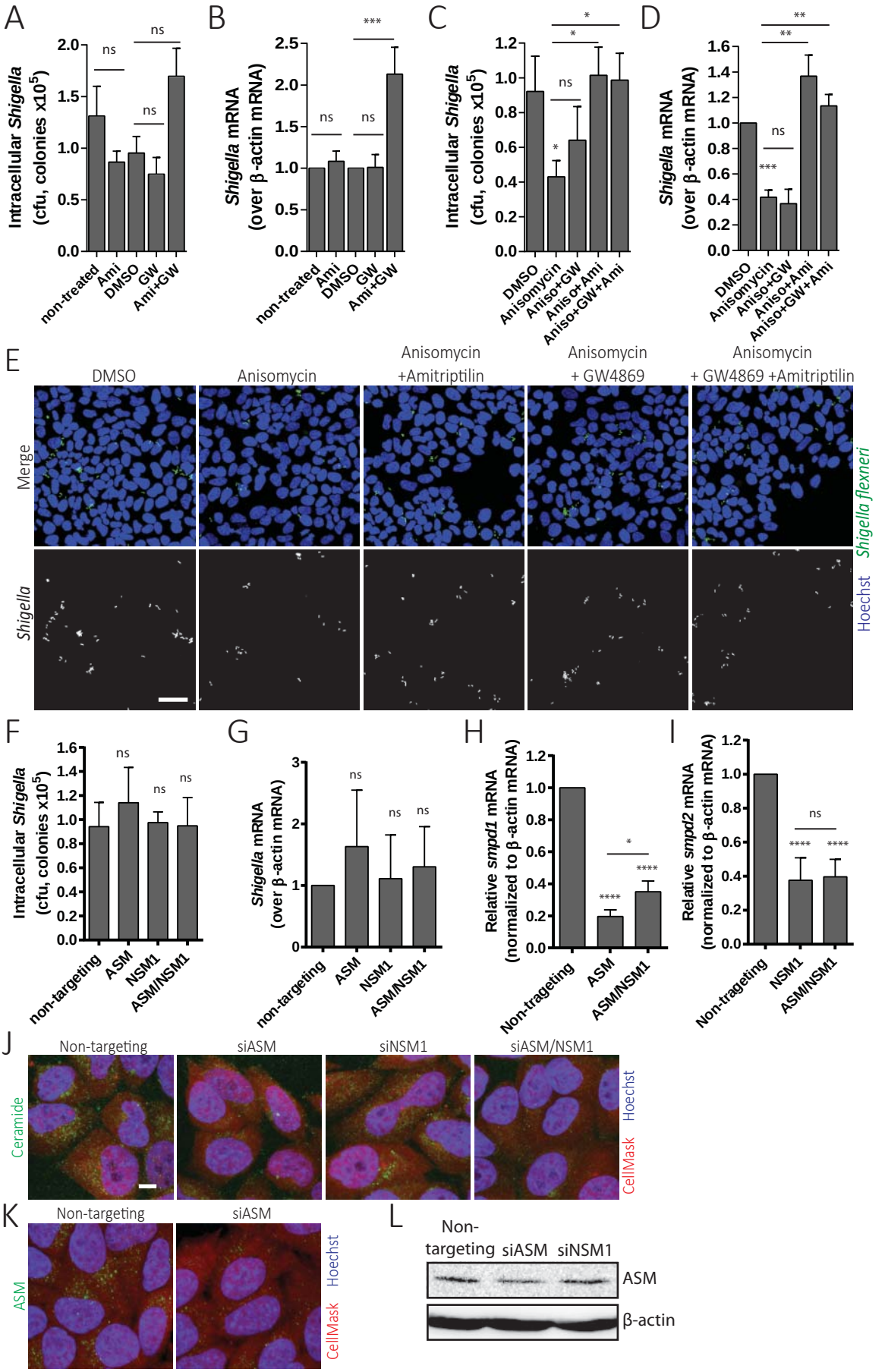
A
Intracellular Shigella (cfu, colonies x10^5)
non-treated
Ami
DMSO
GW
Ami+GW
B
Shigella mRNA (over β-actin mRNA)
C
Intracellular Shigella (cfu, colonies x10^5)
DMSO
Anisomycin
Aniso+GW
Aniso+Ami
Aniso+GW+Ami
D
Shigella mRNA (over β-actin mRNA)
E
DMSO
Anisomycin
Anisomycin +Amitriptilin
Anisomycin + GW4869
Anisomycin + GW4869 +Amitriptilin
Merge
Shigella
Shigella flexneri
Hoechst
F
Intracellular Shigella (cfu, colonies x10^5)
non-targeting
ASM
NSM1
ASM/NSM1
G
Shigella mRNA (over β-actin mRNA)
H
Relative smpd1 mRNA (normalized to β-actin mRNA)
Non-trageting
I
Relative smpd2 mRNA (normalized to β-actin mRNA)
J
Non-targeting
siASM
siNSM1
siASM/NSM1
Ceramide
Hoechst
CellMask
K
ASM
L
Non-targeting
siASM
siNSM1
ASM
β-actin

Figure 4.3 Sphingolipid-rafts depletion by the stress-activated ASM and NSM inhibits *Shigella* infection

(A) CFU and (B) qRT-PCR quantification of *Shigella* infection at 0.5hpi in cells treated with the sphingomyelinase inhibitors alone, DMSO is the vehicle for GW4869. (C) CFU and (D) qRT-PCR quantification of *Shigella* infection at 0.5hpi in cells treated with anisomycin in combination with the sphingomyelinase inhibitors, DMSO is the vehicle for anisomycin and GW4869. (E) Representative images of *Shigella*-GFP infection at 0.5hpi same as in (C, D). Scale-bar 50μm. (F) CFU and (G) qRT-PCR quantification of *Shigella* infection at 0.5hpi in cells transfected with different siRNAs (50nM) in the absence of stress. (H, I) qRT-PCR quantification of (H) *smpd1* mRNA (ASM) or (I) *smpd2* mRNA (NSM-1) in cells transfected with siRNAs. (J, K) representative images of cells transfected with siRNAs and treated with arsenite for 1h, and stained for (J) Ceramide or (K) ASM (green). The cell-body was stained with CellMask (red), and cell nuclei with Hoechst (blue). Scale-bar 10μm. (L) WB analysis of ASM protein levels in cells transfected with siRNAs. β-actin was used as a loading control. Results are shown as mean ± s.e.m. n ≥ 3, *p<0.05, **p<0.01, ***p<0.001, ****p<0.0001, ns: non-significant; two-way ANOVA.

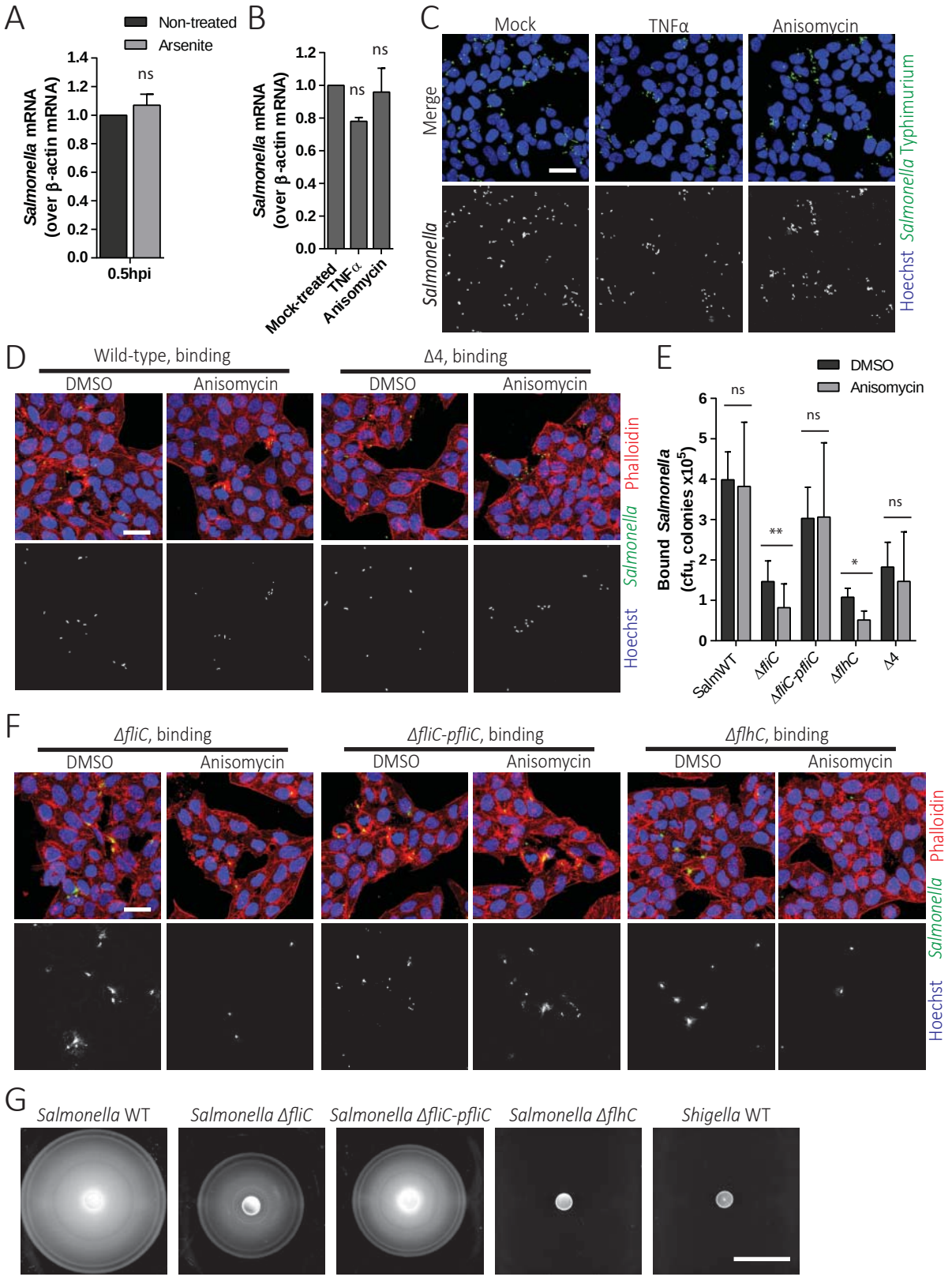
A
Non-treated
Arsenite
Salmonella mRNA (over β-actin mRNA)
ns
0.5hpi
B
Salmonella mRNA (over β-actin mRNA)
ns
ns
Mock-treated
TNFα
Anisomycin
C
Mock
TNFα
Anisomycin
Merge
Salmonella
Hoechst Salmonella Typhimurium
D
Wild-type, binding
Δ4, binding
DMSO
Anisomycin
DMSO
Anisomycin
Phalloidin
Salmonella
Hoechst
E
DMSO
Anisomycin
Bound Salmonella (cfu, colonies x10^5)
ns
**
ns
*
ns
SalmWT
ΔfliC
ΔfliC-pfliC
ΔflhC
Δ4
F
ΔfliC, binding
ΔfliC-pfliC, binding
ΔflhC, binding
DMSO
Anisomycin
DMSO
Anisomycin
DMSO
Anisomycin
Phalloidin
Salmonella
Hoechst
G
Salmonella WT
Salmonella ΔfliC
Salmonella ΔfliC-pfliC
Salmonella ΔflhC
Shigella WT

Figure 4.4 *Salmonella* motility compensates for the depletion of lipid-rafts in stressed cells

(A, B) qRT-PCR quantification of intracellular *Salmonella* at 0.5hpi in control cells or cells treated with (A) arsenite, or (B) with anisomycin or TNF-α. (C) Representative images of *Salmonella*-GFP infections at 0.5hpi. Scale-bar 50μm. (D) Representative images of adhesion assays with *Salmonella* WT and *Δ4* expressing GFP in DMSO or anisomycin treated cells. The cell F-actin network was stained with Phalloidin (red) and the nuclei with Hoechst. Scale-bar 25μm. (E) CFU analysis of adhesion assays with *Salmonella* WT, *ΔfliC*, *ΔfliC* complemented strain by ectopic expression of FliC, *ΔflhC*, and *Δ4* in DMSO or anisomycin treated cells. (F) Representative images of adhesion assays performed same as in (E). Scale-bar 25μm. (G) Representative images of motility assays performed with the different strains. Scale-bar 4cm. Results are shown as mean ± s.e.m. n ≥ 3; two-way ANOVA, ns: non-significant; *p<0.05; **P<0.01.

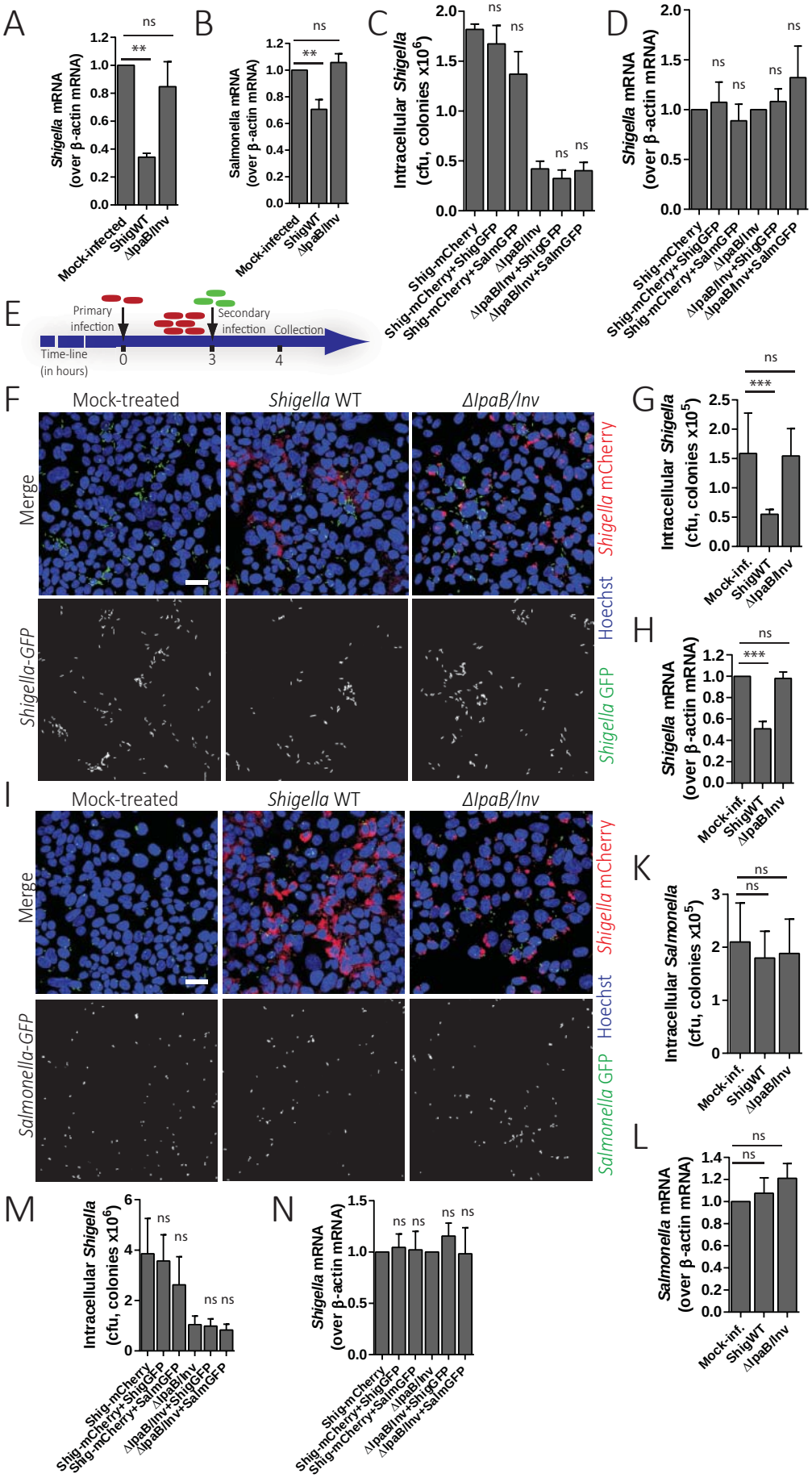
A
Shigella mRNA (over β-actin mRNA)
ns
**
Mock-infected
ShigWT
ΔIpaB/Inv
B
Salmonella mRNA (over β-actin mRNA)
ns
**
Mock-infected
ShigWT
ΔIpaB/Inv
C
Intracellular Shigella (cfu, colonies x10^6)
ns
ns
ns
ns
Shig-mCherry
Shig-mCherry+ShigGFP
Shig-mCherry+SalmGFP
ΔIpaB/Inv
ΔIpaB/Inv+ShigGFP
ΔIpaB/Inv+SalmGFP
D
Shigella mRNA (over β-actin mRNA)
ns
ns
ns
ns
Shig-mCherry
Shig-mCherry+ShigGFP
Shig-mCherry+SalmGFP
ΔIpaB/Inv
ΔIpaB/Inv+ShigGFP
ΔIpaB/Inv+SalmGFP
E
Primary infection
Secondary infection
Collection
Time-line (in hours)
0
3
4
F
Mock-treated
Shigella WT
ΔIpaB/Inv
Merge
Shigella-GFP
Shigella mCherry
Hoechst
Shigella GFP
G
Intracellular Shigella (cfu, colonies x10^5)
ns
***
Mock-inf.
ShigWT
ΔIpaB/Inv
H
Shigella mRNA (over β-actin mRNA)
ns
***
Mock-inf.
ShigWT
ΔIpaB/Inv
I
Mock-treated
Shigella WT
ΔIpaB/Inv
Merge
Salmonella-GFP
Shigella mCherry
Hoechst
Salmonella GFP
K
Intracellular Salmonella (cfu, colonies x10^5)
ns
ns
Mock-inf.
ShigWT
ΔIpaB/Inv
L
Salmonella mRNA (over β-actin mRNA)
ns
ns
Mock-inf.
ShigWT
ΔIpaB/Inv
M
Intracellular Shigella (cfu, colonies x10^6)
ns
ns
ns ns
Shig-mCherry
Shig-mCherry+ShigGFP
Shig-mCherry+SalmGFP
ΔIpaB/Inv
ΔIpaB/Inv+ShigGFP
ΔIpaB/Inv+SalmGFP
N
Shigella mRNA (over β-actin mRNA)
ns ns
ns ns
Shig-mCherry
Shig-mCherry+ShigGFP
Shig-mCherry+SalmGFP
ΔIpaB/Inv
ΔIpaB/Inv+ShigGFP
ΔIpaB/Inv+SalmGFP

Figure 4.5 *Shigella* replication in cells inhibits re-infection by extracellular bacteria

(A) qRT-PCR quantification of intracellular *Shigella*-GFP in re-infection assays with mock-infected, *Shigella* WT-mCherry infected, and *Shigella ΔipaB*/invasin-mCherry infected cells. (B) qRT-PCR quantification of intracellular *Salmonella*-GFP in re-infection assays ame as in (A). (C) CFU and (D) qRT-PCR quantification of the primary infection with *Shigella*-mCherry or *Shigella ΔipaB*/invasin-mCherry. (E) Schematic representation of the experimental design for the re-infection assays. Cells are infected with mCherry labelled *Shigella*, and at 3hpi re-infected with GFP labelled *Shigella*, and collected at 0.5hpi. (F) Representative images of *Shigella*-GFP re-infection assays with mock-infected, *Shigella* WT-mCherry infected, and *Shigella ΔipaB*/invasin-mCherry infected HCT-8 cells. (G) CFU and (H) qRT-PCR quantification of intracellular *Shigella*-GFP in re-infection assays in HCT-8 cells. (I) Representative images of *Salmonella*-GFP re-infection assays in HCT-8 cells. (K) CFU and (L) qRT-PCR quantification of intracellular *Salmonella*-GFP in re-infection assays in HCT-8 cells. (M) CFU and (N) qRT-PCR quantification of the primary infection with *Shigella*-mCherry or *Shigella ΔipaB*/invasin-mCherry in HCT-8 cells. Scale-bar 50μm. Results are shown as mean ± s.e.m. n ≥ 3; two-way ANOVA ns: non-significant; *p<0.05; **p<0.01; ***p<0.001.

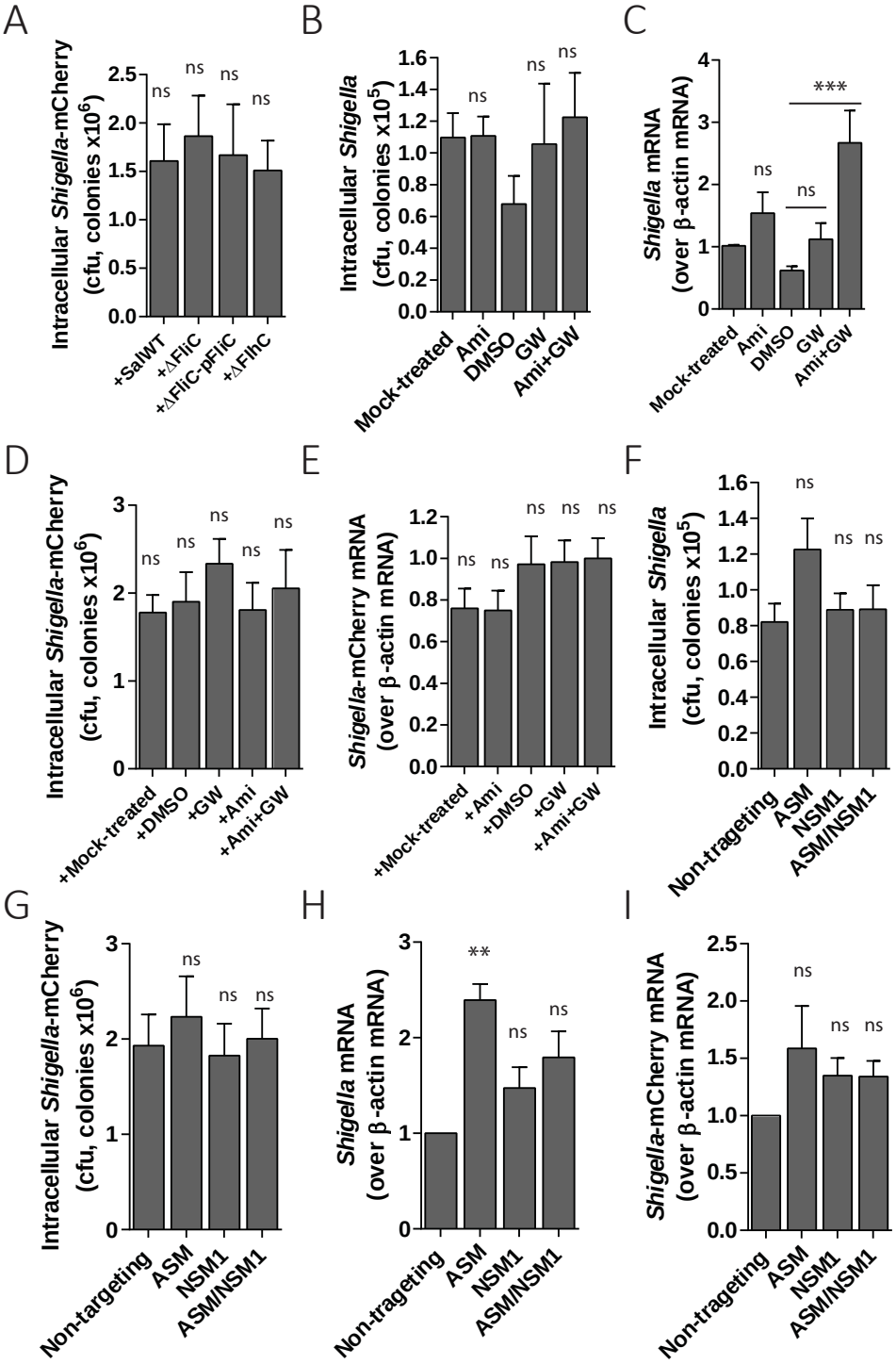
A
Intracellular Shigella-mCherry (cfu, colonies x10^6)
ns
+SalWT
+ΔFliC
+ΔFliC-pFliC
+ΔFlhC
B
Intracellular Shigella (cfu, colonies x10^5)
Mock-treated
Ami
DMSO
GW
Ami+GW
C
Shigella mRNA (over β-actin mRNA)
***
D
+Mock-treated
+DMSO
+GW
+Ami
+Ami+GW
E
Shigella-mCherry mRNA (over β-actin mRNA)
F
Non-trageting
ASM
NSM1
ASM/NSM1
G
Non-targeting
H
**
I

Figure 4.6 *Shigella* replication in cells induces host-cell membrane remodeling

(A) CFU quantification of *Shigella*-mCherry in combination with different *Salmonella* strains. (B) CFU and (C) qRT-PCR quantification of *Shigella*-GFP infection at 0.5hpi of different treated cells. (D) CFU and (E) qRT-PCR quantification of the primary infection with *Shigella*-mCherry with different treatments. (F) CFU quantification of *Shigella*-GFP infection at 0.5hpi of cells transfected with different siRNAs. (G) CFU quantification of the primary infection by *Shigella*-mCherry of cells transfected with different siRNAs. (H) qRT-PCR quantification of infections same as in (F). (I) qRT-PCR quantification of infections same as in (G). Results are shown as mean ± s.e.m. n ≥ 3. two-way ANOVA, ns: non-significant; **p<0.01, ***p<0.001.

Table 4.1 Single effector knockout mutants of *Shigella flexneri* M90T serotype 5a

Deletion	Infection phenotype in HeLa cells	Strain number
ΔospG	same as wild-type	AE-77
ΔospI	same as wild-type	AE-78
ΔospB	same as wild-type	AE-79
ΔvirA	same as wild-type	AE-87
ΔipaA	same as wild-type	AE-88
ΔvirG	defective in intracellular spreading	AE-89
ΔospE2	same as wild-type	AE-90
ΔipgB2	same as wild-type	AE-91
ΔipgD	defective in invasion	AE-92
ΔipaJ	same as wild-type	AE-93
Δspa15	defective in invasion	AE-94
ΔipaH9.8	same as wild-type	AE-95
ΔipaH4.5	defective in invasion	AE-96
ΔipaH7.8	same as wild-type	AE-97
ΔipaH3	same as wild-type	AE-98
ΔipaH2.5	same as wild-type	AE-99
ΔospC3	~2-fold less replication compared to WT	AE-100
ΔospZ	same as wild-type	AE-101
ΔipaH1.4	same as wild-type	AE-102
ΔicsB	more than 2-fold less replication compared to WT	AE-103
ΔipgB1	same as wild-type	AE-110
ΔospE1	same as wild-type	AE-111
ΔospC1	same as wild-type	AE-112
ΔospC2	same as wild-type	AE-113
ΔospF	same as wild-type	AE-114
ΔipaB	defective in invasion	AE-115
ΔospD1	same as wild-type	AE-164
ΔospD2	same as wild-type	AE-165
ΔospD3	same as wild-type	AE-166
ΔshiA	same as wild-type	AE-167

Table 4.2.1 TIAR and TIA-1 RNA-targets upregulated during *Shigella* infection

Gene name	Shigella infection*	TIA-1 enriched*	Gene name	Shigella infection*	TIAR enriched*
CREB5	3,7	3,7	CREB5	3,7	5,2
CCL2	3,3	7,0	SOD2	2,8	6,3
SOD2	2,8	9,8	ZBTB10	2,7	3,4
SAMD4A	2,7	6,0	SAMD4A	2,7	6,8
SLC7A2	2,5	6,8	ATF3	2,7	5,5
FAM84B	2,2	6,0	SLC7A2	2,5	6,8
PPP1R14C	2,0	4,9	FAM84B	2,2	7,8
SLIT2	1,8	8,9	PPP1R14C	2,0	6,0
MAML3	1,7	5,7	HIVEP2	1,8	3,3
NTN1	1,7	4,5	SLIT2	1,8	10,3
JUN	1,7	6,4	MAML3	1,7	4,5
AIM2	1,7	6,4	MB21D2	1,7	5,1
ITGB8	1,5	6,9	NTN1	1,7	6,5
PMAIP1	1,5	5,6	SOX6	1,7	2,7
ZC3HAV1	1,5	6,0	AIM2	1,7	6,1
NAMPT	1,5	3,5	ABTB2	1,6	6,0
COL8A1	1,4	7,3	AKT3	1,6	4,4
KDM7A	1,4	5,1	LRRC49	1,6	3,2
ZC3H12C	1,4	3,9	ITGB8	1,5	4,5
ABCA5	1,4	4,3	COL4A1	1,5	3,9
EGLN1	1,3	3,8	PMAIP1	1,5	5,3
DISC1	1,3	5,5	ZC3HAV1	1,5	5,6
NHS	1,3	4,3	DNER	1,5	4,4
ERN1	1,3	4,5	SHB	1,5	5,6
TNFRSF21	1,3	5,3	NAMPT	1,5	3,4
EGFR	1,3	5,5	PRICKLE2	1,5	5,3
SNAP25	1,3	3,9	COL8A1	1,4	4,6
PTPRG	1,3	4,9	WTAP	1,4	3,5
SLC1A3	1,2	3,7	SLC39A8	1,4	3,4
OCLN	1,2	4,8	C5orf56	1,4	3,0
LRIG1	1,2	4,9	TSPAN9	1,4	4,3
SERTAD2	1,2	5,3	KDM7A	1,4	6,4
REL	1,2	5,7	ZC3H12C	1,4	4,3
DIRC3	1,2	6,3	HIVEP1	1,4	3,7
SULF1	1,2	4,2	ABCA5	1,4	4,9
THSD4	1,2	3,6	EGLN1	1,3	3,9
ATP13A3	1,2	7,6	DISC1	1,3	7,2
USP54	1,1	5,8	FRMD6	1,3	5,2
RHOB	1,1	6,7	GNG7	1,3	3,1
ADAMTS1	1,1	5,8	NHS	1,3	3,4
FBLN5	1,1	8,0	EGFR	1,3	4,6

ZCCHC24	1,1	6,5
IFNGR1	1,1	3,4
GCA	1,1	4,4
DDAH1	1,0	3,6
ANKLE2	1,0	6,5
KLF5	1,0	6,9
CALD1	1,0	6,0
DCBLD1	1,0	6,4
BACH1	1,0	4,3
ARHGAP29	1,0	6,0
GPC6	1,0	4,1
CRIM1	1,0	7,4
ABL2	1,0	4,1
BMP2K	1,0	7,1
SASH1	1,0	5,3
SLC25A28	1,0	6,1
MCL1	1,0	5,4
FOXC1	1,0	5,6
GRB10	1,0	6,9
SMURF2	0,9	7,2
FAM110B	0,9	5,4
MYBL1	0,9	5,4
LHFP	0,9	5,1
RASSF8	0,9	6,9
NABP1	0,9	6,8
PPP3CC	0,9	5,9
PICALM	0,9	8,1
MBNL2	0,9	10,6
CDC14A	0,9	6,2
DNAJC1	0,9	3,5
CCSER2	0,9	3,7
TLE1	0,9	4,8
ARL5B	0,9	5,9
PARP8	0,9	5,2
EIF2AK2	0,9	5,7
NT5C2	0,9	7,5
PTPRF	0,9	5,9
KCNQ5	0,9	5,1
TIAM1	0,9	4,7
FAM219A	0,9	5,4
FEM1B	0,8	6,1
CHST11	0,8	5,9
MAML2	0,8	4,5
CDKL5	0,8	5,8
RASA2	0,8	4,6
SPAG1	0,8	4,9
PALM2-AKAP2	1,3	3,9
AKAP2	1,3	3,9
PTPRG	1,3	8,6
RAPH1	1,3	5,6
CYLD	1,2	5,0
SLC1A3	1,2	4,9
OCLN	1,2	5,6
LRIG1	1,2	5,9
MID2	1,2	4,6
SERTAD2	1,2	6,2
REL	1,2	5,6
DIRC3	1,2	6,5
GPR176	1,2	5,7
PRKCH	1,2	5,6
PAPSS2	1,2	5,1
TDRD7	1,2	5,0
SULF1	1,2	5,2
THSD4	1,2	2,7
ATP13A3	1,2	7,8
USP54	1,1	5,8
RHOB	1,1	5,5
FOSL2	1,1	3,8
ADAMTS1	1,1	6,3
FBLN5	1,1	4,4
ZCCHC24	1,1	5,2
IFNGR1	1,1	3,9
ANKLE2	1,0	6,7
KLF5	1,0	3,6
SLC25A37	1,0	4,1
CALD1	1,0	5,2
DCBLD1	1,0	6,1
BACH1	1,0	4,1
EPHA2	1,0	3,3
DUSP1	1,0	4,1
ARHGAP29	1,0	4,6
GPC6	1,0	9,2
CRIM1	1,0	7,4
ABL2	1,0	4,9
BMP2K	1,0	6,8
FMNL2	1,0	2,9
SAV1	1,0	5,3
SASH1	1,0	5,5
MCL1	1,0	4,6
CDK6	1,0	2,9
FOXC1	1,0	6,1
GRB10	1,0	7,4

PPP1R15B	0,8	7,1
USP53	0,8	10,8
FERMT2	0,8	7,2
FYN	0,8	7,5
C10orf11	0,8	6,7
NID1	0,8	6,0
UXS1	0,8	5,9
RAB3IP	0,8	5,1
TMEFF1	0,8	3,4
MSANTD3-TMEFF1	0,8	3,4
COL27A1	0,8	4,7
COTL1	0,8	6,2
DENND5A	0,8	4,7
GSK3B	0,8	3,9
SLC41A2	0,8	9,5
ST3GAL1	0,8	7,3
HDX	0,7	6,0
PLCE1	0,7	4,7
FLNB	0,7	8,4
LRRC8C	0,7	4,6
TMEM47	0,7	6,7
SLC39A14	0,7	7,7
APBB2	0,7	8,1
SHROOM3	0,7	5,2
ADAM17	0,7	6,2
GBE1	0,7	5,7
C12orf79	0,7	5,6
LYN	0,7	3,6
MED9	0,7	6,1
TLL1	0,7	8,3
TPST1	0,7	11,5
DNAH11	0,7	6,6
TRAF3	0,7	4,1
RNF217	0,7	7,1
BICC1	0,7	4,5
MASTL	0,7	5,4
CAPRIN2	0,7	4,6
CRY1	0,7	5,7
CORO1C	0,7	7,1
DDR2	0,6	4,9
RRAS2	0,6	7,1
CYTH1	0,6	5,8
MAP3K1	0,6	7,6
DLX2	0,6	4,9
EIF1	0,6	5,3
WWC1	0,9	5,6
SMURF2	0,9	7,4
ATP2B1	0,9	2,7
FAM110B	0,9	5,2
MREG	0,9	5,4
MYBL1	0,9	5,6
FAM171A1	0,9	3,1
LHFP	0,9	6,4
IPMK	0,9	5,6
COL7A1	0,9	3,5
CHST15	0,9	5,1
RASSF8	0,9	5,7
PPP3CC	0,9	5,1
PICALM	0,9	7,5
MBNL2	0,9	6,9
CDC14A	0,9	6,5
DNAJC1	0,9	3,9
CCSER2	0,9	4,0
TLE1	0,9	6,3
ARL5B	0,9	6,7
PARP8	0,9	6,7
EIF2AK2	0,9	5,6
NT5C2	0,9	6,0
KIF26B	0,9	5,4
PTPRF	0,9	6,8
KCNQ5	0,9	8,2
TIAM1	0,9	7,9
RBPMS	0,8	5,3
FEM1B	0,8	6,3
CHST11	0,8	7,0
MAML2	0,8	3,8
LYPD6B	0,8	5,2
SLC35G1	0,8	5,5
CDKL5	0,8	5,9
RASA2	0,8	4,9
SPAG1	0,8	4,5
PPP1R15B	0,8	6,5
USP53	0,8	7,1
FERMT2	0,8	6,0
FYN	0,8	8,4
BTBD10	0,8	5,6
C10orf11	0,8	6,4
NID1	0,8	7,3
UXS1	0,8	6,0
MCTP1	0,8	2,7

ELL2	0,6	11,0
LRRFIP2	0,6	7,2
TMEM2	0,6	5,8
TGFBR1	0,6	4,7
C5orf15	0,6	6,9
RUSC2	0,6	4,2
B4GALT1	0,6	4,9
HIF1A	0,6	5,9
SEC24D	0,6	5,7
PSMB5	0,6	6,2
FGFR1	0,6	4,9
TMEM165	0,6	6,9
NAB1	0,6	6,7
DNAJC3	0,6	7,0
C1orf198	0,6	6,0
SDCBP	0,6	6,6
SIK2	0,6	6,1
RHOF	0,6	6,5
RPS6KA3	0,6	3,9
FBXL3	0,6	4,0
CSGALNACT1	0,6	5,4
ALKBH6	0,6	6,2
SDK2	0,6	5,1
GPR137C	0,6	5,1
MCTP2	0,6	3,9
VHL	0,6	5,7
MEF2A	0,6	4,4
WWTR1	0,6	9,7
NUDCD1	0,6	3,5
UAP1	0,6	8,2
HELB	0,6	4,2
LIMS1	0,6	3,7
MYO1D	0,6	5,4
UBE2H	0,6	3,7
FAM160A1	0,6	9,7
BRIP1	0,6	3,5
UBE2E2	0,6	5,7
BZW1	0,6	6,3
CCNL1	0,6	6,2
ITGAV	0,6	8,5
WDR45B	0,6	5,9
MORC4	0,6	5,5
SMIM13	0,6	6,4
C1GALT1	0,6	3,9
CEP135	0,6	5,4
CDV3	0,8	5,8
RAB3IP	0,8	5,3
DUSP16	0,8	5,3
PDE5A	0,8	4,3
TMEFF1	0,8	4,1
STAT3	0,8	5,7
MSANTD3-TMEFF1	0,8	4,1
COL27A1	0,8	6,3
COTL1	0,8	5,8
DENND5A	0,8	5,5
GSK3B	0,8	3,5
SLC41A2	0,8	5,7
ST3GAL1	0,8	5,3
ITGA1	0,8	5,4
HDX	0,7	5,4
PLCE1	0,7	5,0
KLF7	0,7	5,3
MYADM	0,7	4,4
SRGAP1	0,7	3,0
AGRN	0,7	5,3
FLNB	0,7	6,9
ACOT9	0,7	5,4
LRRC8C	0,7	5,2
CAMK4	0,7	2,8
SLC39A14	0,7	6,7
APBB2	0,7	6,3
SHROOM3	0,7	4,0
TNFRSF10B	0,7	3,4
GPRC5A	0,7	4,1
ADAM17	0,7	6,3
PDLIM7	0,7	3,2
GBE1	0,7	3,0
C12orf79	0,7	6,6
LRRC1	0,7	5,6
LYN	0,7	5,0
TLL1	0,7	5,3
TPST1	0,7	6,4
DNAH11	0,7	5,7
TRAF3	0,7	5,3
RNF217	0,7	7,3
PDK1	0,7	3,8
BICC1	0,7	4,4
PPTC7	0,7	6,2
MASTL	0,7	5,7
CAPRIN2	0,7	5,3

ASAP2	0,5	6,8
CD47	0,5	6,6
RASSF3	0,5	5,0
AFAP1	0,5	5,3
CHIC2	0,5	4,9
RREB1	0,5	3,9
N4BP1	0,5	5,0
SPRED2	0,5	7,0
TMTC2	0,5	9,1
JARID2	0,5	7,9
SERAC1	0,5	4,6
LIMA1	0,5	4,2
FCGR2B	0,5	5,1
ADAM19	0,5	6,2
INO80D	0,5	6,1
PLOD2	0,5	3,7
FSTL1	0,5	7,1
XPO6	0,5	7,1
EFNA5	0,5	4,2
ENAH	0,5	3,9
TMEM184B	0,5	6,5
AK4	0,5	5,3
PPM1K	0,5	4,5
ZNF281	0,5	6,3
CD55	0,5	7,9
MAPKAPK2	0,5	7,4
DSE	0,5	6,1
ARL8B	0,5	4,2
CCDC82	0,5	4,1
SLC37A3	0,5	5,4
C8orf88	0,5	4,5
TGFB1	0,5	4,7
ZFP36L1	0,5	7,3
IGFBP7	0,5	3,9
AKIRIN1	0,5	6,4
SPINK6	0,5	3,9
PEAK1	0,5	3,5
RP11-302B13.5	0,5	6,7
MCC	0,5	3,9
USP12	0,5	5,8
TMEM39A	0,5	5,3
LIFR	0,5	5,7
TM2D2	0,5	6,6
UHRF1BP1	0,5	6,7
RASAL2	0,5	3,9
FGFR1OP2	0,7	5,4
RAB23	0,7	5,6
CRY1	0,7	6,0
CORO1C	0,7	6,7
HMCN1	0,7	3,4
DDR2	0,6	5,4
RRAS2	0,6	6,3
CYTH1	0,6	6,1
MAP3K1	0,6	5,8
DLX2	0,6	6,0
RAB9A	0,6	5,1
EIF1	0,6	6,5
ELL2	0,6	5,7
LRRFIP2	0,6	6,8
TMEM2	0,6	5,7
TGFBR1	0,6	4,7
C5orf15	0,6	6,8
HIF1A	0,6	3,5
SEC24D	0,6	6,1
SPIRE1	0,6	3,0
PSMB5	0,6	5,3
PIEZO1	0,6	5,4
DTWD1	0,6	5,1
TWISTNB	0,6	5,6
FGFR1	0,6	6,2
TMEM165	0,6	6,6
NAB1	0,6	5,6
SSH1	0,6	5,5
DNAJC3	0,6	6,5
C1orf198	0,6	6,0
RP2	0,6	5,2
SDCBP	0,6	6,6
SIK2	0,6	6,4
RHOF	0,6	5,4
RPS6KA3	0,6	2,8
FBXL3	0,6	4,1
CSGALNACT1	0,6	3,7
PRICKLE1	0,6	5,4
GPR137C	0,6	6,0
SDK2	0,6	7,2
VHL	0,6	6,1
MEF2A	0,6	3,7
WWTR1	0,6	6,4
DIAPH2	0,6	2,7
SPEN	0,6	3,7

ZNF483	0,5	5,2
AGFG1	0,5	6,5
TBC1D12	0,5	5,5
NUP153	0,5	3,7
WDFY2	0,5	10,8
CD70	0,5	6,6
MED15	0,5	5,4
TFG	0,5	4,5
TAB2	0,5	6,3
FRAS1	0,5	4,7
ST3GAL6	0,5	5,2
HSPA13	0,5	5,4
PTPN1	0,5	3,8
NUDCD1	0,6	3,1
C12orf75	0,6	3,0
UAP1	0,6	5,8
LIMS1	0,6	3,3
MYO1D	0,6	6,4
UBE2H	0,6	2,9
FAM160A1	0,6	6,7
BRIP1	0,6	3,4
UBE2E2	0,6	5,6
BZW1	0,6	5,6
CCNL1	0,6	6,7
ITGAV	0,6	7,0
WDR45B	0,6	5,9
MORC4	0,6	6,1
SLC2A1	0,6	5,7
SMIM13	0,6	5,9
CEP135	0,6	5,8
ASAP2	0,5	6,0
CD47	0,5	6,4
RASSF3	0,5	4,8
AFAP1	0,5	4,5
RREB1	0,5	4,5
N4BP1	0,5	5,8
TMTC2	0,5	7,2
JARID2	0,5	7,5
SERAC1	0,5	5,5
LIMA1	0,5	4,0
FCGR2B	0,5	4,7
PRRG1	0,5	5,3
CNTNAP3B	0,5	5,3
INO80D	0,5	5,7
MAN1A1	0,5	3,0
PLOD2	0,5	3,1
OTUD4	0,5	4,1
FSTL1	0,5	4,8
XPO6	0,5	7,4
EFNA5	0,5	3,5
ENAH	0,5	3,9
TMEM184B	0,5	6,3
AK4	0,5	5,0
PPM1K	0,5	5,4
ZNF281	0,5	5,7
GFOD1	0,5	5,7
CD55	0,5	6,0
UBE2F	0,5	5,2
MAPKAPK2	0,5	5,9

DSE	0,5	7,0
ARL8B	0,5	2,8
CCDC82	0,5	3,6
SLC37A3	0,5	6,4
CEP85L	0,5	3,6
C8orf88	0,5	5,2
MAPKBP1	0,5	4,8
ZFP36L1	0,5	5,2
BID	0,5	3,6
FEM1C	0,5	5,1
AKIRIN1	0,5	5,8
PEAK1	0,5	2,8
RP11-302B13.5	0,5	5,7
MCC	0,5	4,7
USP12	0,5	6,0
TMEM39A	0,5	6,5
LIFR	0,5	6,1
UHRF1BP1	0,5	6,3
MAP2K4	0,5	3,5
RASAL2	0,5	3,5
ANXA11	0,5	5,0
ZNF483	0,5	5,5
UBAP1	0,5	5,8
AGFG1	0,5	7,9
TBC1D12	0,5	5,8
NUP153	0,5	4,1
CNN2	0,5	4,5
WDFY2	0,5	5,8
MED15	0,5	3,7
TFG	0,5	4,8
TAB2	0,5	7,4
OSBPL6	0,5	2,9
FRAS1	0,5	5,0
ST3GAL6	0,5	5,7
HSPA13	0,5	5,9
STAMBPL1	0,5	3,6
PTPN1	0,5	4,2
FHOD3	0,5	6,5

* Values are log2 fold-change

Table 4.2.2 TIAR and TIA-1 RNA-targets downregulated during *Shigella* infection

Gene name	Shigella infection*	TIA-1 enriched*	Gene name	Shigella infection*	TIAR enriched*
PDE1A	-1,5	3,7	FAM13C	-2,4	4,4
STXBP5L	-1,4	6,2	STXBP5L	-1,4	6,0
DFFB	-1,4	6,4	ZNF711	-1,3	5,0
RP11-758M4.1	-1,3	5,1	RP11-758M4.1	-1,3	6,0
L3MBTL3	-1,2	3,4	L3MBTL3	-1,2	4,8
VAV3	-1,1	5,8	TBC1D8B	-1,2	5,2
EPHA5	-1,1	9,9	CDON	-1,1	3,4
GPR98	-1,0	4,2	EEPD1	-1,1	5,6
HMMR	-1,0	7,0	DZIP1	-1,1	4,0
TSHZ1	-1,0	3,9	ARHGAP18	-1,1	5,0
PTCH1	-1,0	4,5	GPR63	-1,1	2,8
PDE8B	-1,0	5,2	VAV3	-1,1	4,6
OSBPL1A	-0,9	8,5	EPHA5	-1,1	5,5
OMA1	-0,9	4,2	GPR98	-1,0	5,6
DOPEY1	-0,9	5,7	TRIM62	-1,0	4,4
ENPP1	-0,9	4,0	HMMR	-1,0	5,1
IQGAP2	-0,9	5,3	TSHZ1	-1,0	4,4
SESN3	-0,9	4,7	PTCH1	-1,0	5,4
CRB1	-0,8	6,8	MEGF9	-1,0	4,6
DLGAP5	-0,8	5,0	PDE8B	-1,0	2,7
VWDE	-0,8	6,5	CRYL1	-0,9	3,9
DEPDC1	-0,8	6,7	ARHGEF9	-0,9	5,3
MTBP	-0,8	4,6	INTU	-0,9	3,5
RNF146	-0,7	5,9	OSBPL1A	-0,9	6,5
MRS2	-0,7	4,6	OMA1	-0,9	5,4
DFNB31	-0,7	8,0	DOPEY1	-0,9	6,8
NXPE3	-0,7	5,9	CRADD	-0,9	5,8
SGOL2	-0,7	5,6	GPR155	-0,9	5,7
DHRS3	-0,7	6,3	IQGAP2	-0,9	5,0
TSEN2	-0,7	5,3	ENPP1	-0,9	4,9
BCKDHB	-0,7	7,7	SESN3	-0,9	4,3
ATG4C	-0,7	5,9	SLC22A3	-0,8	3,7
ARMCX4	-0,7	6,4	DLGAP5	-0,8	5,6
PRR16	-0,7	5,0	VWDE	-0,8	6,6
GIPC2	-0,7	5,4	INPP5F	-0,8	5,3
PFKM	-0,7	4,3	DEPDC1	-0,8	6,6
TTC8	-0,7	4,8	LMF1	-0,8	4,1
PDE7B	-0,7	6,4	MTBP	-0,8	5,3
PLS1	-0,7	5,4	RPGRIP1L	-0,8	4,0
GLDC	-0,7	4,2	SESN1	-0,8	5,5
MRE11A	-0,6	4,4	PTGR2	-0,7	3,0
TRMT1L	-0,6	6,3	RNF146	-0,7	5,9

BBS9	-0,6	7,3
ELP4	-0,6	6,3
CBR4	-0,6	10,4
PCMTD2	-0,6	5,0
PLEKHG1	-0,6	5,1
TTC23	-0,6	5,0
BTBD3	-0,6	4,2
ALG6	-0,6	5,4
C6orf211	-0,6	5,0
ACAT1	-0,6	3,4
CCDC18	-0,6	4,9
FIGN	-0,6	6,9
ERMP1	-0,6	5,9
HOXB3	-0,6	4,9
HSPA1B	-0,6	6,7
HSPA1A	-0,6	6,1
FBXL4	-0,6	5,8
DCAF16	-0,6	5,9
ZNF138	-0,6	6,1
WDR12	-0,6	4,9
E2F5	-0,6	5,6
KIAA1009	-0,6	8,7
RANBP17	-0,6	3,9
GALNT13	-0,6	4,0
PEX7	-0,6	4,9
KIF11	-0,6	7,4
SLC2A13	-0,6	11,2
TMEM68	-0,6	5,1
FASTKD1	-0,6	5,4
LDLRAD4	-0,6	3,8
TBCK	-0,6	6,3
BRMS1L	-0,6	5,3
DEPDC1B	-0,5	5,5
COL25A1	-0,5	4,9
CEP44	-0,5	6,1
GTF2H3	-0,5	8,2
KIAA0586	-0,5	3,4
DTNA	-0,5	6,4
FANCM	-0,5	8,7
EXPH5	-0,5	4,6
PLXDC2	-0,5	4,7
GALNT10	-0,5	5,9
CLYBL	-0,5	5,6
SNCA	-0,5	6,7
RPAP2	-0,5	6,1
DHX29	-0,5	5,0

NEIL3	-0,7	2,9
CDHR3	-0,7	5,6
MSH5	-0,7	5,7
KIAA1549	-0,7	3,3
RGS5	-0,7	3,4
DFNB31	-0,7	4,9
TLN2	-0,7	2,8
NXPE3	-0,7	5,9
SGOL2	-0,7	5,4
SLX4IP	-0,7	3,2
RDH10	-0,7	3,1
TSEN2	-0,7	6,3
BCKDHB	-0,7	6,5
CDH12	-0,7	3,4
ATG4C	-0,7	6,6
PRR16	-0,7	5,1
OBSCN	-0,7	5,8
GIPC2	-0,7	5,7
PFKM	-0,7	4,5
KBTBD6	-0,7	5,6
MUM1	-0,7	5,3
TTC8	-0,7	5,1
PDE7B	-0,7	3,8
PLS1	-0,7	5,9
SLC29A1	-0,7	5,7
GLDC	-0,7	5,3
MTERF	-0,6	5,3
MRE11A	-0,6	4,4
TRMT1L	-0,6	5,4
DNAJB4	-0,6	5,3
BBS9	-0,6	7,0
ELP4	-0,6	7,0
ARHGAP22	-0,6	5,7
CBR4	-0,6	6,2
PCMTD2	-0,6	5,3
EML1	-0,6	5,2
PLEKHG1	-0,6	5,2
TTC23	-0,6	5,4
ZNF280C	-0,6	3,2
ALG6	-0,6	6,6
C6orf211	-0,6	4,0
ACAT1	-0,6	3,2
CCDC18	-0,6	5,2
FIGN	-0,6	6,6
SLC35A1	-0,6	4,5
ERMP1	-0,6	6,0

ZNF510	-0,5	6,2
PDE3B	-0,5	7,4
SMARCA2	-0,5	4,6
ADCK3	-0,5	4,7
C4orf27	-0,5	4,8
COG6	-0,5	7,0
SPDL1	-0,5	6,1
MBTD1	-0,5	5,4
XRRA1	-0,5	4,8
PGRMC2	-0,5	5,9
UBE3D	-0,5	7,3
ACN9	-0,5	4,8
B3GALNT2	-0,5	6,7
KIF15	-0,5	5,0
L3HYPDH	-0,5	6,9
CCNA2	-0,5	4,4
WDR60	-0,5	5,2
FSBP	-0,5	7,3
TDRD3	-0,5	6,1
TMEM241	-0,5	5,6
ANKRD26	-0,5	5,2
PRTG	-0,5	8,7
LANCL1	-0,5	7,2
MXI1	-0,5	5,0
PLEKHA2	-0,5	6,9
TBC1D32	-0,5	6,0
ZNF589	-0,5	4,9
UBE2T	-0,5	5,3
LRRC45	-0,5	6,4
DSC2	-0,5	5,3
MRPS14	-0,5	5,1
RNF182	-0,5	4,8

HOXB3	-0,6	6,5
BBS2	-0,6	5,2
MACROD1	-0,6	5,7
HSPA1B	-0,6	6,9
FBXL4	-0,6	6,6
RNPC3	-0,6	5,0
DCAF16	-0,6	6,3
ZNF138	-0,6	5,9
WDR12	-0,6	5,6
E2F5	-0,6	6,2
KIAA1009	-0,6	5,8
RANBP17	-0,6	4,8
PEX7	-0,6	5,8
TTLL11	-0,6	5,4
KIF11	-0,6	6,9
SLC2A13	-0,6	7,6
FAM83D	-0,6	5,7
FASTKD1	-0,6	6,5
MOB3B	-0,6	2,8
TBCK	-0,6	7,1
SDCCAG8	-0,6	2,9
BRMS1L	-0,6	6,0
PLA2G12A	-0,6	5,3
ZNF618	-0,5	4,6
DEPDC1B	-0,5	6,0
COL25A1	-0,5	3,1
CEP44	-0,5	6,3
GTF2H3	-0,5	5,9
ASPM	-0,5	3,0
KIAA0586	-0,5	3,8
DTNA	-0,5	8,5
FANCM	-0,5	6,5
NSUN6	-0,5	3,3
EXPH5	-0,5	5,2
PLXDC2	-0,5	3,0
GALNT10	-0,5	5,6
CLYBL	-0,5	6,4
SNCA	-0,5	5,9
RPAP2	-0,5	6,7
PDE3B	-0,5	7,2
SMARCA2	-0,5	3,6
ADCK3	-0,5	6,1
AASDHPPT	-0,5	5,9
TYW1B	-0,5	3,1
COG6	-0,5	6,6
C4orf27	-0,5	5,5

	SPDL1	-0,5	6,2
	MBTD1	-0,5	5,0
	XRRA1	-0,5	4,4
	PGRMC2	-0,5	5,8
	ACACA	-0,5	2,8
	UBE3D	-0,5	7,5
	ACN9	-0,5	5,6
	WIPF1	-0,5	5,5
	DBT	-0,5	5,3
	B3GALNT2	-0,5	6,3
	WDR3	-0,5	3,3
	KIF20B	-0,5	2,7
	KIF15	-0,5	4,5
	L3HYPDH	-0,5	6,1
	CCNA2	-0,5	4,2
	WDR60	-0,5	6,4
	FSBP	-0,5	5,6
	NUDT4	-0,5	5,5
	TDRD3	-0,5	6,6
	FAM173B	-0,5	3,8
	TMEM241	-0,5	6,2
	FHIT	-0,5	3,3
	ANKRD26	-0,5	6,0
	PRTG	-0,5	5,9
	LANCL1	-0,5	6,4
	MXI1	-0,5	6,0
	RILPL1	-0,5	5,9
	PLEKHA2	-0,5	4,3
	TBC1D32	-0,5	9,1
	ZNF589	-0,5	5,6
	AKAP7	-0,5	5,1
	UBE2T	-0,5	5,8
	DSC2	-0,5	5,4
	CCNB2	-0,5	4,0
	RNF182	-0,5	2,7

* Values are log2 fold-change

5 MATERIALS AND METHODS

5.1 General equipment

Table 5.1 Instruments

Instrument	Manufacturer
centrifuge Eppendorf 5424	Eppendorf
Bio TDB-100, Dry block thermostat	Biosan
C1000 Touch™ Thermal Cycler	Bio-Rad
centrifuge Eppendorf 5424R	Eppendorf
CFX96 RealTime System	Bio-Rad
Confocal Leica TCS SP5 microscope	Leica
Eclipse TS100 Inverted Routine Microscope	Nikon
electroporator MicroPulser	Bio-Rad
Eppendorf Research® plus 10, 20, 200, 1000	Eppendorf
eraser for imaging plates FLA	GE Healthcare
gel documentation system Gel iX Imager	Intas
Heraeus™ Multifuge™ X3 Centrifuge	Thermo Fischer
horizontal electrophoresis systems PerfectBlue Mini S, M, L	Peqlab
imaging plates BAS-IP MS 2325, 2340	Fujifilm
imaging plates cassettes BAS 2325, 2340	Fujifilm
imaging System Image Quant LAS 4000	GE Healthcare
Incubator Hood TH 15	Edmund Bühler GmbH
Incubator I	Memmert
Infinite® 200 PRO plate reader	Tecan
New Brunswick GALAXY 170S CO2 incubator	Eppendorf
Optima MAX-XP table-top ultracentrifuge	Beckman-Coulter
phosphorimager Typhoon FLA 7000	GE Healthcare
photometer Ultrospec 10 Cell Density Meter	Gilson
power supplies peqPOWER E250, E300	Peqlab
Safe 2020 Class II Biological Safety Cabinets	Thermo Fischer
semi-dry electroblotter PerfectBlue SEDEC M	Peqlab
spectrophotometer NanoDrop 2000	Perkin-Elmer
TS-100C, Thermo-Shaker	Biosan
UV crosslinker for Southern and Northern Blotting (254 nm).	Vilber
vertical electrophoresis systems PerfectBlue Twin S, ExW S, L	Peqlab

5.2 Consumables and commercial kits

Table 5.2 Consumables and commercial kits

Consumables	Manufacturer
Amplex® Red Sphingomyelinase Assay Kit	Thermo Fischer
Corning® Costar® Spin-X® Centrifuge tubes	Sigma
Disposable glass Pasteur pipettes	Kimble
dNTPs	Thermo Fischer
Dynabeads™ Protein G	Thermo Fischer
Fisherbrand™ Cell Scrapers	Fisher Scientific
Hard-Shell® 96-Well PCR Plates	Bio-Rad
Low Molecular Weight DNA ladder	NEB
Millex® Syringe Filter	Merk Millipore
Nitrocellulose membranes for Western blot 0.45 µm	GE Healthcare
NucleoSpin® Gel and PCR Clean-up	Machrey-Nagel
NucleoSpin® Plasmid EasyPure	Machrey-Nagel
OptiPlate-96, White Opaque 96-well Microplate	Perkin Elmer
PCR tubes 0.2 ml	Thermo Fischer
Phase Lock Gel tubes 2 ml	5 Prime
Pipette filter tips	Sarstedt
pipette tips	Sarstedt
PolyScreen PVDF Transfer Membrane	Perkin Elmer
Protease Inhibitor Cocktail Tablets in EASYpacks.	Roche
Random primers	Invitrogen
reagent and centrifuge tubes 15, 50 ml	Sarstedt
RNaseOUT	Thermo Fischer
safe-lock tubes 1.5 ml, 2.0 ml	Eppendorf
spectrophotometer cuvettes	Sarstedt
SsoAdvanced™ Universal SYBR® Green Supermix	Bio-Rad
SYBR Gold nucleic acid stain	Invitrogen
Whatmann Glass Microfiber Filters	GE Healthcare

5.3 Chemicals

Table 5.3 Chemicals

Chemicals	Manufacturer
Albumin Fraktion V	Roth
ampicillin sodium salt	Roth
chloramphenicol	Roth
Difco Agar	Merck
dimethyl sulfoxide (DMSO)	Roth
EDTA	Roth
EGTA	Roth
ethanol	Roth
ethanol (absolute for analysis)	Merck
glycerol (99%)	Sigma
GlycoBlue	Ambion
H2O2 30%	AppliChem
isopropanol	Roth
kanamycin sulfate	Roth
L(+)-Arabinose	Roth
luminol	Sigma
methanol	Roth
milk powder (blotting grade)	Roth
Nutrient broth Difco	BD
p-Coumaric acid	Sigma
PEG400	Sigma
RedSafe	ChemBio
rifampicin	Fluka
Roti-Aqua-P/C/I	Roth
Rotiphorese gel 40 (37.5:1)	Roth
SYBR Gold Nucleic Acid Gel Stain	Invitrogen
Triton-X100	Sigma
TRIzol Reagent	Invitrogen
γ-32P-ATP (222TBq (6000Ci)/mmol 370MBq (10mCi)/ml)	Hartmann Analytic

Additional chemicals were purchased from Sigma, Roth and Merck.

5.4 Enzymes

Table 5.4 Enzymes

Enzyme	Manufacturer
Accuprime supermix 1 enzyme	Invitrogen
CircLigase	Epicenter
DNase I	NEB
Polynucleotide kinase (PNK)	NEB
Phusion High-Fidelity DNA polymerase	Fermentas
RNase I	Ambion
RT M-MLV	Thermo Fischer
SuperScript® III Reverse Transcriptase	Thermo Fischer
T4 DNA ligase	NEB
T4 RNA ligase	NEB
Taq polymerase	Fermentas

5.5 Antibiotics

Table 5.5 Antibiotics

Antibiotic	Solvent	Working concentration
ampicillin	H2O	100 µg/ml
chloramphenicol	ethanol absolute	20 µg/ml
kanamycin	H2O	50 µg/ml

5.6 Drugs, inhibitors, and chemicals for cell culture

Table 5.6 Drugs, inhibitors, and chemicals for cell culture

Name	conditions of use	manufacturer
Actinomycin D	5µg/ml for 1h	Sigma
Amitryptiline hydrochloride	50µM for 1h 15min	Sigma
Anisomycin	10µg/ml for 20min	Sigma
Arsenite	0.1-0.5µM for 0.5-1h	Sigma
Cyclohexamide	100µM for 1h	Sigma
DMSO	v/v as vehicle control	Roth
GW4869	0.5µM for 1h 15min	Sigma
Hydrogen peroxide	0.5mM for 3h	AppliChem
Puromycin dihydrochloride	100µg/ml for 1h	Sigma
SB203580	5µM for 1h 15min	Sigma
TNFalpha	10ng/ml for 15min	Sigma

5.7 Antibodies

Table 5.7 Antibodies

Antibody	Source	Manufacturer	Conditions of use
ASM (4H2)	Mouse	Santa Cruz	IF: 1:250 ON at 4˚C; WB: 1:200
Ceramide monocl. Antibody	Mouse	Enzo Life Sciences	IF: 1:50 for 1h at RT
eIF3η (N-20)	Goat	Santa Cruz	IF: 1:500 for 1h at RT; WB: 1:3000
G3BP	Mouse	BD	IF: 1:250 for 2h at RT; WB: 1:1500
Lamin B	goat	Santa Cruz	WB: 1:200
Listeria monocytogenes	Rabbit	antibodies-online	IF: 1:750 for 2h at RT
p38 MAPK Antib.	Rabbit	Cell Signaling Technology	WB: 1:1000
Phospho-p38 MAPK	Mouse	Cell Signaling Technology	WB: 1:2000
Salmonella typhimurium0-4 [1E6]	Mouse	abcam	IF: 1:1000 for 1h at RT
Shigella flexneri	Rabbit	Gentaur	IF: 1:150 for 2h at RT
TIA-1 (C-20)	Goat	Santa Cruz	IF: 1:350 for 1h at RT; WB: 1:2000
TIAR-1 (C-18)	Goat	Santa Cruz	IF: 1:400 for 1h at RT; WB: 1:3000
α-Tubulin	Mouse	Sigma-Aldrich	WB: 1:3000
β-Actin	Mouse	Sigma-Aldrich	WB: 1:3000

Table 5.8 Secondary antibodies

Secondary antibodies	Source	Manufacturer	Conditions of use
Anti-Goat IgG Alexa Flour 488	Goat	Lifetechnologies	IF: 1:400
Anti-Goat IgG Alexa Flour 647	Goat	Lifetechnologies	IF: 1:400
Anti-Mouse IgG Alexa Flour 488	Mouse	Lifetechnologies	IF: 1:400
Anti-Mouse IgG Alexa Flour 594	Mouse	Lifetechnologies	IF: 1:400
Anti-Mouse IgG Alexa Flour 647	Mouse	Lifetechnologies	IF: 1:400
Anti-Rabbit IgG Alexa Flour 488	Rabbit	Lifetechnologies	IF: 1:400
Anti-Rabbit IgG Alexa Flour 594	Rabbit	Lifetechnologies	IF: 1:400
Anti-Rabbit IgG Alexa Flour 647	Rabbit	Lifetechnologies	IF: 1:400
ECL anti-goat IgG	Goat	Amersham/GE Healthcare	WB: 1:10000
ECL anti-Mouse IgG	Mouse	Amersham/GE Healthcare	WB: 1:10000
ECL anti-Rabbit IgG	Rabbit	Amersham/GE Healthcare	WB: 1:10000

Table 5.9 Cell dyes

Cell dyes	Manufacturer	Conditions of use
Alexa Fluor 594 Phalloidin	Thermo F. Sc. (Lifetech.)	IF 1:50 for 1h at RT
Cell Mask	Thermo F. Sc. (Lifetech.)	IF 1:10000 for 1h at RT
Hoechst	Thermo F. Sc. (Lifetech.)	IF 1:5000 for 15min at RT

5.8 Bacterial strains

Table 5.10 Bacterial strains

Genotype	Stock name	plasmid	Species	reference/source
Wild-type	AE-41		*Shigella flexneri* M90T serotype 5a	Sansonetti et al., 1982; from A. Zychlinsky
WT-GFP	AE-107	pXG-1	*Shigella flexneri* M90T serotype 5a	This study
WT-mCherry	AE-172	pSB4004	*Shigella flexneri* M90T serotype 5a	This study
Wild-type	AE-205	pKD46	*Shigella flexneri* M90T serotype 5a	from A. Zychlinsky
*ΔipaB/*invasin	AE-176	pRI203	*Shigella flexneri* M90T serotype 5a	This study
*ΔipaB/*invasin-mCherry	AE-178	pSB4004	*Shigella flexneri* M90T serotype 5a	This study
ΔospG	AE-77		*Shigella flexneri* M90T serotype 5a	This study
ΔospI	AE-78		*Shigella flexneri* M90T serotype 5a	This study
ΔospB	AE-79		*Shigella flexneri* M90T serotype 5a	This study
ΔvirA	AE-87		*Shigella flexneri* M90T serotype 5a	This study
ΔipaA	AE-88		*Shigella flexneri* M90T serotype 5a	This study
ΔvirG	AE-89		*Shigella flexneri* M90T serotype 5a	This study
ΔospE2	AE-90		*Shigella flexneri* M90T serotype 5a	This study
ΔipgB2	AE-91		*Shigella flexneri* M90T serotype 5a	This study

ΔipgD	AE-92	*Shigella flexneri* M90T serotype 5a	This study
ΔipaJ	AE-93	*Shigella flexneri* M90T serotype 5a	This study
Δspa15	AE-94	*Shigella flexneri* M90T serotype 5a	This study
ΔipaH9.8	AE-95	*Shigella flexneri* M90T serotype 5a	This study
ΔipaH4.5	AE-96	*Shigella flexneri* M90T serotype 5a	This study
ΔipaH7.8	AE-97	*Shigella flexneri* M90T serotype 5a	This study
ΔipaH3	AE-98	*Shigella flexneri* M90T serotype 5a	This study
ΔipaH2.5	AE-99	*Shigella flexneri* M90T serotype 5a	This study
ΔospC3	AE-100	*Shigella flexneri* M90T serotype 5a	This study
ΔospZ	AE-101	*Shigella flexneri* M90T serotype 5a	This study
ΔipaH1.4	AE-102	*Shigella flexneri* M90T serotype 5a	This study
ΔicsB	AE-103	*Shigella flexneri* M90T serotype 5a	This study
ΔipgB1	AE-110	*Shigella flexneri* M90T serotype 5a	This study
ΔospE1	AE-111	*Shigella flexneri* M90T serotype 5a	This study
ΔospC1	AE-112	*Shigella flexneri* M90T serotype 5a	This study
ΔospC2	AE-113	*Shigella flexneri* M90T serotype 5a	This study
ΔospF	AE-114	*Shigella flexneri* M90T serotype 5a	This study
ΔipaB	AE-115	*Shigella flexneri* M90T serotype 5a	This study
ΔospD1	AE-164	*Shigella flexneri* M90T serotype 5a	This study
ΔospD2	AE-165	*Shigella flexneri* M90T serotype 5a	This study

ΔospD3	AE-166		*Shigella flexneri* M90T serotype 5a	This study
ΔshiA	AE-167		*Shigella flexneri* M90T serotype 5a	This study
Wild-type	AE-45		*Salmonella enterica* serovar Typhimurium SL1344	from J.Galan
WT-pTetGFP	AE-35		*Salmonella enterica* serovar Typhimurium SL1344	from J.Vogel; Papenfort et al,2009
ΔsifA-mCherry	AE-203	pSB4004	*Salmonella enterica* serovar Typhimurium SL1344	from J.Galan; Spano et al, 2011
Δ4 (ΔsopBΔsipAΔsopEΔsopE2)-pTetGFP	AE-168		*Salmonella enterica* serovar Typhimurium SL1344	This study
ΔFliC	AE-206		*Salmonella enterica* serovar Typhimurium SL1344	From J.Vogel
ΔFlhC5213	AE-207		*Salmonella enterica* serovar Typhimurium SL1344	From J.Vogel
ΔFliC-FliC	AE-208	pXG1-FliC	*Salmonella enterica* serovar Typhimurium SL1344	This study
Wild-type	AE-121		*Listeria monocytogenes EGD-e*	From J.Vogel
TOP10	AE-39		*Escherichia coli*	Invitrogen

5.9 Plasmids

Table 5.11 List of plasmids

Name	expression	source/reference
pXG-1	GFP	Urban and Vogel, 2007
pSB4004	mCherry	Spano et al, 2011
pKD46	lambda red recombinase	Datsenko & Wanner, 2000
pRI203	*Yersinia* invasin	Isberg et al, 1985
pXG-1_FliC	*Salmonella* FliC	This study

5.10 Synthetic oligonucleotides

Table 5.12 Synthetic Oligonucleotides

Name	Sequence	description
AE171	AATCTCTTGTGATTTTTAAATATCGTAACAAAGGTATGACG TGTAGGCTGGAGCTGCTTC	delete Shigella ospG
AE172	TCATAGAAGAGCCTCTGGCTTATAGCATCAACAAATACGTgg tccatatgaatatcctccttag	
AE173	GACCACACAAGGTAGCGTG	verify deletion Shigella ospG
AE174	GTTAATATCGCGAGGGAATG	
AE175	TTCAAGGGGCCGGCTCAAATCTATGTACAGGCTCTCAGCAGT GTAGGCTGGAGCTGCTTC	delete Shigella ospl
AE176	GAAGAAAATATAGTGAGTATATATACTGTCAGGATACAATg gtccatatgaatatcctccttag	
AE177	ACACGAATAGCTGCAGTTC	verify deletion Shigella ospl
AE178	GACATATATCCAAGCCTATCTC	
AE179	GAACGTTTTTTTACAGTCTGGCAGCCAATATAATATTGGCG TGTAGGCTGGAGCTGCTTC	delete Shigella VirA
AE180	TATATTGGCATTAATAGGAAAATACATCAGGAGAAATCAAg gtccatatgaatatcctccttag	
AE181	GCTGAGATTCTATTGGTCC	verify deletion Shigella VirA
AE182	ATGCAATAACTGCATAATTG	
AE183	CTTAAATGCAAACAATTAACTATAGGTTAAAAATTTTATAG TGTAGGCTGGAGCTGCTTC	delete Shigella OpsB
AE184	ACTATGATGTTTATAAAACAATATATGGAGTCATGTAGGTg gtccatatgaatatcctccttag	
AE185	ACAAAGAAGCTTGCATACTATATG	verify deletion Shigella
AE186	TTCCCTCATAGGGAAGCAC	
AE187	ATTGTTATTTTTTAAATCAGATATATCATCTGTAAGTAATG TGTAGGCTGGAGCTGCTTC	delete Shigella IpaA
AE188	TCAACAGAATACAGCGAGTTAAAAAGCAAAATATCCGATAg gtccatatgaatatcctccttag	
AE189	ACACCAGCATCAGTGTCTG	verify deletion Shigella IpaA
AE190	TAGTTTGCTGTACGCTATACC	
AE265	TTTTCTTATTATTTCTCTTTTAATTTCAGCATCCTGCATAGT GTAGGCTGGAGCTGCTTC	delete Shigella IpgD

AE266	AACTGCAATCAATGCCCCATTTATGACTGAGGATAATTAAG GTCCATATGAATATCCTCCTTAG	
AE267	AAGTGCCTGATGTATCAGG	verify deletion Shigella IpgD
AE268	TGCTAAATCTTCCATATATTCC	
AE273	GGACAGTTCAATGACGTAACGCAGCCATTTTTCTGGCTCCGT GTAGGCTGGAGCTGCTTC	delete Shigella OspE2
AE274	TTCTTTTGAAAATGGAGCTTAAACGAGTCTGAAATTAACTG GTCCATATGAATATCCTCCTTAG	
AE275	TGTCAACTTAAGATACAACGAC	verify deletion Shigella OspE2
AE276	TCTGAAATAGAATTACTGCTCTAC	
AE277	TTTTCAGGGGTTTATCAACCACTTACTGATAATATAGTGCG TGTAGGCTGGAGCTGCTTC	delete Shigella VirG/IcsA
AE278	AGAGAAATGCAGGACATCAACACGCCCTGCATTTTTATTAG GTCCATATGAATATCCTCCTTAG	
AE279	AACACAGCTCTCATGTTTTGG	verify deletion Shigella VirG/IcsA
AE280	AGGCATACCATCATGTGCAC	
AE289	TAATGACAATGTTACTATTTTACATGACAAGGTGATTATAG TGTAGGCTGGAGCTGCTTC	delete Shigella IpgB2
AE290	ATTTACTTTTCTTAGTTTCTTTACTCGGGATGTTCTGTCAGG TCCATATGAATATCCTCCTTAG	
AE291	TCTCAGAGAGTTTAGTCTCTGG	verify deletion Shigella IpgB2
AE292	TCAATATATTAGGACTTACTTGCG	
AE297	CCAGTCCGTAAATTCATTCTCTTCACGGCTTCTGACCATGGT GTAGGCTGGAGCTGCTTC	delete Shigella IpaH2.5
AE298	TCACTAGAGTTCTTATCGTTGATAAGAAATTCTGGTTATAG GTCCATATGAATATCCTCCTTAG	
AE299	AGCAATACCTGGAGAAAGAGTAC	verify deletion Shigella IpaH2.5
AE300	TGACTTTCCAGAACCATACG	
AE301	ACAAAGCCATTTGTCCACCGGCTTTAACTGGATGCCCATCGT GTAGGCTGGAGCTGCTTC	delete Shigella IpaH9.8
AE302	TCTGAGGGTACTCATTCTCCAGCATCTCATATTTCTGCTCGG TCCATATGAATATCCTCCTTAG	
AE303	AGGCCATTCACGGTTAAC	verify deletion Shigella IpaH9.8
AE304	TATGGCAGAGGAGTAAAACC	
AE309	CCATAGCTTCGGCAGTGCGGAGGTCATTTGCTGTCACTCCGT GTAGGCTGGAGCTGCTTC	delete Shigella IpaH4.5
AE310	TTTTTCGTTCCCTTTGTGGCTTATCATGTATATCTCGTTTGG TCCATATGAATATCCTCCTTAG	
AE311	AGACAGGAACATATTCCTCC	verify deletion Shigella IpaH4.5
AE312	TGACTTTCCAGAACCATACG	
AE313	AGCTTCGGCAGTGCGGAGGTCATTTGCTGTCACTCCCGACGT GTAGGCTGGAGCTGCTTC	delete Shigella IpaH7.8
AE314	TAAATATTTATTCTCACAAATATAAGGTTGACCTAGCATTG GTCCATATGAATATCCTCCTTAG	
AE315	AACTTAATATCGGAAATGGTAAG	verify deletion Shigella IpaH7.8
AE316	TTATGCTTATGCGACGTG	

AE329	TTTCTTTTAACAAAGCCATTTGTCCATCGGCTTTAACTGAGT GTAGGCTGGAGCTGCTTC	delete Shigella IpaH3
AE330	CTCAGACCTGATGCTTTCAGCCGGTCAGCCACCCTCTGAGGG TCCATATGAATATCCTCCTTAG	
AE331	AACAAGAACAATACGGTGC	verify deletion Shigella IpaH3
AE332	AGTCAGTCCGGTCTGTGG	
AE333	CGCATTGCTGGATGCAATACTGTGCTGCAATTACTCGTCGGT GTAGGCTGGAGCTGCTTC	delete Shigella IpaJ
AE334	CCAAAATATTCAAGCTCCTTCACAGATAAAAAACGACAATG GTCCATATGAATATCCTCCTTAG	
AE335	TGATGACGACGGAAAAGAG	verify deletion Shigella IpaJ
AE336	TTCGTCTTCCCACACAAC	
AE337	GTGAACGTAGTCATCTTTAATAACAACTCTTAACTGTAAGG TGTAGGCTGGAGCTGCTTC	delete Shigella Spa15
AE338	GGTTGTCCTCCATCAATTATTACAGATTTAGACAGCCATTGG TCCATATGAATATCCTCCTTAG	
AE339	TACTCGTTATATCGTATGCTGAG	verify deletion Shigella Spa15
AE340	ATCGCTAAGACTTGTTTCC	
AE408	AGTTAGATAATGTTATCTAAATAACCACAGATAAAAACGCG TGTAGGCTGGAGCTGCTTC	delete OspC3
AE409	TTATTGATAAAATATTCTAGCACTTTATAGTTGGCACCATG GTCCATATGAATATCCTCCTTAG	
AE410	TTGCCTTCAGTAAAGGAAAC	verify deletion OspC3
AE411	AATCACTCATGATGACTTCG	
AE502	TGTTTATATTTGAGTATAGAGATTAAAAATGATTAGTCCCG TGTAGGCTGGAGCTGCTTC	delete Shigella OspZ
AE503	CATTTCACGAGCAATAATAATCTCAGATTTAATAGACTTTG GTCCATATGAATATCCTCCTTAG	
AE504	AGCGATTGTAATCGCACTCG	verify deletion Shigella OspZ
AE505	ACATTAAGTAACAGGCATTCGAG	
AE506	TGAACTAACATATAGGGGGTATCATGCAAATTCTAAACAAA GTGTAGGCTGGAGCTGCTTC	delete Shigella IpgB1
AE507	AAGATTTAATATAAAAGATTTAATTTGTATTGCTTTGACGG GGTCCATATGAATATCCTCCTTAG	
AE508	TCTTTCACCTGATGAACTCATTG	verify deletion Shigella IpgB1
AE509	TCAATTACTGCAGTAGAGATGC	
AE510	ACATCGTTAGGTGTAGCAACCAATTTAACGTCAGGGAGTGG TGTAGGCTGGAGCTGCTTC	delete Shigella IcsB
AE511	ATGGAGAGTTAATAAAGTATGAGCCTCAAAATTAGCAATTG GTCCATATGAATATCCTCCTTAG	
AE512	ATCTGGCATCACATAACATC	verify deletion Shigella OspC1
AE513	TCTATCGCTGTAAGCAGTGC	
AE514	TTCCTTTCAGTAAAGGAAGTGTG	verify deletion Shigella OspC2
AE515	ACCACATGCAATGTGTTGTTG	
AE516	TTAACTAGAATTCTTATCGTTGATAAGAATTCTAGTTATAG TGTAGGCTGGAGCTGCTTC	delete Shigella IpaH1.4

AE517	GCGAGCATGGTCTGGAAGGCCAGGTAGACTTCTATCTCATG GTCCATATGAATATCCTCCTTAG	
AE518	AGAAAGGGTACAAAGCAAACTG	verify deletion Shigella IpaH1.4
AE519	AATGCGGAACTAACTGACCATC	
AE564	AAAATAAATTTTTTGCCAAAATATAACATAAGGAAGTAATG TGTAGGCTGGAGCTGCTTC	delete Shigella OspE1
AE565	TCAGAAATCAGAATACCGTTGGCTTTGTTTTTCATCAATTG GTCCATATGAATATCCTCCTTAG	
AE566	AGTCATCGGCTCCTTCATTG	verify deletion Shigella OspE1
AE567	AGATGGAGTTACTCCTCTCTG	
AE570	AAGATATTAATTAAAACTGTTTTCATATAAGGTTCATTTTG TGTAGGCTGGAGCTGCTTC	delete Shigella OspC1
AE571	GTAACAGCCTCCTCTAAGGATATTTCTCTAATCTTAACTTGG TCCATATGAATATCCTCCTTAG	
AE572	AATAACTGCAGATAAAAACGCACATAATGGGGGATGTTTTG TGTAGGCTGGAGCTGCTTC	delete Shigella OspC2
AE573	GATATATCTCTGAGTCTTATCTTTTTGAAGTTATCTGTGCGG TCCATATGAATATCCTCCTTAG	
AE574	AATATAAGATAATATATCTATTTTATAGAGGACGTTTTCTG TGTAGGCTGGAGCTGCTTC	delete Shigella OspF
AE575	CCAGTTTTCAAGCTACAAGGTGGTGTAGCTGGCATCTTCTGG TCCATATGAATATCCTCCTTAG	
AE576	ATGATCGGAGAAGACCCTTAC	verify deletion Shigella OspF
AE577	TTCGGATTTCAGATGAGTAGC	
AE578	CTGGTTTTCCTCTTGCCAAAATATTGACTTCCACTGAGCTGT GTAGGCTGGAGCTGCTTC	delete Shigella IpaB
AE579	GGTATAAGGTCTGTGAGGGTTTTACCTATTATTTTGCCAAG GTCCATATGAATATCCTCCTTAG	
AE580	AGTGCTTCGAACTCGTAATTC	verify deletion Shigella IpaB
AE581	TATGCGCTGCAATCTGCTG	
AE630	TATGTTAACAGGCTCAAGTTTC	verify deletion Shigella IcsB
AE631	ACTTTCAATGCGTTGCCTAAC	
AE662	GCAAAAAGGATGAACAAAAATGTCAATAAATAACTATGGAG TGTAGGCTGGAGCTGCTTC	delete Shigella OspD1
AE663	GATCCTTCTAAGTGCAATTCTTTGCAGCTATTTAGCACACGG TCCATATGAATATCCTCCTTAG	
AE664	TGAATATAGCCATTCAATGTGGC	verify deletion Shigella OspD1
AE665	TGGTTCTATGGGTAGTATCG	
AE666	GCAATCTAATAGTATTATAACATCTCTATGGTTGTCTTCTGT GTAGGCTGGAGCTGCTTC	delete Shigella OspD2
AE667	TCACTACTAAGCATTTTCTTATTAAGCAGACTTCCGAACAGG TCCATATGAATATCCTCCTTAG	
AE668	AGGAGCATTCTGAATAAGCTACC	verify deletion Shigella OspD2
AE669	CTACACCTTGTTGGAGTGAACAT	
AE670	AGTCTGCGTCACAACCCATCAATGAAAGGAATATATACATG TGTAGGCTGGAGCTGCTTC	delete Shigella OspD3

AE671	CTCATTCAAGATATCACCATAAGCTAAGATTGCATCAGCCGG TCCATATGAATATCCTCCTTAG	
AE672	ACCACATCAATCTTTGCCATC	verify deletion Shigella OspD3
AE673	ATTCAGTGTATCACCACGAG	
AE674	CTCTCAGACTATATCACCACATGTTTTACAGGCTCAGAAAGT GTAGGCTGGAGCTGCTTC	delete Shigella ShiA
AE675	ATAAATTATTACTTGTTTTAAAGTTACACTAATGCAATATG GTCCATATGAATATCCTCCTTAG	
AE676	TCGTAAGCAATATTCATTCGGTG	verify deletion Shigella ShiA
AE677	ATGAGTTCATGGAGTAATTCG	verify deletion Shigella ShiA
AE993	[Phos]NNAACCNNNAGATCGGAAGAGCGTCGTGgatcCTGAA CCGC	Rt1clip
AE994	[Phos]NNACAANNNAGATCGGAAGAGCGTCGTGgatcCTGAA CCGC	Rt2clip
AE995	[Phos]NNATTGNNNAGATCGGAAGAGCGTCGTGgatcCTGAA CCGC	Rt3clip
AE996	[Phos]NNAGGTNNNAGATCGGAAGAGCGTCGTGgatcCTGAA CCGC	Rt4clip
AE997	[Phos]NNCGCCNNNAGATCGGAAGAGCGTCGTGgatcCTGAA CCGC	Rt5clip
AE998	[Phos]NNCCGGNNNAGATCGGAAGAGCGTCGTGgatcCTGAA CCGC	Rt6clip
AE999	[Phos]NNCTAANNNAGATCGGAAGAGCGTCGTGgatcCTGAA CCGC	Rt7clip
AE1000	[Phos]NNCATTNNNAGATCGGAAGAGCGTCGTGgatcCTGAA CCGC	Rt8clip
AE1001	[Phos]NNGCCANNNAGATCGGAAGAGCGTCGTGgatcCTGAA CCGC	Rt9clip
AE1002	[Phos]NNGACCNNNAGATCGGAAGAGCGTCGTGgatcCTGAA CCGC	Rt10clip
AE1003	[Phos]NNGGTTNNNAGATCGGAAGAGCGTCGTGgatcCTGAA CCGC	Rt11clip
AE1004	[Phos]NNGTGGNNNAGATCGGAAGAGCGTCGTGgatcCTGAA CCGC	Rt12clip
AE1005	[Phos]NNTCCGNNNAGATCGGAAGAGCGTCGTGgatcCTGAA CCGC	Rt13clip
AE1006	[Phos]NNTGCCNNNAGATCGGAAGAGCGTCGTGgatcCTGAA CCGC	Rt14clip
AE1007	[Phos]NNTATTNNNAGATCGGAAGAGCGTCGTGgatcCTGAA CCGC	Rt15clip
AE1008	[Phos]NNTTAANNNAGATCGGAAGAGCGTCGTGgatcCTGAA CCGC	Rt16clip
AE1009	GTTCAGGATCCACGACGCTCTTCaaaa	Cut-Oligo
AE1010	AATGATACGGCGACCACCGAGATCTACACTCTTTCCCTACAC GACGCTCTTCCGATCT	P5Solexa
AE1011	CAAGCAGAAGACGGCATACGAGATCGGTCTCGGCATTCCTGC TGAACCGCTCTTCCGATCT	P3Solexa
AE1012	rAppAGATCGGAAGAGCGGTTCAG/ddC/	L3-App, Pre-adenylated 3' linker

* oligonucleotides were purchased from Sigma, and the pre-adenylated 3' linker was purchased from IDT

Table 5.13 Primers for Sybr Realtime qRT-PCR

Name	Sequence	Description
AE1	ATGCTTTTCCCGTTATCCGG	Sybr Realtime sense oligo for gfp
AE2	GCGTCTTGTAGTTCCCGTCATC	Sybr Realtime antisense oligo for gfp
AE99	GGCGAGTTCATCTACAAG	Sybr Realtime sense oligo for mcherry
AE100	GGTCTTCTTCTGCATTACG	Sybr Realtime antisense oligo for mcherry
AE109	TACCTCCGTCAGCGAACC	SyBr Realtime sense oligo *Salmonella* rfaH
AE110	TGGCGTTGATTGTAGTGGTATG	SyBr Realtime antisense oligo *Salmonella* rfaH
AE129	GCAGTCAGTGAACCGTTA	SyBr Realtime sense oligo for *Shigella flexneri* rfaH ORF set2
AE130	TGATGGTCGTGGTATGAATC	SyBr Realtime antisense oligo for *Shigella flexneri* rfaH ORF set2
AE341	CCTGTACGCCAACACAGTGC	Sense oligo for amplification of human beta-actin for qRT-PCR
AE342	ATACTCCTGCTTGCTGATCC	Anti-sense oligo for amplification of human beta-actin for qRT-PCR
AE39	ATTGAAATCAGCCAGCACGC	Sybr Realtime sense oligo for RPL37A
AE40	GCAGGAACCACAGTGCCAGATCC	Sybr Realtime antisense oligo for RPL37A
AE1229	GCTGGAATTATTACCGAAT	SyBr Realtime sense oligo for human SMPD1 (ASMase)
AE1230	TCATCATAGAAGACCTCAA	SyBr Realtime antisense oligo for human SMPD1 (ASMase)
AE1233	ATGGTGCTCAACGCCTAT	SyBr Realtime sense oligo for human SMPD2 (NSMase-1)
AE1234	ACGATGTGCTAGGTAGATGT	SyBr Realtime antisense oligo for human SMPD2 (NSMase-1)

Table 5.14 siRNAs

Name	Target
Non-targeting 5	no specific target in human
ASM	*smpd1* human gene
NSM-1	*smpd2* human gene

siRNAs were purchased from Dharmacon

5.11 Media

5.11.1 Bacterial media

Luria broth (LB) liquid medium and LB Agar

5.0 g tryptone
2.5 g Bacto-yeast extract
5.0 g NaCl
7.5 g agar (for LB agar)
500 ml H_2O

LB agar for motility assays

0.3% agar or agarose was added to the LB medium. After autoclaving, 20ml of agar at 55˚C was poured into petri dishes on the bench. After 15min of solidification, 10µl of ON culture was spotted in the middle of the plate without disturbing the agar. The plates were incubated at 37˚C for 8h. The diameters of migration were measured, and images were taken with the imaging system Image Quant LAS 4000 at 2h intervals.

Tryptic soy broth (TSB)-Congo red agar

7.5 g Agar
15 g TSB (BBL Trypticase Soy Broth)
500 ml H_2O
0.05 g Congo Red

Brain heart infusion (BHI)-Agar

7.5 g Agar
18.5 g BHI (Brain Heart Infusion)
500 ml H_2O

15.11.2 Cell culture media

DMEM GlutaMAX containing 1.0 g/l glucose (Life Technologies)

RPMI 1640 Medium, GlutaMAX™ (Life Technologies)

Opti-MEM® I Reduced Serum Medium (Life Technologies)

Fetal bovine serum (Biochrom)

5.12 Buffers and solutions

10x Phosphate-buffered saline (PBS) (1 L):

2 g KCl
2.4 g KH_2PO_4
80 g NaCl
14.4 g Na_2HPO_4
pH 7.4

Lysis buffer for sphingomyelinase assays

20 mM Tris-HCl
2 mM EDTA
5 mM EGTA
1 mM Na_3VO_4
10 mM β-glycerol phosphate
1 mM PMSF
1X protease inhibitors cocktail
pH 7.5

Hypotonic lysis buffer (HLB) for cell fractionation

10 mM Tris-HCl
10 mM NaCl
3 mM $MgCl_2$
0.3 % IGEPAL CA-630
1 mM DTT
1X protease inhibitors cocktail
pH 7.5

1X DNase I buffer

10 mM Tris-HCl
2.5 mM $MgCl_2$
0.5 mM $CaCl_2$
pH 7.6

5X First-Strand buffer

250 mM Tris-HCl
375 mM KCl
15 mM $MgCl_2$
pH 8.3

Chemiluminescence solution

2 ml chemiluminescence solution A
200 µl chemiluminescence solution B
0.6 µl 3% (v/v) H2O2

Chemiluminescence solution A

0.1 M Tris-Cl (pH=8.6)
0.025% (w/v) luminol

Chemiluminescence solution B

	0.11% (w/v) p-coumaric acid in DMSO
SDS running buffer (10X)	
	30.275 g Tris base 144 g glycin 10 g SDS 1 l H_2O
PAA solution resolving gel (10%)	
	3.75 ml Tris solution (lower buffer) 2.5 ml Rotiphorese gel 40 (37.5:1) 3.75 ml H_2O 75 µl 10% (w/v) APS 7.5 µl TEMED
PAA solution stacking gel (4%)	
	1.25 ml Tris solution (upper buffer) 1 ml Rotiphorese gel 40 (37.5:1) 7.5 ml H_2O 150 µl 10% (w/v) APS 15 µl TEMED
Tris solution (lower buffer)	
	1.5 M Tris-HCl (pH=8.8) 0.4% (w/v) SDS
Tris solution (upper buffer)	
	0.5 M Tris-HCl (pH=6.8) 0.4% (w/v) SDS
TBS (10X)	
	24.11 g Tris base 72.6 g NaCl pH=7.4 adjusted with HCl 1 l H_2O
TBST (1X)	
	1X TBS 0.1% (v/v) Tween20
Transfer buffer (1X)	
	100 ml transfer buffer stock (10X) 200 ml methanol 1 l H_2O
Transfer buffer stock (10X)	

TAE (50X)	30 g Tris base 144 g glycin 1 l H_2O
TBE (10X)	242 g Tris base 51.7 ml acetic acid 10 mM EDTA (pH=8.0) 1 l H_2O
Agarose gel solution	108 g Tris base 55 g boric acid 20 mM EDTA (pH=8.0) 1 l H_2O
DNA loading buffer (5X)	1-2% (w/v) agarose in 1X TAE
TE buffer (1X)	10 mM Tris-Cl (pH=7.6) 60% (v/v) glycerol 60 mM EDTA (pH=8.0) 0.025% (w/v) bromophenol blue
5x Protein loading buffer	10 mM Tris-Cl (pH=8.0) 1 mM EDTA (pH=8.0) Sterile filtered (0.22 µm)
5X MOPS-SDS Running buffer	15 g SDS pellets 46.95 mL Tris-HCl 1M (pH=6.8) 0.075 g Bromophenol blue 75 mL Glycerol 100% 11,56 g DTT 150 ml H_2O
3.5X Bis-Tris gel buffer	250 mM Tris 250 mM MOPS 5 mM EDTA 0.5 % SDS 5 mM Sodium bisulfite (added fresh) pH7.7
	1.25 M Bis-Tris HCl pH6.8

Bis-Tris 10% separation gel

2.86 ml Bis-Tris buffer
2.5 ml Rotiphorese gel 40 (37.5:1)
4.64 ml H_2O
100 µl 10% (w/v) APS
4 µl TEMED

Bis-Tris 4% stacking gel

2.86 ml Bis-Tris buffer
1 ml Rotiphorese gel 40 (37.5:1)
6.14 ml H_2O
150 µl 10% (w/v) APS
15 µl TEMED

Solutions for iCLIP

Lysis Buffer

50 mM Tris-HCl, pH 7.4
100 mM NaCl
1% NP-40
0.1% SDS
0.5% sodium deoxycholate
1X protease inhibitor cocktail (fresh)

High-salt Wash buffer

50 mM Tris-HCl, pH 7.4
1 M NaCl
1 mM EDTA
1% NP-40
0.1% SDS
0.5% sodium deoxycholate

PNK Buffer

20 mM Tris-HCl, pH 7.4
10 mM MgCl2
0.2% Tween-20

5x PNK *pH 6.5* Buffer:

350 mM Tris-HCl, pH 6.5
50 mM MgCl2
25 mM dithiothreitol
(freeze aliquots of the buffer)

4x Ligation Buffer

200 mM Tris-HCl, pH 7.8
40 mM MgCl2
40 mM dithiothreitol

PK Buffer

100 mM Tris-HCl, pH 7.4
50 mM NaCl

	10 mM EDTA
PK Buffer + 7 M Urea	
	100 mM Tris-HCl, pH 7.4 50 mM NaCl 10 mM EDTA 7 M urea
GLII (RNA loading buffer II; 2X)	
	0.025% (w/v) bromophenol blue 0.025% (w/v) xylene cyanol 18 µM EDTA (pH=8.0) 0.13% (w/v) SDS 95% formamide
6% TBE-urea gel	
	10 ml Rotiphorese gel 40 (37.5:1) 7 M Urea 100 µl 10% APS 10 µl TEMED

5.13 Methods

5.13.1 Cell lines and cell culture

Human epithelial HeLa-229 cells (ATCC) were cultured in DMEM and human colon epithelial HCT-8 cells (ATCC) were cultured in RPMI. Media were supplemented with 10% fetal bovine serum. Cells were maintained at 37°C in a 5% CO2 humidified atmosphere.

Cells were exposed to heat-shock by incubation at 45°C in a 5% CO2 humidified atmosphere for 1h.

5.13.2 Treatment of cells

All drugs, inhibitors, and the corresponding vehicles were added directly to the culture medium. The cell supernatant was exchanged with 500 µl of medium containing the drug/inhibitor. The cells were incubated at 37°C in a 5% CO2 humidified atmosphere for the designated time. The cells were washed 1 time in PBS before any downstream manipulation.

5.13.3 siRNA reverse transfections

The siRNAs (50nM for single-knockdown and 25nM for double-knockdown) were added to 0.8µl Lipofectamine RNAiMAX in 120µl of Opti-MEM® I Reduced Serum Medium (after 5min incubation at RT). This mix was incubated for 30min at RT, then added to $6x10^5$ cells in 240µl culture medium, and seeded in 24-well plates. The transfections were incubated for 66h and the medium was exchanged 24h before infection.

5.13.4 Plasma membrane sphingomyelin activity assays

$3.5x10^5$ cells were seeded in 6-well plates 2 days prior to the experiment. Cells were harvested after treatment or infection with PBS+5mM EDTA (detached) and washed 3 times in ice-cold PBS+100 µM Na_3VO_4 at 4˚C. Cells were resuspended in 100 µl of lysis buffer and disrupted by five cycles of freezing and thawing in a methanol/dry-ice bath. The lysate was centrifuged for 10 min at 1000 g at 4˚C, and the supernatant (post-nuclear homogenate) was transferred to a new tube. The supernatant was centrifuged for 1h at 100000 g at 4˚C. The resulting pellet (membrane fraction) was resuspended in 40 µl 1X reaction buffer provided with the sphingomyelinase assay kit. 10 µl were used for the measurement of neutral and acid sphingomyelinase each. The Amplex® Red Sphingomyelinase Assay Kit was used to measure the enzyme activity following the manufacturer's instructions.

5.13.5 Nuclear and cytoplasmic cell fractionation

$3.5x10^5$ cells were seeded in 6-well plates 2 days prior to the experiment. Cells were harvested after treatment or infection with PBS+5mM EDTA (detached) and washed 2 times in ice-cold PBS at 4˚C. The cells were resuspended in 400 µl of ice-cold hypotonic lysis buffer (HLB), and incubated on ice for 12 min with gentle pipetting. The lysate was centrifuged at 800g for 5 min at 4˚C. The supernatant was kept as the cytosolic fraction by adding 90 µl of 5X protein loading buffer (PL). The pelleted nuclei were washed 3 times in 800 µl HLB with 5 min incubation on ice each, pipetting and vortexing, and centrifuged at 150 g for 2 min at 4˚C. The nuclei were resuspended in 200 µl (1/2 the volume of the cytoplasmic fraction) lysis buffer (iCLIP), with 1mM DTT and 1X protease inhibitors cocktail, and 40 µl 5X PL. All samples were boiled for 5 min and stored at -20˚C. (modified from Gagnon et al, 2014).

5.13.6 Infection assays

i) *Shigella*

Bacteria were streaked freshly on TSB/Congo Red agar plates. An overnight culture was started from a single colony in 2 ml LB at 37˚C, 220rpm (12-14 h). The next day, the ON culture was diluted 1/10 in 10ml LB and grown until an OD_{600} of 0.4 at 37˚C, 220rpm. 1 ml of the bacterial culture was centrifuged at 12000rpm for 2min at RT, and resuspended in 1 ml cell culture medium. The culture was diluted further in cell culture medium to reach the required multiplicity of infection (MOI).

For infection, cells were seeded 2 days prior to the experiment. The supernatant of the cells was exchanged with the prepared bacterial suspension and centrifuged at 2000 g for 15 min at RT. The cells with the bacteria were incubated at 37˚C for 15 min in a 5% CO2 humidified atmosphere. The remaining extracellular bacteria were killed by exchanging the supernatant with medium containing 50 µg/ml of gentamycin, and further incubated for 30 min at 37˚C, this step was considered as the start of infection (time 0). The

supernatant was then exchanged with medium containing 10 µg/ml of gentamycin, and incubated at 37˚C until the cells were collected.

ii) *Salmonella*

The infections with *Salmonella* were performed similarly to *Shigella*, except the day of the infection the diluted culture was grown until an OD_{600} of 2. The cells and bacteria were centrifuged at 250 g for 10 min and then incubated at 37˚C for 20 min.

iii) *Listeria*

The infections with *Listeria* were performed similarly to *Salmonella*, except the day of the infection the diluted culture was grown until an OD_{600} of 0.7.

Number of bacteria per ml for
Shigella OD_{600} of 1 ⇒ $4x10^8$ bacteria/ml
Salmonella OD_{600} of 2 ⇒ $2x10^9$ bacteria/ml
Listeria OD_{600} of 0.7 ⇒ $1x10^9$ bacteria/ml

iv) Adhesion assays

For adhesion, cells were infected with bacteria following the standard procedure. For *Shigella*, cells were centrifuged at 2000 g for 15 min and incubated for 10 min at 37°C, 5% CO2. For *Salmonella*, cells were centrifuged at 250 g for 10 min. The cells were washed thoroughly 5 times with PBS and collected for downstream analysis.

v) Re-infection assays

Cells were infected with *Shigella* following the standard protocol. The cells were washed with PBS at 3 hpi and re-infected using the standard infection protocol. In case of treatment with inhibitors, the inhibitors were directly added to culture medium containing 10 µg/ml of gentamycin and added to the cells at 2hpi, then the cells were washed with PBS and re-infected.

5.13.7 Quantification of colony forming units (CFU)

Cells were lysed by adding 0.5 ml PBST (PBS containing 0.1% Triton X-100). After incubation for > 5 min, cells were collected by scraping. Dilutions of the lysate were made in 500 µl PBS, vortexed, and plated on LB agar plates using glass beads and incubated at 37°C ON. The colonies were counted and calculated according to the dilution factor, for total number of bacteria.

5.13.8 Isolation of total RNA

Cells were lysed in TRIzol, and incubated for > 5 min at RT. 100 µl chloroform was added to the lysate and the mixture was mixed by shaking for 15 sec. The lysate was centrifuged for 10 min at 12000 rpm at 4°C, and the top aqueous phase was transferred into a new tube. An equal volume of isopropanol was added to the supernatant, mixed by shaking, and incubated at -20°C for >20 min for RNA precipitation. The RNA was centrifuged at >13000 rpm for >20 min and washed 3 times with 85% Ethanol absolute. The pellet was dried for 10 min and resuspended in RNase-free water, and the RNA was stored at -20°C.

5.13.9 Determination of concentration of nucleic acids
DNA and RNA concentrations were determined using NanoDrop2000.

5.13.10 cDNA synthesis and Quantitative reverse transcription PCR (qRT-PCR)

i) DNase treatment

500 ng of total RNA in 12.5 µl of RNase-free was used for complementary DNA (cDNA) synthesis. The following mixture was added to the RNA and incubated at 37°C for 10 min:

1.5 µl 10X DNase I buffer
0.5 µl of RNaseOUT
0.5 µl of DNase I

Then 1.5 µl of 0.05 M EDTA was added, mixed by pipetting, and incubated for 10 min at 75°C for heat denaturation of the DNase. RNA was cooled down on ice for 1 min.

ii) reverse transcription

2 µl dNTP mix 10 mM
2 µl random primers (1:20 dilution of the stock)
3.5 µl H_2O

was further added to the RNA and incubated at 65°C for 5 min and then quick-chilled on ice.

8 µl 5X First-Strand buffer
4 µl DTT 0.1 M
2 µl H_2O

was added and mixed by pipetting, then incubated at 37°C for 2 min. 0.5 µl of M-MLV reverse transcriptase was added to the reaction and incubated with the following program in a thermal cycler:

25°C for 10 min
30°C for 50 min
75°C for 15 min

iii) Quantitative reverse transcription PCR (qRT-PCR)

The cDNA was diluted 1:5 and 1-2 µl were used for qRT-PCR by adding to the following mix

3 µl H_2O
1 µl primer mix 18 µM (primers for qRT-PCR table 5.13)
5 µl SsoAdvanced™ Universal SYBR® Green Supermix

The mix was pipetted into 96-well plates, sealed with PCR plate seal, and centrifuged at 1500 g for 1 min at RT. The qRT-PCR was read on the CFX96 Touch™ Real-Time PCR Detection System from Biorad with the following cycling protocol:

Step1 95°C for 3 min
Step2 95°C for 10 min
Step3 59°C for 60 sec, repeat step2-3 40 times

5.13.11 Microscopy methods

i) Immunofluorescence staining and confocal imaging

Cells grown on glass coverslips were fixed with 4% paraformaldehyde (PFA) for 15 min at RT, permeabilized with 0.5% Triton-X-100 in PBS for 10 min, and washed once in PBS Blocking was performed for 30 min in 1% Bovine Serum Albumin (BSA) in PBS. Cells were then stained with a primary antibody diluted in blocking buffer, and washed 3 times in PBS. The cells were then incubated with the corresponding secondary antibody conjugated with a fluorophore.
Images were acquired with the Confocal Leica TCS SP5 microscope.

ii) 3D conversion

The 3D conversion of images was performed using the Imaris (Bitplane) software. An average of 20-25 Z-stacks were acquired for each image; the blue and green channels were surface converted by voxel distance.

5.13.12 Western blot analysis

Proteins were transferred onto a polyvinylidene fluoride (PVDF) or nitrocellulose membrane by semidry blotting. Prior to assembly of the blotting sandwich, the PVDF membrane was equilibrated in methanol and the nitrocellulose membrane in transfer buffer. Likewise, Whatman paper as well as the gel were wetted in transfer buffer. Transfer was carried out in a semidry blotter at 2 mA/cm^2 of membrane for 1.5 h.

Subsequently, immunoblots were blocked with 5% (w/v) non-fat dry milk in 1X TBST for 1 h. Blots were rinsed with 1X TBST 3 times and hybridized with antibodies (diluted in 5% (w/v) non-fat dry milk in 1X TBST) at 4°C overnight on a shaker. After three washing steps (10 min; 1X TBST), membranes were incubated with secondary antibodies conjugated to horseradish peroxidase (HRP; diluted in 5% (w/v) non-fat dry milk in 1X TBST) on a shaker for 1.5 h at room temperature. Blots were again washed with TBST 2 times 10 min each, the membrane was developed using chemiluminescence detection solution. Signals were detected with an ImageQuant LAS 4000 CCD camera.

5.13.13 Cloning

i) Preparation of plasmid DNA

Plasmid DNA was extracted from bacterial cells using the NucleoSpin® Plasmid EasyPure kit (Machrey-Nagel) according to the manufacturer's instructions.

ii) Polymerase chain reaction (PCR)

DNA fragments of interest were amplified by PCR using *Taq* DNA polymerase or Phusion polymerase and the DNA oligonucleotides listed in Table 5.12. PCR products were purified using the NucleoSpin® Gel and PCR Clean-up kit (Machrey-Nagel) according to the manufacturer's instructions. For screening of bacterial transformants, cells were picked from plates and streaked into tubes to serve as template in colony PCR.

iii) Agarose gel electrophoresis of DNA

DNA fragments of different sizes were separated using 1-2% (w/v) agarose gels in 1X TAE buffer as described in (Sambrook, 2001). Prior to loading, samples were mixed with DNA loading buffer (ratio 5:1) and separated at 120 V for 20-60 min. GeneRuler 1kB DNA ladder served as size standards. DNA fragments were visualized by the addition of RedSafe (0.02% (v/v)) to agarose gel solutions. If desired, DNA fragments were excised from gels under UV light and recovered using the the NucleoSpin® Gel and PCR Clean-up kit (Machrey-Nagel).

iv) Restriction digest and DNA ligation

All restriction enzyme digests were performed in the buffers and under the conditions suggested by the manufacturer.
Digested DNA fragments and linearized vectors were ligated by T4 DNA ligase and reactions as described in (Sambrook, 2001) prior to transformation into chemically competent *E. coli*.

5.13.14 Single-gene inactivation in bacteria

Bacteria carrying pKD46 (recombinase expressing plasmid, temperature sensitive) were grown ON with Amp at 28˚C. The next day, the culture was diluted 1/100 in 20-25ml LB containing Ampicillin and 0.2% arabinose, and grown at 28˚C until OD 0.45-0.5. Electrocompetent cells were prepared and transformed with 400-500ng PCR product (gel purified).
The kanamycin cassette was amplified by PCR from the pKD4 plasmid using primers containing the flanking region of the gene of interest.
The next day, clones were verified by PCR and restreaked on agar medium containing kanamycin, or ampicillin.

5.13.15 Growth curve

Bacteria were grown in 500µl LB for 15h at 37˚C in 24-well transparent plates, and the OD_{600} was measured with the Tecan Infinite 200Pro plate reader.

5.13.16 DNA transformation

i) Transformation of chemically competent *E. coli*

DNA (1 µl of plasmid DNA or 5 µl of ligation reactions) was mixed with 20 µl of chemically competent *E. coli* TOP10 cells. Cells were incubated on ice for 20 min, and heat-shocked at 37°C for 1min. Cells were chilled on ice for 1 min and resuspended in 300 µl LB medium. Recovery was carried out for 60 min at 37°C, 220 rpm. Then the bacteria were plated on agar medium with the selection antibiotic.

ii) Transformation of electrocompetent bacteria

Bacteria were grown ON at 37°C, 220 rpm after inoculation with a single colony. The next day, the culture was diluted 1/100 in 20-25ml medium, and grown at 37°C, 220 rpm until OD 0.45-0.5. The culture was immediately cooled on ice for 30min, centrifuged at 4500rpm for 20min. The pellet was washed in 25-30ml ice-cold sterile MilliQ water 3 times with centrifugation at 4500rpm for 10min. After the last wash, the pellet was resuspended in 100µl ice-cold water and mixed with the DNA in cuvettes (2 mm gap size). The electroporator was set-up to: manual at 2.5KV and the pulse 5.5-6ms (200 Ω; 25 µF; 2.5 kV).
Immediately 300ul of pre-warmed LB medium was added, and the bacteria were recovered in the at 37˚C for 1.5-2h, 220 rpm. 200ul was plated on agar medium and incubated ON at 37˚C.

5.13.17 Individual-nucleotide resolution UV crosslinking and immunoprecipitation (iCLIP)

(modified from Huppertz et al, 2014)

i) Seeding cells
Two days prior to the infection, HeLa cells ($3.5x10^5$ cells/well) were seeded in 6-well plates.

ii) Infection assays
Infection assays were performed with *Shigella ΔvirG* at MOI 250 using the standard protocol.

iii) UV Cross-linking

At 3hpi, cells were washed in PBS, and 0.5 ml ice-cold PBS was added per well. The lid of the plates was removed and the cells were irradiate once with 150 mJ/cm2 in a Stratlinker 2400 at 254 nm. The cells were harvested by scraping using cell lifters, 2 wells per condition, and centrifuged at 3000 g for 3 min. The pellet was snap-frozen in liquid nitrogen and stored at -80°C until use.

iv) Bead preparation

100 µl of protein G Dynabeads per experiment were washed 2 times with lysis buffer. Then the beads were resuspended in 100 µl lysis buffer with 4 µg (TIAR antibody) and 6 µg (TIA-1 antibody) per experiment. The beads were rotated at room temperature for 60 min, and washed 3x with lysis buffer and left in the last wash.

v) Partial RNA digestion and centrifugation

Cell pellets were resuspended cell pellet (from step iii) in 1 ml lysis buffer (with 1X protease inhibitors cocktail), and sonicated 2 times with 10s bursts at 20% intensity. RNase I was diluted 1:1500 from the stock in lysis buffer, and 10µl was added to the lysate together with 2 µl DNase I and incubated for 3 min at 37°C shaking at 1100 rpm. Then the lysate was cooled on ice for >3 min.
The lysate was centrifuged at 4°C at top speed for 10 minutes, the supernatant carefully collected. And 1 ml of cold-lysis buffer was added.

vi) Immunoprecipitation

The prepared beads (step iv) were added to the prepared lysate (step v) and rotated for 3 h at 4°C. (100 µl of lysate was saved for WB)
The supernatant was discarded (100 µl was saved for WB) and the beads were washed 2 times with high-salt wash (rotated for at least 5min in the cold room). Then the beads were washed 2 times with PNK buffer and resuspended in 1 ml PNK buffer.

vii) 3' end RNA dephosphorylation

The supernatant was discarded and the beads were resuspended in 20 µl of the following mixture:

4.0 µl 5x PNK *pH 6.5* buffer
0.5 µl PNK (with 3' phosphatase activity)
0.5 µl RNasin
15.0µl water

The reaction was incubated for 20 min at 37°C, washed 1 time with PNK buffer, washed 1 time with high-salt wash (rotated for at least 1 min in cold room), and washed 2 times with PNK buffer.

viii) L3 Linker ligation

The supernatant was carefully removed and the beads were resuspended in 20 µl of the following mix:

9.0 µl water
4.0 µl 4X ligation buffer
1.0 µl RNA ligase
0.5 µl RNasin
1.5 µl pre-adenylated linker L3-App (20 µM)
4.0 µl PEG400

The reaction was incubate overnight (~16 h) at 16°C. Then 500 µl PNK buffer was added, and the beads were washed 2 times with 1 ml high-salt buffer, rotating in the wash for 5 min in the cold room. The beads were washed 2 times with 1 ml PNK buffer, and left in 1 ml of the second wash.

ix) 5' end labelling

200 µl (20%) of beads were collected (from step viii) and the supernatant removed. 4 µl of hot PNK mix was added to the beads and incubated for 5min at 37°C:

0.2 µl PNK
0.4 µl ^{32}P-γ-ATP
0.4 µl 10x PNK buffer
3.0 µl water

The supernatant was removed and 20 µl of 1X PL was added to the beads, and added to the remaining cold beads after removing the supernatant and incubate at 70°C for 5 min.

x) SDS-PAGE and nitrocellulose transfer

The samples were loaded on a 10% Bis-Tris gel and the Western blot standard protocol was followed by transfer on a nitrocellulose membrane.

After the transfer, the membrane was sealed and exposed to imaging plates. Signals were determined on a Typhoon FLA 7000 phosphorimager after 0.5 h, 1h, and ON of exposure.

xi) RNA isolation from the membrane

The protein-RNA complexes were isolated using the autoradiograph as a mask by cutting the respective regions out of the nitrocellulose membrane. The pieces of membrane were added to 10 µl proteinase K in 200 µl PK buffer (all submerged), and incubated at 1100 rpm for 20 min at 37°C. 200 µl of PK buffer + 7 M urea was added to the membrane pieces and further incubated for 20 min at 37°C and 1100 rpm.
The solution was collected, and added together with 400 µl Roti-Aqua-P/C/I to a 2 ml Phase Lock Gel Heavy tube, and incubated for 5 min at 30°C at 1100 rpm. The RNA was centrifuged for 5 min at 13000 rpm at room temperature.
The aqueous layer was transferred into a new tube and precipitated by addition of 0.5 µl glycoblue, 40 µl 3 M sodiumacetate pH 5.5, and 1 ml 100% ethanol, mixed, and incubated over night at -20°C.
The RNA was centrifuged for 20 min at 15000 rpm at 4°C and washed with 0.5 ml 85% ethanol. Then the pellet was resuspended in 6.25 µl water.

xii) Reverse transcription

The following reagents were added to the RNA (step xi):

0.5 µl primer Rt#clip (0.5 pmol/µl)
0.5 µl dNTP mix (10 mM)

RT thermal programme:

70°C 5 min
25°C hold until the RT mix is added, mixed by pipetting.

RT mix
2.0 µl 5x RT buffer

0.5 µl 0.1 M DTT

0.25 µl Superscript III RT
25°C 5 min
42°C 20 min
50°C 40 min
80°C 5 min
4°C hold

100 µl of TE buffer was added, then 0.5 µl glycoblue was added and mixed. 15 µl of sodium
acetate was added pH 5.5, and mixed, then 300 µl 100% ethanol. Mixed and precipitated over night at -20°C.

xiii) Gel purification

The cDNA (from step xii) was centrifuged for 20 min at 15000 rpm at 4°C and the pellet was washed with 0.5 ml 85% ethanol and resuspended in 6 µl water.
An equal volume of GLII was added. 6 µl size marker was prepared with equal volume of GLII (low molecular weight marker, diluted 1:30). Samples were incubated at 80°C for 3 min, and loaded on a 6% TBE-urea gel for 40 min at 180 V until the lower (dark blue) dye is close to the bottom.
The last lane containing the size marker was cut out and stain by incubation for 10 min shaking in 10 ml TBE buffer with 2 µl SYBR gold, wash 1 time with TBE and visualised by UV transillumination and used as reference.
The gel pieces were cut out and placed into a 0.5 ml microtube with a perforated bottom using a needle and placed into a 1.5 ml Epp. tube with 400 µl TE. The crushed gel was incubated at 1100 rpm for 1 h at 37°C, then place on dry ice for 2 min, and place back at 1100 rpm for 1 h at 37°C.
The liquid portion was transferred a Costar SpinX column into which two 1 cm glass prefilters were placed, and centrifuged at 13000 rpm for 1 min.
0.5 µl glycoblue, 40 µl sodium acetate, and 1 ml 100% ethanol were added, mixed and precipitated ON at -20°C.

xiv) Ligation of the primer to the 5'end of the cDNA

The cDNA was centrifuged and washed as described above, and the pellet resuspended in 8 µl ligation mix and incubate for 1 h at 60°C:

6.5 µl water
0.8 µl 10x CircLigase Buffer II
0.4 µl 50 mM MnCl2
0.3 µl CircLigase II

Then 30 µl oligo annealing mix was added:

26 µl water
3 µl Cutsmart Buffer
1 µl 10 µM Cut_oligo

The oligos were annealed with following programme:

95°C 2 min successive cycles of 20 s, starting from 95°C and decreasing the temperature by 1°C each cycle down to 25°C 25°C hold

2 µl BamHI was added and incubated for 30 min at 37°C. 50 µl TE, 0.5 µl glycoblue, 10 µl sodium acetate, pH 5.5, and 250 µl 100% ethanol were added mixed and precipitated ON at - 20°C.

xv) PCR amplification

The cDNA was centrifuged and washed as described above, then resuspended in 11 µl water.

Optimization of the PCR amplification

PCR mix:

0.5 µl cDNA
0.25 µl primer mix P5Solexa/P3Solexa, 10 µM each
5.0 µl Accuprime Supermix 1 enzyme
4.25 µl water

PCR program:

94°C 2 min
25-35 cycles of
94°C 15 s
65°C 30 s
68°C 30 s
68°C 3min
25°C hold

8 µl PCR product with 2 µl of GLII buffer was loaded on a 6% TBE gel and stain with SYBR I gold.

Preparative PCR

PCR mix:

10 µl cDNA (from step 8 A)
9 µl water
20 µl primer mix P5Solexa/P3Solexa, 10 µM each
20 l Accuprime Supermix 1 enzyme

Same PCR program but with the determined number of cycles. And 10 µl of the PCR library were submitted for sequencing.

5.13.18 Sequencing

i) Sanger sequencing

DNA Sanger sequencing was performed at GATC Biotech.

Sample preparation:

Template DNA in 5µl H_2O with the following concentrations:

Plasmid DNA (purified): 80-100ng/µl (we use 500ng)
PCR product (purified): 20-80ng/µl
5µl of primer 5µM

ii) Whole-transcriptome sequencing

Library preparation and deep-sequencing was performed by Vertis Biotechnology AG, as described previously (Maudet et al., 2014). RNA-seq analysis was performed using the READemption pipeline version 0.3.0 (Forstner et al., 2014), with Segemehl version 0.1.7 (Otto et al., 2014). Reads were mapped against the human genome (build GRCh37) and *Shigella flexneri*. The analysis of differential gene expression was performed with DESeq 1.18.0 (Anders and Huber, 2010).

iii) MiSeq

The Illumina MiSeq system was used for the deep-sequencing of iCLIP RNA using single-end 50 nt reads.

5.13.19 Statistical analysis

All data are presented as mean ± standard error of the mean (s.e.m.), of at least three independent experiments, as indicated in the figure legends. Statistical analysis was performed using Prism Software (GraphPad). For statistical comparison of datasets from two conditions, two-tailed Student's t-test was used; for data from three or more conditions, two-way ANOVA was used. A P-value of 0.05 or lower was considered significant.

6 REFERENCES

Akira, S., Uematsu, S., and Takeuchi, O. (2006). Pathogen recognition and innate immunity. Cell *124*, 783-801.

Anders, S., and Huber, W. (2010). Differential expression analysis for sequence count data. Genome Biol *11*, R106.

Anderson, P. (2008). Post-transcriptional control of cytokine production. Nat Immunol *9*, 353-359.

Anderson, P., and Kedersha, N. (2008). Stress granules: the Tao of RNA triage. Trends Biochem Sci *33*, 141-150.

Ardestani, S., Deskins, D.L., and Young, P.P. (2013). Membrane TNF-alpha-activated programmed necrosis is mediated by Ceramide-induced reactive oxygen species. J Mol Signal *8*, 12.

Arimoto-Matsuzaki, K., Saito, H., and Takekawa, M. (2016). TIA1 oxidation inhibits stress granule assembly and sensitizes cells to stress-induced apoptosis. Nat Commun *7*, 10252.

Arimoto, K., Fukuda, H., Imajoh-Ohmi, S., Saito, H., and Takekawa, M. (2008). Formation of stress granules inhibits apoptosis by suppressing stress-responsive MAPK pathways. Nat Cell Biol *10*, 1324-1332.

Badger, J.L., and Miller, V.L. (1998). Expression of invasin and motility are coordinately regulated in Yersinia enterocolitica. J Bacteriol *180*, 793-800.

Bae, Y.S., Oh, H., Rhee, S.G., and Yoo, Y.D. (2011). Regulation of reactive oxygen species generation in cell signaling. Mol Cells *32*, 491-509.

Baxt, L.A., Garza-Mayers, A.C., and Goldberg, M.B. (2013). Bacterial subversion of host innate immune pathways. Science *340*, 697-701.

Becker, K.A., Grassme, H., Zhang, Y., and Gulbins, E. (2010a). Ceramide in Pseudomonas aeruginosa infections and cystic fibrosis. Cell Physiol Biochem *26*, 57-66.

Becker, K.A., Riethmuller, J., Zhang, Y., and Gulbins, E. (2010b). The role of sphingolipids and ceramide in pulmonary inflammation in cystic fibrosis. Open Respir Med J *4*, 39-47.

Becker, K.A., Tummler, B., Gulbins, E., and Grassme, H. (2010c). Accumulation of ceramide in the trachea and intestine of cystic fibrosis mice causes inflammation and cell death. Biochem Biophys Res Commun *403*, 368-374.

Bernardini, M.L., Mounier, J., d'Hauteville, H., Coquis-Rondon, M., and Sansonetti, P.J. (1989). Identification of icsA, a plasmid locus of Shigella flexneri that governs bacterial

intra- and intercellular spread through interaction with F-actin. Proc Natl Acad Sci U S A *86*, 3867-3871.

Bernstam, L., and Nriagu, J. (2000). Molecular aspects of arsenic stress. J Toxicol Environ Health B Crit Rev *3*, 293-322.

Beutler, B. (2000). Tlr4: central component of the sole mammalian LPS sensor. Curr Opin Immunol *12*, 20-26.

Beuzon, C.R., Meresse, S., Unsworth, K.E., Ruiz-Albert, J., Garvis, S., Waterman, S.R., Ryder, T.A., Boucrot, E., and Holden, D.W. (2000). Salmonella maintains the integrity of its intracellular vacuole through the action of SifA. EMBO J *19*, 3235-3249.

Bianco, F., Perrotta, C., Novellino, L., Francolini, M., Riganti, L., Menna, E., Saglietti, L., Schuchman, E.H., Furlan, R., Clementi, E.*, et al.* (2009). Acid sphingomyelinase activity triggers microparticle release from glial cells. EMBO J *28*, 1043-1054.

Bishop, A., House, D., Perkins, T., Baker, S., Kingsley, R.A., and Dougan, G. (2008). Interaction of Salmonella enterica serovar Typhi with cultured epithelial cells: roles of surface structures in adhesion and invasion. Microbiology *154*, 1914-1926.

Bogdan, C., Rollinghoff, M., and Diefenbach, A. (2000). Reactive oxygen and reactive nitrogen intermediates in innate and specific immunity. Curr Opin Immunol *12*, 64-76.

Bonifield, H.R., and Hughes, K.T. (2003). Flagellar phase variation in Salmonella enterica is mediated by a posttranscriptional control mechanism. J Bacteriol *185*, 3567-3574.

Brotcke Zumsteg, A., Goosmann, C., Brinkmann, V., Morona, R., and Zychlinsky, A. (2014). IcsA is a Shigella flexneri adhesin regulated by the type III secretion system and required for pathogenesis. Cell Host Microbe *15*, 435-445.

Buchan, J.R., and Parker, R. (2009). Eukaryotic stress granules: the ins and outs of translation. Mol Cell *36*, 932-941.

Buchmann, K. (2014). Evolution of Innate Immunity: Clues from Invertebrates via Fish to Mammals. Front Immunol *5*, 459.

Burdette, D.L., Monroe, K.M., Sotelo-Troha, K., Iwig, J.S., Eckert, B., Hyodo, M., Hayakawa, Y., and Vance, R.E. (2011). STING is a direct innate immune sensor of cyclic di-GMP. Nature *478*, 515-518.

Burton, N.A., Schurmann, N., Casse, O., Steeb, A.K., Claudi, B., Zankl, J., Schmidt, A., and Bumann, D. (2014). Disparate impact of oxidative host defenses determines the fate of Salmonella during systemic infection in mice. Cell Host Microbe *15*, 72-83.

Bylund, J., Goldblatt, D., and Speert, D.P. (2005). Chronic granulomatous disease: from genetic defect to clinical presentation. Adv Exp Med Biol *568*, 67-87.

Cao, X., Surma, M.A., and Simons, K. (2012). Polarized sorting and trafficking in epithelial cells. Cell Res *22*, 793-805.

Carneiro, L.A., Travassos, L.H., Soares, F., Tattoli, I., Magalhaes, J.G., Bozza, M.T., Plotkowski, M.C., Sansonetti, P.J., Molkentin, J.D., Philpott, D.J.*, et al.* (2009). Shigella induces mitochondrial dysfunction and cell death in nonmyleoid cells. Cell Host Microbe *5*, 123-136.

Carpenter, S., Ricci, E.P., Mercier, B.C., Moore, M.J., and Fitzgerald, K.A. (2014). Post-transcriptional regulation of gene expression in innate immunity. Nat Rev Immunol *14*, 361-376.

Carrascoso, I., Sanchez-Jimenez, C., and Izquierdo, J.M. (2014). Genome-wide profiling reveals a role for T-cell intracellular antigens TIA1 and TIAR in the control of translational specificity in HeLa cells. Biochem J *461*, 43-50.

Casadevall, A., and Pirofski, L.A. (2003). The damage-response framework of microbial pathogenesis. Nat Rev Microbiol *1*, 17-24.

Chen, C.L., Lin, C.F., Chang, W.T., Huang, W.C., Teng, C.F., and Lin, Y.S. (2008). Ceramide induces p38 MAPK and JNK activation through a mechanism involving a thioredoxin-interacting protein-mediated pathway. Blood *111*, 4365-4374.

Chen, G.Y., and Nunez, G. (2010). Sterile inflammation: sensing and reacting to damage. Nat Rev Immunol *10*, 826-837.

Chovatiya, R., and Medzhitov, R. (2014). Stress, inflammation, and defense of homeostasis. Mol Cell *54*, 281-288.

Clarke, C.J., Truong, T.G., and Hannun, Y.A. (2007). Role for neutral sphingomyelinase-2 in tumor necrosis factor alpha-stimulated expression of vascular cell adhesion molecule-1 (VCAM) and intercellular adhesion molecule-1 (ICAM) in lung epithelial cells: p38 MAPK is an upstream regulator of nSMase2. J Biol Chem *282*, 1384-1396.

Coburn, B., Grassl, G.A., and Finlay, B.B. (2007). Salmonella, the host and disease: a brief review. Immunol Cell Biol *85*, 112-118.

Cok, S.J., Acton, S.J., and Morrison, A.R. (2003). The proximal region of the 3'-untranslated region of cyclooxygenase-2 is recognized by a multimeric protein complex containing HuR, TIA-1, TIAR, and the heterogeneous nuclear ribonucleoprotein U. J Biol Chem *278*, 36157-36162.

Colgan, S.P., and Taylor, C.T. (2010). Hypoxia: an alarm signal during intestinal inflammation. Nat Rev Gastroenterol Hepatol *7*, 281-287.

Croxen, M.A., and Finlay, B.B. (2010). Molecular mechanisms of Escherichia coli pathogenicity. Nat Rev Microbiol *8*, 26-38.

Cruz-Gallardo, I., Aroca, A., Gunzburg, M.J., Sivakumaran, A., Yoon, J.H., Angulo, J., Persson, C., Gorospe, M., Karlsson, B.G., Wilce, J.A., *et al.* (2014). The binding of TIA-1 to RNA C-rich sequences is driven by its C-terminal RRM domain. RNA Biol *11*, 766-776.

Dang, Y., Kedersha, N., Low, W.K., Romo, D., Gorospe, M., Kaufman, R., Anderson, P., and Liu, J.O. (2006). Eukaryotic initiation factor 2alpha-independent pathway of stress granule induction by the natural product pateamine A. J Biol Chem *281*, 32870-32878.

de Jong, H.K., Parry, C.M., van der Poll, T., and Wiersinga, W.J. (2012). Host-pathogen interaction in invasive Salmonellosis. PLoS Pathog *8*, e1002933.

Decker, C.J., and Parker, R. (2012). P-bodies and stress granules: possible roles in the control of translation and mRNA degradation. Cold Spring Harb Perspect Biol *4*, a012286.

Decourt, B., Munnamalai, V., Lee, A.C., Sanchez, L., and Suter, D.M. (2009). Cortactin colocalizes with filopodial actin and accumulates at IgCAM adhesion sites in Aplysia growth cones. J Neurosci Res *87*, 1057-1068.

Del Gatto-Konczak, F., Bourgeois, C.F., Le Guiner, C., Kister, L., Gesnel, M.C., Stevenin, J., and Breathnach, R. (2000). The RNA-binding protein TIA-1 is a novel mammalian splicing regulator acting through intron sequences adjacent to a 5' splice site. Mol Cell Biol *20*, 6287-6299.

Du, J., Reeves, A.Z., Klein, J.A., Twedt, D.J., Knodler, L.A., and Lesser, C.F. (2016). The type III secretion system apparatus determines the intracellular niche of bacterial pathogens. Proc Natl Acad Sci U S A *113*, 4794-4799.

Duncan, M.J., Shin, J.S., and Abraham, S.N. (2002). Microbial entry through caveolae: variations on a theme. Cell Microbiol *4*, 783-791.

DuPont, H.L., Levine, M.M., Hornick, R.B., and Formal, S.B. (1989). Inoculum size in shigellosis and implications for expected mode of transmission. J Infect Dis *159*, 1126-1128.

Emara, M.M., Fujimura, K., Sciaranghella, D., Ivanova, V., Ivanov, P., and Anderson, P. (2012). Hydrogen peroxide induces stress granule formation independent of eIF2alpha phosphorylation. Biochem Biophys Res Commun *423*, 763-769.

Esclatine, A., Taddeo, B., and Roizman, B. (2004). Herpes simplex virus 1 induces cytoplasmic accumulation of TIA-1/TIAR and both synthesis and cytoplasmic accumulation of tristetraprolin, two cellular proteins that bind and destabilize AU-rich RNAs. J Virol *78*, 8582-8592.

Eulalio, A., Frohlich, K.S., Mano, M., Giacca, M., and Vogel, J. (2011). A candidate approach implicates the secreted Salmonella effector protein SpvB in P-body disassembly. PLoS One *6*, e17296.

Fabrega, A., and Vila, J. (2013). Salmonella enterica serovar Typhimurium skills to succeed in the host: virulence and regulation. Clin Microbiol Rev *26*, 308-341.

Falcone, S., Perrotta, C., De Palma, C., Pisconti, A., Sciorati, C., Capobianco, A., Rovere-Querini, P., Manfredi, A.A., and Clementi, E. (2004). Activation of acid sphingomyelinase and its inhibition by the nitric oxide/cyclic guanosine 3',5'-monophosphate pathway: key events in Escherichia coli-elicited apoptosis of dendritic cells. J Immunol *173*, 4452-4463.

Fang, F.C. (2004). Antimicrobial reactive oxygen and nitrogen species: concepts and controversies. Nat Rev Microbiol *2*, 820-832.

Faulstich, M., Hagen, F., Avota, E., Kozjak-Pavlovic, V., Winkler, A.C., Xian, Y., Schneider-Schaulies, S., and Rudel, T. (2015). Neutral sphingomyelinase 2 is a key factor for PorB-dependent invasion of Neisseria gonorrhoeae. Cell Microbiol *17*, 241-253.

Feuillet, V., Medjane, S., Mondor, I., Demaria, O., Pagni, P.P., Galan, J.E., Flavell, R.A., and Alexopoulou, L. (2006). Involvement of Toll-like receptor 5 in the recognition of flagellated bacteria. Proc Natl Acad Sci U S A *103*, 12487-12492.

Fierer, J., and Guiney, D.G. (2001). Diverse virulence traits underlying different clinical outcomes of Salmonella infection. J Clin Invest *107*, 775-780.

Flora, S.J. (2011). Arsenic-induced oxidative stress and its reversibility. Free Radic Biol Med *51*, 257-281.

Forch, P., Puig, O., Kedersha, N., Martinez, C., Granneman, S., Seraphin, B., Anderson, P., and Valcarcel, J. (2000). The apoptosis-promoting factor TIA-1 is a regulator of alternative pre-mRNA splicing. Mol Cell *6*, 1089-1098.

Forstner, K.U., Vogel, J., and Sharma, C.M. (2014). READemption-a tool for the computational analysis of deep-sequencing-based transcriptome data. Bioinformatics *30*, 3421-3423.

Fros, J.J., Domeradzka, N.E., Baggen, J., Geertsema, C., Flipse, J., Vlak, J.M., and Pijlman, G.P. (2012). Chikungunya virus nsP3 blocks stress granule assembly by recruitment of G3BP into cytoplasmic foci. J Virol *86*, 10873-10879.

Gallucci, S., and Matzinger, P. (2001). Danger signals: SOS to the immune system. Curr Opin Immunol *13*, 114-119.

Garner, M.J., Hayward, R.D., and Koronakis, V. (2002). The Salmonella pathogenicity island 1 secretion system directs cellular cholesterol redistribution during mammalian cell entry and intracellular trafficking. Cell Microbiol *4*, 153-165.

Gewirtz, A.T., Navas, T.A., Lyons, S., Godowski, P.J., and Madara, J.L. (2001). Cutting edge: bacterial flagellin activates basolaterally expressed TLR5 to induce epithelial proinflammatory gene expression. J Immunol *167*, 1882-1885.

Gilks, N., Kedersha, N., Ayodele, M., Shen, L., Stoecklin, G., Dember, L.M., and Anderson, P. (2004). Stress granule assembly is mediated by prion-like aggregation of TIA-1. Mol Biol Cell *15*, 5383-5398.

Grassme, H., Jendrossek, V., Riehle, A., von Kurthy, G., Berger, J., Schwarz, H., Weller, M., Kolesnick, R., and Gulbins, E. (2003). Host defense against Pseudomonas aeruginosa requires ceramide-rich membrane rafts. Nat Med *9*, 322-330.

Gueydan, C., Droogmans, L., Chalon, P., Huez, G., Caput, D., and Kruys, V. (1999). Identification of TIAR as a protein binding to the translational regulatory AU-rich element of tumor necrosis factor alpha mRNA. J Biol Chem *274*, 2322-2326.

Hannun, Y.A., and Luberto, C. (2000). Ceramide in the eukaryotic stress response. Trends Cell Biol *10*, 73-80.

Hansen-Wester, I., and Hensel, M. (2001). Salmonella pathogenicity islands encoding type III secretion systems. Microbes Infect *3*, 549-559.

Hardt, W.D., Chen, L.M., Schuebel, K.E., Bustelo, X.R., and Galan, J.E. (1998). S. typhimurium encodes an activator of Rho GTPases that induces membrane ruffling and nuclear responses in host cells. Cell *93*, 815-826.

Hayashi, F., Smith, K.D., Ozinsky, A., Hawn, T.R., Yi, E.C., Goodlett, D.R., Eng, J.K., Akira, S., Underhill, D.M., and Aderem, A. (2001). The innate immune response to bacterial flagellin is mediated by Toll-like receptor 5. Nature *410*, 1099-1103.

Hemmi, H., Takeuchi, O., Kawai, T., Kaisho, T., Sato, S., Sanjo, H., Matsumoto, M., Hoshino, K., Wagner, H., Takeda, K.*, et al.* (2000). A Toll-like receptor recognizes bacterial DNA. Nature *408*, 740-745.

High, N., Mounier, J., Prevost, M.C., and Sansonetti, P.J. (1992). IpaB of Shigella flexneri causes entry into epithelial cells and escape from the phagocytic vacuole. EMBO J *11*, 1991-1999.

Hoffmann, C., Berking, A., Agerer, F., Buntru, A., Neske, F., Chhatwal, G.S., Ohlsen, K., and Hauck, C.R. (2010). Caveolin limits membrane microdomain mobility and integrin-mediated uptake of fibronectin-binding pathogens. J Cell Sci *123*, 4280-4291.

Holmes, B., Page, A.R., and Good, R.A. (1967). Studies of the metabolic activity of leukocytes from patients with a genetic abnormality of phagocytic function. J Clin Invest *46*, 1422-1432.

Ibarra, J.A., and Steele-Mortimer, O. (2009). Salmonella--the ultimate insider. Salmonella virulence factors that modulate intracellular survival. Cell Microbiol *11*, 1579-1586.

Imaeda, A.B., Watanabe, A., Sohail, M.A., Mahmood, S., Mohamadnejad, M., Sutterwala, F.S., Flavell, R.A., and Mehal, W.Z. (2009). Acetaminophen-induced hepatotoxicity in mice is dependent on Tlr9 and the Nalp3 inflammasome. J Clin Invest *119*, 305-314.

Isberg, R.R., Voorhis, D.L., and Falkow, S. (1987). Identification of invasin: a protein that allows enteric bacteria to penetrate cultured mammalian cells. Cell *50*, 769-778.

Janeway, C.A., Jr., and Medzhitov, R. (2002). Innate immune recognition. Annu Rev Immunol *20*, 197-216.

Kafasla, P., Skliris, A., and Kontoyiannis, D.L. (2014). Post-transcriptional coordination of immunological responses by RNA-binding proteins. Nat Immunol *15*, 492-502.

Kalischuk, L.D., Inglis, G.D., and Buret, A.G. (2009). Campylobacter jejuni induces transcellular translocation of commensal bacteria via lipid rafts. Gut Pathog *1*, 2.

Kandasamy, K., Joseph, K., Subramaniam, K., Raymond, J.R., and Tholanikunnel, B.G. (2005). Translational control of beta2-adrenergic receptor mRNA by T-cell-restricted intracellular antigen-related protein. J Biol Chem *280*, 1931-1943.

Karin, M., Lawrence, T., and Nizet, V. (2006). Innate immunity gone awry: linking microbial infections to chronic inflammation and cancer. Cell *124*, 823-835.

Kasper, C.A., Sorg, I., Schmutz, C., Tschon, T., Wischnewski, H., Kim, M.L., and Arrieumerlou, C. (2010). Cell-cell propagation of NF-kappaB transcription factor and MAP kinase activation amplifies innate immunity against bacterial infection. Immunity *33*, 804-816.

Katabami, S., Matsuura, A., Chen, H.Z., Imai, K., and Kikuchi, K. (1998). Structural organization of rat CD1 typifies evolutionarily conserved CD1D class genes. Immunogenetics *48*, 22-31.

Kathariou, S., Kanenaka, R., Allen, R.D., Fok, A.K., and Mizumoto, C. (1995). Repression of motility and flagellin production at 37 degrees C is stronger in Listeria monocytogenes than in the nonpathogenic species Listeria innocua. Can J Microbiol *41*, 572-577.

Katsanou, V., Papadaki, O., Milatos, S., Blackshear, P.J., Anderson, P., Kollias, G., and Kontoyiannis, D.L. (2005). HuR as a negative posttranscriptional modulator in inflammation. Mol Cell *19*, 777-789.

Kawai, T., Lal, A., Yang, X., Galban, S., Mazan-Mamczarz, K., and Gorospe, M. (2006). Translational control of cytochrome c by RNA-binding proteins TIA-1 and HuR. Mol Cell Biol *26*, 3295-3307.

Kawakami, A., Tian, Q., Duan, X., Streuli, M., Schlossman, S.F., and Anderson, P. (1992). Identification and functional characterization of a TIA-1-related nucleolysin. Proc Natl Acad Sci U S A *89*, 8681-8685.

Kedersha, N., and Anderson, P. (2007). Mammalian stress granules and processing bodies. Methods Enzymol *431*, 61-81.

Kedersha, N., Cho, M.R., Li, W., Yacono, P.W., Chen, S., Gilks, N., Golan, D.E., and Anderson, P. (2000). Dynamic shuttling of TIA-1 accompanies the recruitment of mRNA to mammalian stress granules. J Cell Biol *151*, 1257-1268.

Kedersha, N., Ivanov, P., and Anderson, P. (2013). Stress granules and cell signaling: more than just a passing phase? Trends Biochem Sci *38*, 494-506.

Kedersha, N., Stoecklin, G., Ayodele, M., Yacono, P., Lykke-Andersen, J., Fritzler, M.J., Scheuner, D., Kaufman, R.J., Golan, D.E., and Anderson, P. (2005). Stress granules and processing bodies are dynamically linked sites of mRNP remodeling. J Cell Biol *169*, 871-884.

Kedersha, N.L., Gupta, M., Li, W., Miller, I., and Anderson, P. (1999). RNA-binding proteins TIA-1 and TIAR link the phosphorylation of eIF-2 alpha to the assembly of mammalian stress granules. J Cell Biol *147*, 1431-1442.

Khaperskyy, D.A., Hatchette, T.F., and McCormick, C. (2012). Influenza A virus inhibits cytoplasmic stress granule formation. FASEB J *26*, 1629-1639.

Killackey, S.A., Sorbara, M.T., and Girardin, S.E. (2016). Cellular Aspects of Shigella Pathogenesis: Focus on the Manipulation of Host Cell Processes. Front Cell Infect Microbiol *6*, 38.

Kim, H.S., Kuwano, Y., Zhan, M., Pullmann, R., Jr., Mazan-Mamczarz, K., Li, H., Kedersha, N., Anderson, P., Wilce, M.C., Gorospe, M.*, et al.* (2007). Elucidation of a C-rich signature motif in target mRNAs of RNA-binding protein TIAR. Mol Cell Biol *27*, 6806-6817.

Kim, J.J., Lee, S.B., Park, J.K., and Yoo, Y.D. (2010). TNF-alpha-induced ROS production triggering apoptosis is directly linked to Romo1 and Bcl-X(L). Cell Death Differ *17*, 1420-1434.

Kim, W.J., Back, S.H., Kim, V., Ryu, I., and Jang, S.K. (2005). Sequestration of TRAF2 into stress granules interrupts tumor necrosis factor signaling under stress conditions. Mol Cell Biol *25*, 2450-2462.

Kimball, S.R., Horetsky, R.L., Ron, D., Jefferson, L.S., and Harding, H.P. (2003). Mammalian stress granules represent sites of accumulation of stalled translation initiation complexes. Am J Physiol Cell Physiol *284*, C273-284.

Kono, H., Onda, A., and Yanagida, T. (2014). Molecular determinants of sterile inflammation. Curr Opin Immunol *26*, 147-156.

Kotloff, K.L., Winickoff, J.P., Ivanoff, B., Clemens, J.D., Swerdlow, D.L., Sansonetti, P.J., Adak, G.K., and Levine, M.M. (1999). Global burden of Shigella infections: implications for

vaccine development and implementation of control strategies. Bull World Health Organ *77*, 651-666.

Kotlyarov, A., Neininger, A., Schubert, C., Eckert, R., Birchmeier, C., Volk, H.D., and Gaestel, M. (1999). MAPKAP kinase 2 is essential for LPS-induced TNF-alpha biosynthesis. Nat Cell Biol *1*, 94-97.

Kumar, Y., and Valdivia, R.H. (2009). Leading a sheltered life: intracellular pathogens and maintenance of vacuolar compartments. Cell Host Microbe *5*, 593-601.

Kutsukake, K., Ohya, Y., Yamaguchi, S., and Iino, T. (1988). Operon structure of flagellar genes in Salmonella typhimurium. Mol Gen Genet *214*, 11-15.

Lafont, F., Abrami, L., and van der Goot, F.G. (2004). Bacterial subversion of lipid rafts. Curr Opin Microbiol *7*, 4-10.

Lafont, F., Tran Van Nhieu, G., Hanada, K., Sansonetti, P., and van der Goot, F.G. (2002). Initial steps of Shigella infection depend on the cholesterol/sphingolipid raft-mediated CD44-IpaB interaction. EMBO J *21*, 4449-4457.

Langereis, M.A., Feng, Q., and van Kuppeveld, F.J. (2013). MDA5 localizes to stress granules, but this localization is not required for the induction of type I interferon. J Virol *87*, 6314-6325.

LaRock, D.L., Chaudhary, A., and Miller, S.I. (2015). Salmonellae interactions with host processes. Nat Rev Microbiol *13*, 191-205.

Le Guiner, C., Lejeune, F., Galiana, D., Kister, L., Breathnach, R., Stevenin, J., and Del Gatto-Konczak, F. (2001). TIA-1 and TIAR activate splicing of alternative exons with weak 5' splice sites followed by a U-rich stretch on their own pre-mRNAs. J Biol Chem *276*, 40638-40646.

Lee, M.S., and Kim, Y.J. (2007). Signaling pathways downstream of pattern-recognition receptors and their cross talk. Annu Rev Biochem *76*, 447-480.

Lee, T.K., Denny, E.M., Sanghvi, J.C., Gaston, J.E., Maynard, N.D., Hughey, J.J., and Covert, M.W. (2009). A noisy paracrine signal determines the cellular NF-kappaB response to lipopolysaccharide. Sci Signal *2*, ra65.

Leung, A.K., Calabrese, J.M., and Sharp, P.A. (2006). Quantitative analysis of Argonaute protein reveals microRNA-dependent localization to stress granules. Proc Natl Acad Sci U S A *103*, 18125-18130.

Li, H., Xu, H., Zhou, Y., Zhang, J., Long, C., Li, S., Chen, S., Zhou, J.M., and Shao, F. (2007). The phosphothreonine lyase activity of a bacterial type III effector family. Science *315*, 1000-1003.

Li, X., Gulbins, E., and Zhang, Y. (2012). Oxidative stress triggers Ca-dependent lysosome trafficking and activation of acid sphingomyelinase. Cell Physiol Biochem *30*, 815-826.

Liao, B., Hu, Y., and Brewer, G. (2007). Competitive binding of AUF1 and TIAR to MYC mRNA controls its translation. Nat Struct Mol Biol *14*, 511-518.

Lingwood, D., and Simons, K. (2010). Lipid rafts as a membrane-organizing principle. Science *327*, 46-50.

Lopez de Silanes, I., Galban, S., Martindale, J.L., Yang, X., Mazan-Mamczarz, K., Indig, F.E., Falco, G., Zhan, M., and Gorospe, M. (2005). Identification and functional outcome of mRNAs associated with RNA-binding protein TIA-1. Mol Cell Biol *25*, 9520-9531.

Lorkowski, M., Felipe-Lopez, A., Danzer, C.A., Hansmeier, N., and Hensel, M. (2014). Salmonella enterica invasion of polarized epithelial cells is a highly cooperative effort. Infect Immun *82*, 2657-2667.

Manes, S., del Real, G., and Martinez, A.C. (2003). Pathogens: raft hijackers. Nat Rev Immunol *3*, 557-568.

Marchesini, N., and Hannun, Y.A. (2004). Acid and neutral sphingomyelinases: roles and mechanisms of regulation. Biochem Cell Biol *82*, 27-44.

Marteyn, B., Gazi, A., and Sansonetti, P. (2012). Shigella: a model of virulence regulation in vivo. Gut Microbes *3*, 104-120.

Maudet, C., Mano, M., Sunkavalli, U., Sharan, M., Giacca, M., Forstner, K.U., and Eulalio, A. (2014). Functional high-throughput screening identifies the miR-15 microRNA family as cellular restriction factors for Salmonella infection. Nat Commun *5*, 4718.

Mazan-Mamczarz, K., Lal, A., Martindale, J.L., Kawai, T., and Gorospe, M. (2006). Translational repression by RNA-binding protein TIAR. Mol Cell Biol *26*, 2716-2727.

McCollister, B.D., Myers, J.T., Jones-Carson, J., Voelker, D.R., and Vazquez-Torres, A. (2007). Constitutive acid sphingomyelinase enhances early and late macrophage killing of Salmonella enterica serovar Typhimurium. Infect Immun *75*, 5346-5352.

Menard, R., Prevost, M.C., Gounon, P., Sansonetti, P., and Dehio, C. (1996). The secreted Ipa complex of Shigella flexneri promotes entry into mammalian cells. Proc Natl Acad Sci U S A *93*, 1254-1258.

Meylan, E., Tschopp, J., and Karin, M. (2006). Intracellular pattern recognition receptors in the host response. Nature *442*, 39-44.

Mitchell, G., Ge, L., Huang, Q., Chen, C., Kianian, S., Roberts, M.F., Schekman, R., and Portnoy, D.A. (2015). Avoidance of autophagy mediated by PlcA or ActA is required for Listeria monocytogenes growth in macrophages. Infect Immun *83*, 2175-2184.

Muralidharan, S., and Mandrekar, P. (2013). Cellular stress response and innate immune signaling: integrating pathways in host defense and inflammation. J Leukoc Biol *94*, 1167-1184.

Nadezhdina, E.S., Lomakin, A.J., Shpilman, A.A., Chudinova, E.M., and Ivanov, P.A. (2010). Microtubules govern stress granule mobility and dynamics. Biochim Biophys Acta *1803*, 361-371.

Nathan, C., and Cunningham-Bussel, A. (2013). Beyond oxidative stress: an immunologist's guide to reactive oxygen species. Nat Rev Immunol *13*, 349-361.

Neininger, A., Kontoyiannis, D., Kotlyarov, A., Winzen, R., Eckert, R., Volk, H.D., Holtmann, H., Kollias, G., and Gaestel, M. (2002). MK2 targets AU-rich elements and regulates biosynthesis of tumor necrosis factor and interleukin-6 independently at different post-transcriptional levels. J Biol Chem *277*, 3065-3068.

Ng, C.G., and Griffin, D.E. (2006). Acid sphingomyelinase deficiency increases susceptibility to fatal alphavirus encephalomyelitis. J Virol *80*, 10989-10999.

Ng, C.S., Jogi, M., Yoo, J.S., Onomoto, K., Koike, S., Iwasaki, T., Yoneyama, M., Kato, H., and Fujita, T. (2013). Encephalomyocarditis virus disrupts stress granules, the critical platform for triggering antiviral innate immune responses. J Virol *87*, 9511-9522.

Niethammer, P., Grabher, C., Look, A.T., and Mitchison, T.J. (2009). A tissue-scale gradient of hydrogen peroxide mediates rapid wound detection in zebrafish. Nature *459*, 996-999.

Nizet, V., and Johnson, R.S. (2009). Interdependence of hypoxic and innate immune responses. Nat Rev Immunol *9*, 609-617.

Ohn, T., Kedersha, N., Hickman, T., Tisdale, S., and Anderson, P. (2008). A functional RNAi screen links O-GlcNAc modification of ribosomal proteins to stress granule and processing body assembly. Nat Cell Biol *10*, 1224-1231.

Onomoto, K., Jogi, M., Yoo, J.S., Narita, R., Morimoto, S., Takemura, A., Sambhara, S., Kawaguchi, A., Osari, S., Nagata, K*., et al.* (2012). Critical role of an antiviral stress granule containing RIG-I and PKR in viral detection and innate immunity. PLoS One *7*, e43031.

Onomoto, K., Yoneyama, M., Fung, G., Kato, H., and Fujita, T. (2014). Antiviral innate immunity and stress granule responses. Trends Immunol *35*, 420-428.

Otto, C., Stadler, P.F., and Hoffmann, S. (2014). Lacking alignments? The next-generation sequencing mapper segemehl revisited. Bioinformatics *30*, 1837-1843.

Panday, A., Sahoo, M.K., Osorio, D., and Batra, S. (2015). NADPH oxidases: an overview from structure to innate immunity-associated pathologies. Cell Mol Immunol *12*, 5-23.

Pedron, T., Thibault, C., and Sansonetti, P.J. (2003). The invasive phenotype of Shigella flexneri directs a distinct gene expression pattern in the human intestinal epithelial cell line Caco-2. J Biol Chem *278*, 33878-33886.

Phalipon, A., and Sansonetti, P.J. (2007). Shigella's ways of manipulating the host intestinal innate and adaptive immune system: a tool box for survival? Immunol Cell Biol *85*, 119-129.

Piecyk, M., Wax, S., Beck, A.R., Kedersha, N., Gupta, M., Maritim, B., Chen, S., Gueydan, C., Kruys, V., Streuli, M.*, et al.* (2000). TIA-1 is a translational silencer that selectively regulates the expression of TNF-alpha. EMBO J *19*, 4154-4163.

Pizarro-Cerda, J., and Cossart, P. (2006). Bacterial adhesion and entry into host cells. Cell *124*, 715-727.

Ponta, H., Sherman, L., and Herrlich, P.A. (2003). CD44: from adhesion molecules to signalling regulators. Nat Rev Mol Cell Biol *4*, 33-45.

Quinn, M.T., Ammons, M.C., and Deleo, F.R. (2006). The expanding role of NADPH oxidases in health and disease: no longer just agents of death and destruction. Clin Sci (Lond) *111*, 1-20.

Raffatellu, M., Wilson, R.P., Chessa, D., Andrews-Polymenis, H., Tran, Q.T., Lawhon, S., Khare, S., Adams, L.G., and Baumler, A.J. (2005). SipA, SopA, SopB, SopD, and SopE2 contribute to Salmonella enterica serotype typhimurium invasion of epithelial cells. Infect Immun *73*, 146-154.

Ray, K., Marteyn, B., Sansonetti, P.J., and Tang, C.M. (2009). Life on the inside: the intracellular lifestyle of cytosolic bacteria. Nat Rev Microbiol *7*, 333-340.

Reineke, L.C., and Lloyd, R.E. (2013). Diversion of stress granules and P-bodies during viral infection. Virology *436*, 255-267.

Riethmuller, J., Riehle, A., Grassme, H., and Gulbins, E. (2006). Membrane rafts in host-pathogen interactions. Biochim Biophys Acta *1758*, 2139-2147.

Ritchie, J.M., and Waldor, M.K. (2009). Vibrio cholerae interactions with the gastrointestinal tract: lessons from animal studies. Curr Top Microbiol Immunol *337*, 37-59.

Rock, K.L., Latz, E., Ontiveros, F., and Kono, H. (2010). The sterile inflammatory response. Annu Rev Immunol *28*, 321-342.

Rodriguez-Gabriel, M.A., and Russell, P. (2008). Control of mRNA stability by SAPKs. Top Curr Genet *20*, 159-170.

Romero, S., Grompone, G., Carayol, N., Mounier, J., Guadagnini, S., Prevost, M.C., Sansonetti, P.J., and Van Nhieu, G.T. (2011). ATP-mediated Erk1/2 activation stimulates bacterial capture by filopodia, which precedes Shigella invasion of epithelial cells. Cell Host Microbe *9*, 508-519.

Rubartelli, A., and Lotze, M.T. (2007). Inside, outside, upside down: damage-associated molecular-pattern molecules (DAMPs) and redox. Trends Immunol *28*, 429-436.

Ruggieri, A., Dazert, E., Metz, P., Hofmann, S., Bergeest, J.P., Mazur, J., Bankhead, P., Hiet, M.S., Kallis, S., Alvisi, G.*, et al.* (2012). Dynamic oscillation of translation and stress granule formation mark the cellular response to virus infection. Cell Host Microbe *12*, 71-85.

Sabio, G., and Davis, R.J. (2014). TNF and MAP kinase signalling pathways. Semin Immunol *26*, 237-245.

Salzano, S., Checconi, P., Hanschmann, E.M., Lillig, C.H., Bowler, L.D., Chan, P., Vaudry, D., Mengozzi, M., Coppo, L., Sacre, S.*, et al.* (2014). Linkage of inflammation and oxidative stress via release of glutathionylated peroxiredoxin-2, which acts as a danger signal. Proc Natl Acad Sci U S A *111*, 12157-12162.

Sansonetti, P.J. (2001). Rupture, invasion and inflammatory destruction of the intestinal barrier by Shigella, making sense of prokaryote-eukaryote cross-talks. FEMS Microbiol Rev *25*, 3-14.

Sansonetti, P.J. (2004). War and peace at mucosal surfaces. Nat Rev Immunol *4*, 953-964.

Sansonetti, P.J., Arondel, J., Cantey, J.R., Prevost, M.C., and Huerre, M. (1996). Infection of rabbit Peyer's patches by Shigella flexneri: effect of adhesive or invasive bacterial phenotypes on follicle-associated epithelium. Infect Immun *64*, 2752-2764.

Schroeder, G.N., and Hilbi, H. (2008). Molecular pathogenesis of Shigella spp.: controlling host cell signaling, invasion, and death by type III secretion. Clin Microbiol Rev *21*, 134-156.

Schuchman, E.H. (2010). Acid sphingomyelinase, cell membranes and human disease: lessons from Niemann-Pick disease. FEBS Lett *584*, 1895-1900.

Schuchman, E.H., and Wasserstein, M.P. (2015). Types A and B Niemann-Pick disease. Best Pract Res Clin Endocrinol Metab *29*, 237-247.

Schuck, S., and Simons, K. (2004). Polarized sorting in epithelial cells: raft clustering and the biogenesis of the apical membrane. J Cell Sci *117*, 5955-5964.

Shweiki, D., Itin, A., Soffer, D., and Keshet, E. (1992). Vascular endothelial growth factor induced by hypoxia may mediate hypoxia-initiated angiogenesis. Nature *359*, 843-845.

Simonis, A., Hebling, S., Gulbins, E., Schneider-Schaulies, S., and Schubert-Unkmeir, A. (2014). Differential activation of acid sphingomyelinase and ceramide release determines invasiveness of Neisseria meningitidis into brain endothelial cells. PLoS Pathog *10*, e1004160.

Simons, K., and Ikonen, E. (1997). Functional rafts in cell membranes. Nature *387*, 569-572.

Simons, K., and Toomre, D. (2000). Lipid rafts and signal transduction. Nat Rev Mol Cell Biol *1*, 31-39.

Sims, G.E., and Kim, S.H. (2011). Whole-genome phylogeny of Escherichia coli/Shigella group by feature frequency profiles (FFPs). Proc Natl Acad Sci U S A *108*, 8329-8334.

Smith, J.A. (1994). Neutrophils, host defense, and inflammation: a double-edged sword. J Leukoc Biol *56*, 672-686.

Speelman, P., Kabir, I., and Islam, M. (1984). Distribution and spread of colonic lesions in shigellosis: a colonoscopic study. J Infect Dis *150*, 899-903.

Stancevic, B., and Kolesnick, R. (2010). Ceramide-rich platforms in transmembrane signaling. FEBS Lett *584*, 1728-1740.

Stender, S., Friebel, A., Linder, S., Rohde, M., Mirold, S., and Hardt, W.D. (2000). Identification of SopE2 from Salmonella typhimurium, a conserved guanine nucleotide exchange factor for Cdc42 of the host cell. Mol Microbiol *36*, 1206-1221.

Stuart, L.M., Paquette, N., and Boyer, L. (2013). Effector-triggered versus pattern-triggered immunity: how animals sense pathogens. Nat Rev Immunol *13*, 199-206.

Swidsinski, A., Loening-Baucke, V., Theissig, F., Engelhardt, H., Bengmark, S., Koch, S., Lochs, H., and Dorffel, Y. (2007). Comparative study of the intestinal mucus barrier in normal and inflamed colon. Gut *56*, 343-350.

Takahashi, M., Higuchi, M., Matsuki, H., Yoshita, M., Ohsawa, T., Oie, M., and Fujii, M. (2013). Stress granules inhibit apoptosis by reducing reactive oxygen species production. Mol Cell Biol *33*, 815-829.

Tattoli, I., Sorbara, M.T., Vuckovic, D., Ling, A., Soares, F., Carneiro, L.A., Yang, C., Emili, A., Philpott, D.J., and Girardin, S.E. (2012). Amino acid starvation induced by invasive bacterial pathogens triggers an innate host defense program. Cell Host Microbe *11*, 563-575.

Taylor, C.T. (2008). Interdependent roles for hypoxia inducible factor and nuclear factor-kappaB in hypoxic inflammation. J Physiol *586*, 4055-4059.

Teichgraber, V., Ulrich, M., Endlich, N., Riethmuller, J., Wilker, B., De Oliveira-Munding, C.C., van Heeckeren, A.M., Barr, M.L., von Kurthy, G., Schmid, K.W.*, et al.* (2008). Ceramide accumulation mediates inflammation, cell death and infection susceptibility in cystic fibrosis. Nat Med *14*, 382-391.

Tilney, L.G., and Portnoy, D.A. (1989). Actin filaments and the growth, movement, and spread of the intracellular bacterial parasite, Listeria monocytogenes. J Cell Biol *109*, 1597-1608.

Torocsik, B., and Szeberenyi, J. (2000). Anisomycin uses multiple mechanisms to stimulate mitogen-activated protein kinases and gene expression and to inhibit neuronal differentiation in PC12 phaeochromocytoma cells. Eur J Neurosci *12*, 527-532.

Tourriere, H., Chebli, K., Zekri, L., Courselaud, B., Blanchard, J.M., Bertrand, E., and Tazi, J. (2003). The RasGAP-associated endoribonuclease G3BP assembles stress granules. J Cell Biol *160*, 823-831.

Triantafilou, M., Miyake, K., Golenbock, D.T., and Triantafilou, K. (2002). Mediators of innate immune recognition of bacteria concentrate in lipid rafts and facilitate lipopolysaccharide-induced cell activation. J Cell Sci *115*, 2603-2611.

Tripathi, D.N., Chowdhury, R., Trudel, L.J., Tee, A.R., Slack, R.S., Walker, C.L., and Wogan, G.N. (2013). Reactive nitrogen species regulate autophagy through ATM-AMPK-TSC2-mediated suppression of mTORC1. Proc Natl Acad Sci U S A *110*, E2950-2957.

Tschopp, J., and Schroder, K. (2010). NLRP3 inflammasome activation: The convergence of multiple signalling pathways on ROS production? Nat Rev Immunol *10*, 210-215.

Utermohlen, O., Karow, U., Lohler, J., and Kronke, M. (2003). Severe impairment in early host defense against Listeria monocytogenes in mice deficient in acid sphingomyelinase. J Immunol *170*, 2621-2628.

van Asten, A.J., and van Dijk, J.E. (2005). Distribution of "classic" virulence factors among Salmonella spp. FEMS Immunol Med Microbiol *44*, 251-259.

Vonaesch, P., Campbell-Valois, F.X., Dufour, A., Sansonetti, P.J., and Schnupf, P. (2016). Shigella flexneri modulates stress granule composition and inhibits stress granule aggregation. Cell Microbiol *18*, 982-997.

Wang, Z., Kayikci, M., Briese, M., Zarnack, K., Luscombe, N.M., Rot, G., Zupan, B., Curk, T., and Ule, J. (2010). iCLIP predicts the dual splicing effects of TIA-RNA interactions. PLoS Biol *8*, e1000530.

Wary, K.K., Mariotti, A., Zurzolo, C., and Giancotti, F.G. (1998). A requirement for caveolin-1 and associated kinase Fyn in integrin signaling and anchorage-dependent cell growth. Cell *94*, 625-634.

Wassef, J.S., Keren, D.F., and Mailloux, J.L. (1989). Role of M cells in initial antigen uptake and in ulcer formation in the rabbit intestinal loop model of shigellosis. Infect Immun *57*, 858-863.

Wasserman, T., Katsenelson, K., Daniliuc, S., Hasin, T., Choder, M., and Aronheim, A. (2010). A novel c-Jun N-terminal kinase (JNK)-binding protein WDR62 is recruited to stress granules and mediates a nonclassical JNK activation. Mol Biol Cell *21*, 117-130.

Watarai, M., Funato, S., and Sasakawa, C. (1996). Interaction of Ipa proteins of Shigella flexneri with alpha5beta1 integrin promotes entry of the bacteria into mammalian cells. J Exp Med *183*, 991-999.

Weber, F., Wagner, V., Rasmussen, S.B., Hartmann, R., and Paludan, S.R. (2006). Double-stranded RNA is produced by positive-strand RNA viruses and DNA viruses but not in detectable amounts by negative-strand RNA viruses. J Virol *80*, 5059-5064.

White, J.P., Cardenas, A.M., Marissen, W.E., and Lloyd, R.E. (2007). Inhibition of cytoplasmic mRNA stress granule formation by a viral proteinase. Cell Host Microbe *2*, 295-305.

Wiegmann, K., Schutze, S., Machleidt, T., Witte, D., and Kronke, M. (1994). Functional dichotomy of neutral and acidic sphingomyelinases in tumor necrosis factor signaling. Cell *78*, 1005-1015.

Wittmann, C., Chockley, P., Singh, S.K., Pase, L., Lieschke, G.J., and Grabher, C. (2012). Hydrogen peroxide in inflammation: messenger, guide, and assassin. Adv Hematol *2012*, 541471.

Wojciak-Stothard, B., Entwistle, A., Garg, R., and Ridley, A.J. (1998). Regulation of TNF-alpha-induced reorganization of the actin cytoskeleton and cell-cell junctions by Rho, Rac, and Cdc42 in human endothelial cells. J Cell Physiol *176*, 150-165.

Wu, S.C., Liao, C.W., Pan, R.L., and Juang, J.L. (2012). Infection-induced intestinal oxidative stress triggers organ-to-organ immunological communication in Drosophila. Cell Host Microbe *11*, 410-417.

Yabu, T., Imamura, S., Yamashita, M., and Okazaki, T. (2008). Identification of Mg2+ -dependent neutral sphingomyelinase 1 as a mediator of heat stress-induced ceramide generation and apoptosis. J Biol Chem *283*, 29971-29982.

Yang, F., Yang, J., Zhang, X., Chen, L., Jiang, Y., Yan, Y., Tang, X., Wang, J., Xiong, Z., Dong, J., *et al.* (2005). Genome dynamics and diversity of Shigella species, the etiologic agents of bacillary dysentery. Nucleic Acids Res *33*, 6445-6458.

Yang, X., Shen, Y., Garre, E., Hao, X., Krumlinde, D., Cvijovic, M., Arens, C., Nystrom, T., Liu, B., and Sunnerhagen, P. (2014). Stress granule-defective mutants deregulate stress responsive transcripts. PLoS Genet *10*, e1004763.

Yoneyama, M., Kikuchi, M., Natsukawa, T., Shinobu, N., Imaizumi, T., Miyagishi, M., Taira, K., Akira, S., and Fujita, T. (2004). The RNA helicase RIG-I has an essential function in double-stranded RNA-induced innate antiviral responses. Nat Immunol *5*, 730-737.

Yoshikawa, Y., Ogawa, M., Hain, T., Yoshida, M., Fukumatsu, M., Kim, M., Mimuro, H., Nakagawa, I., Yanagawa, T., Ishii, T.*, et al.* (2009). Listeria monocytogenes ActA-mediated escape from autophagic recognition. Nat Cell Biol *11*, 1233-1240.

Yu, H., Zeidan, Y.H., Wu, B.X., Jenkins, R.W., Flotte, T.R., Hannun, Y.A., and Virella-Lowell, I. (2009). Defective acid sphingomyelinase pathway with Pseudomonas aeruginosa infection in cystic fibrosis. Am J Respir Cell Mol Biol *41*, 367-375.

Zeitouni, N.E., Dersch, P., Naim, H.Y., and von Kockritz-Blickwede, M. (2016). Hypoxia Decreases Invasin-Mediated Yersinia enterocolitica Internalization into Caco-2 Cells. PLoS One *11*, e0146103.

Zhang, T., Delestienne, N., Huez, G., Kruys, V., and Gueydan, C. (2005). Identification of the sequence determinants mediating the nucleo-cytoplasmic shuttling of TIAR and TIA-1 RNA-binding proteins. J Cell Sci *118*, 5453-5463.

10 CURRICULUM VITAE

11 LIST OF PUBLICATIONS

Manuscripts submitted or in preparation

- **Caroline Tawk**, Malvika Sharan, Ana Eulalio, Jörg Vogel. A paucity of RNA targeting potential amongst bacterial effector proteins. *Submitted*.
- **Caroline Tawk** and Ana Eulalio. Host-stress promotes defense against infection by *Shigella flexneri* by remodeling the epithelial cell surface. *In preparation*.
- **Caroline Tawk** and Ana Eulalio**.** Cytoplasmic bacterial replication reshapes the TIAR/TIA-1 RNA interactome. *In preparation*.
- Ushasree Sunkavalli; Ricardo Jorge Silva; Carmen Aguilar; Malvika Sharan; Ana Rita Cruz; **Caroline Tawk**; Claire Maudet; Miguel Mano; Ana Eulalio. Analysis of Host MicroRNA Function Uncovers a Role for miR-29b-2-5p in *Shigella* Capture by Filopodia. *Submitted*.
- Claire Maudet, Carmen Aguilar, Clivia Lisowski, **Caroline Tawk**, Malvika Sharan, Konrad U. Förstner, Miguel Mano, Ana Eulalio. *Salmonella* decreases let-7i-3p expression to promote multiple steps of bacterial infection. *In preparation*.

Previous publications

Tawk CS, Ghattas IR, Smith CA. 2015. HK022 Nun requires arginine-rich motif residues distinct from λ N. J Bacteriol 197:3573–3582. doi:10.1128/JB.00466-15.

Attended conferences and courses

1. 2nd Mol Micro meeting 2012
   April 25-27, 2012
   Würzburg, Germany
   Poster presentation

2. EPOS, 7th international symposium organized by the students of the GSLS
   October 16-17, 2012
   Würzburg, Germany
   Poster presentation

3. Systems biology of infection

June 23-27, 2013
Ascona, Switzerland
Poster presentation

4. Regulating with RNA in bacteria
   June 4-8, 2013
   Würzburg, Germany
   Poster presentation

5. 3rd Mol Micro meeting 2014
   May 7-8, 2014
   Würzburg, Germany
   Poster presentation

6. Practical course: Current methods in RNP analysis
   July 21-25, 2014
   Regensburg, Germany

7. Eureka 9th international symposium organized by the students of the GSLS
   October 14-15, 2014
   Würzburg, Germany
   Poster presentation

8. Eureka 10th international symposium organized by the students of the GSLS
   October 14-15, 2015
   Würzburg, Germany
   Poster presentation

Affidavit

I hereby confirm that my thesis entitled "The role of host-stress in the infection by the bacterial pathogen Shigella flexneri" is the result of my own work. I did not receive any help or support from commercial consultants. All sources and / or materials applied are listed and specified in the thesis.

Furthermore, I confirm that this thesis has not yet been submitted as part of another examination process neither in identical nor in similar form.

Würzburg
Place, Date

Signature

Caroline Tawk

Eidesstattliche Erklärung

Hiermit erkläre ich an Eides statt, die Dissertation "Die Rolle von Wirtszellstress in der Infektion mit dem bakteriellen Krankheitserreger Shigella flexneri" eigenständig, d.h. insbesondere selbständig und ohne Hilfe eines kommerziellen Promotionsberaters, angefertigt und keine anderen als die von mir angegebenen Quellen und Hilfsmittel verwendet zu haben.

Ich erkläre außerdem, dass die Dissertation weder in gleicher noch in ähnlicher Form bereits in einem anderen Prüfungsverfahren vorgelegen hat.

Würzburg
Ort, Datum

Unterschrift

Caroline Tawk